MODELING AND CONTROL OF A SMALL AUTONOMOUS VEHICLE

by

Jong Young Kim

DEPARTMENT OF ELECTRICAL ENGINEERING AND COMPUTER SCIENCE

in partial fulfillment of the requirements

for the degree of

Master of Science

at the

MASSACHUSETTS INSTITUTE OF TECHNOLOGY

June, 1997

Signature of Author _____
Department of Electrical Engineering and Computer Science, June, 1997

Certified by _____
David Kang, Thesis Supervisor

Certified by _____
Kai-Yeung Siu, Thesis Supervisor

Accepted by _____
Arthur C. Smith, Chair, Department Committee on Graduate Students

I hereby assign my copyright of this thesis to The Charles Stark Draper Laboratory, Inc., Cambridge, Massachusetts.

Permission is hereby granted by the Charles Stark Draper Laboratory, Inc., to the Massachusetts Institute of Technology to reproduce any or all of this thesis.

MODELING AND CONTROL OF A SMALL AUTONOMOUS VEHICLE

by

Jong Young Kim

Submitted to the Department of Electrical Engineering and Computer Science
in partial fulfillment of the requirements
for the degree of
Master of Science

ABSTRACT

Design and implementation of small autonomous vehicles requires specific electronics and control designs to meet space and power constraints. Design of such system requires careful investigation of design constrains and specifications. Motion control of driver motors is very important factor however its been overlooked. A good motor control circuit can increase power efficiency and consumption of overall system, thus operation time can be greatly extended. A devoted microprocessor H-bridge hardware with sliding mode control provides good performance, compactness and power efficiency. Also autonomy of vehicles usually requires precise and robust control of vehicle's dynamics. To be able to achieve these requirements, many sensors are required to feedback vehicle's essential information. A sonar sensor for obstacle detection, Laser Positioning System for absolute positioning of vehicles and an anti-aliasing filter for AD conversion of gyro output are also discussed. In addition mathematical models of a small autonomous vehicle are derived for better design decisions, component selections and control algorithms. With not only qualitative information, but also some quantitative information from mathematical models should help to plan an overall system before individual system developments are begun. Control design of vehicle dynamics are done with above derived mathematical models and evaluated. Sliding mode control enables to simplify driver motor electronics without compromising its performance. Thus a new concept of motor controller is designed and should solve many problems pertained in vehicle development and performance.

Thesis Supervisor: Dr. David Kang
Title: Project Manager

Thesis Supervisor: Dr. Kai-Yeung Siu
Title: Professor of Mechanical Engineering

ACKNOWLEDGMENT

I gratefully thank to Dr. David Kang giving me tremendous opportunity to work on system design and actual implementation of real applications and believing in my ability. Professor Kai-Yeung Siu accepted this project and thesis even at very late notice and understood my situation. I also like to thank to all fellow students in the lab, especially Bill Kaliardos who made me realize importance of small, hidden but important details of system design and integration. Finally I deeply thank to my parents who believed in me and gave me mental strength all the time. This thesis was prepared at the Charles Stark Draper Laboratory, Inc., under contract 15834.

TABLE OF CONTENTS

LIST OF FIGURE

Figure page

LIST OF TABLES

Table page

CHAPTER 1

Introduction

Dropped ordinances for anti-personnel have some failure rate. Clearing these unexploded ordinance (UXO) is a dangerous and slow process due to exposure of human personnel and equipment. But clearing UXO is an important task to provide safe operation area after the purpose of deploying land munitions. An autonomous small vehicle can perform the clearing of UXOs and it is a safer and more efficient way to clear UXOs. A small six wheeled autonomous vehicle has a high mobility and flexibility on rough terrain to perform the task. Its hardware platform is rather unique in a sense that all electronics, sensors, and actuators are specifically designed to able to perform the task. But the problems, that lie on this small autonomous vehicle, also share some common problems in many other robots and unmanned and/or remote vehicles. For instance, all the battery powered vehicles and robots are constrained by the maximum energy and operation condition of batteries. Most of electronics are developed to maximize the energy efficiency. For small vehicles and robots, physical space and weight are serious constraints. All electronics are designed in such a way to fit into a physical space and weight constraint. To navigate and perform the task on rough terrain, several unique sensors are designed and used to meet the task requirements and budget. Sonar sensors are used to detect obstacles that are too big to climb over. A bumper switch is used to register and detour an obstacle that is missed by sonar sensors. Six DC motors are used to provide better mobility of the vehicle. For dead reckoning, a gyro and encoders are used. Also control of the vehicle is an issue to address, and a new DC motor controller circuit is designed with a sliding mode control algorithm. This sliding mode control algorithm provides a new method to design a DC motor control circuit with considerably simpler and fewer components. This new motor controller circuit enables us to provide good position control performance and to meet the space and weight constraint. This thesis provides a method/solution to the vehicle electronics and control problems emphasizing a system integration issue.

1.1. What is EOD?

In the era of a modern warfare, immobilizing and damaging combatants is still one of the most effective way to win a war. Many different methods exist and a dropped mine is one of very effective way. The dropped mines are deployed on the air by ground support aircrafts and detonate once hit the ground. But some dropped mines do not

explode even when those mines hit the ground. After serving the purpose of those dropped mines, unexploded ordinances (UXO) are needed to be cleaned. These clearing UXO job is called Explosive Ordinance Disposal (EOD). Only 3000 EOD technicians are available from all the military services combined, and they must do more than UXO clearing.

In the current manual UXO clearing approach, areas suspected of having UXO are first partitioned into sectors with corners delimited by flags. In each sector, a four-to eight-man sweep team visually scans the area for UXOs. The risk during the manual sweep is considered much less than the risk involved in clearing the UXO. UXOs are dangerous and can detonate even if handled with care by well trained UXO technicians.

Once a UXO is located, all services except the Marines execute blow-in-place (BIP): personnel place a detonation charge, stand off 1000 yd, and return 30 minutes after detonation. The Marines execute a manual pickup and carry-away (PUCA) procedure to gather the UXOs in a common location for later detonation.

An estimate of the efficiencies of the two methods, BIP and PUCA, may be approximated by the rough statistics in Table 1.1.1. gathered from manual EOD operations.

Method	Gross Statistics	1 Day Efficiency [UXOs/Man]	Comment
PUCA (USMC EOD)	1000 UXOs/Day by 8-man team	125	3103 UXOs gathered in period of 4 days including 2 short days due to bad weather. (6 h = one full day)
BIP (Other Services)	100 UXOs/Day by 4-man team	25	Air Force data (4 h = one full day; less than acre area covered by team)

Table 1.1.1.[1] Comparison of BIP and PUCA methods.

The data indicate an approximate efficiency gain of a factor of 5 by using the PUCA method as compared to the BIP method. Increased efficiency not only reduces the time to clear a designated area, but also reduces the manpower required to accomplish the same task.

1.2. Small autonomous vehicles and advances in EOD capabilities

The small autonomous robot vehicle can solve the risk of exposing personnel to UXO and can increase a speed of whole process. Small robotics technology can be used to

[1] Small Robotics for Unexploded Ordnance (UXO) Clearance Workshop, Naval EOD Technology Center, Indian Head, MD, March 16, 1994

clear UXO safely while reducing the number of personnel re uired. This small autonomous vehicle built in Draper laboratory is called the EOD vehicle.

The PUCA operation in UXO clearing is proven to be more efficient than the BIP operation, and is adapted on the small autonomous vehicle operation. It is assumed that the location of the UXOs within the area of operation are known a priori (within an accuracy of 1x1 meter), but that the terrain conditions are not.

The starting UXO position information is assumed to come from a manual visual sweep or a remote detection sensors for automated UXO survey vehicles. Proposed methods of clearing UXO by the EOD small autonomous vehicle are following.

- Either sweep team or helicopter with UXO position sensor scans the area for location of UXO.
- A UXO location map is made based on the above information in a ground station.
- A ground station assigns each vehicle a route with several UXOs on the way.
- The EOD vehicle follows its route to clear UXOs
- The EOD vehicle collects a UXO and drop at the disposal area.
- Once cleared the area, deploy a detonation charge at the disposal area and detonate.

For a partitioned area to be cleared, several EOD vehicles will be deployed to increase speed of UXO clearance operation. Figure 1.2.1. shows a propose baseline EOD operation.

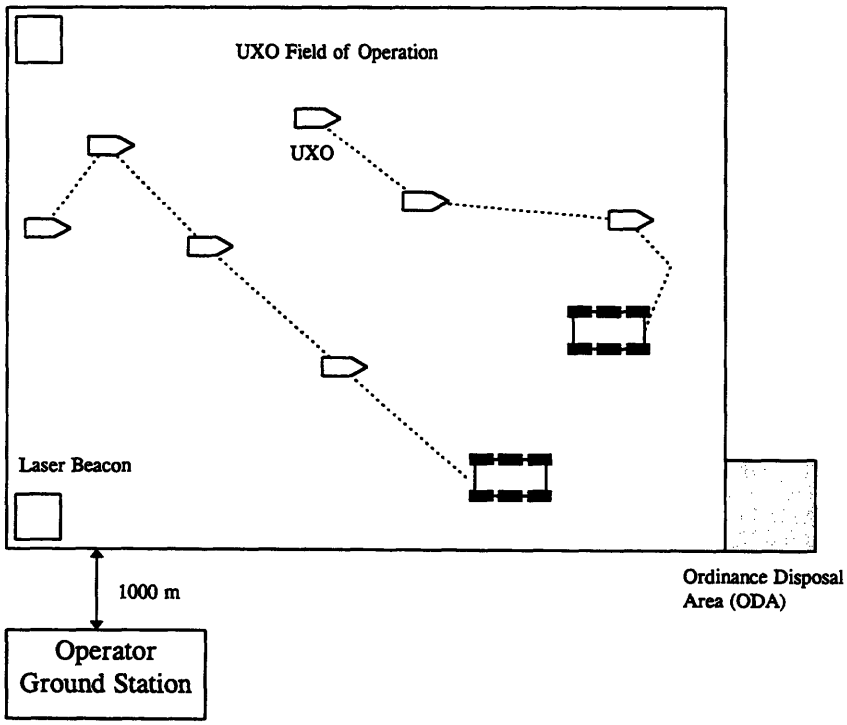

Figure 1.2.1. Baseline EOD operation

The baseline EOD operation, Figure 1.2.1., consists of autonomous EOD vehicles, a Local Positioning System (LPS) for EOD vehicles using laser beacons, and a ground operation station. EOD vehicles will be inexpensive (for a mass production) enough to consider expendable should UXO detonate or explode in their vicinity. The ground station interfaces with a human operator and serves as an Automated Mission Management (AMM) host. It is located at a safe distance from the UXO area and from the ODA. Wireless communications connect EOD vehicles and the ground station. A single operator at one ground station will oversee multiple EOD vehicles that coordinate their activities and safely conduct PUCA operations.

1.3. Specifications to meet mission requirements

The EOD vehicle is designed to operate its major mission autonomously. Autonomy of any vehicle requires more sensors and different architecture than most other common remote controlled vehicle's. Remote controlled vehicles requires only drive motor (any form of actuator) and servo mechanism. A human operator can determine its environment and react to the change of environment. But, for an autonomous vehicle, interpretation of environment is not so trivial as human operators do. For instance, when there is an obstacle in front of a vehicle, it must have some sort of sensor that can detect and identify as an obstacle. On the other hand, human operators detect and identify an obstacle by a vision or by any other human sensors. Mainly an autonomous vehicle needs to have equivalent sensors of humans or other variations.

1.3.1. Drive systems

For the UXO clearance mission, EOD vehicles are expandable during pick-up of a UXO. Those exploded or detonated UXO during pick-ups are ones that more likely to damage EOD technician. Thus EOD vehicles must be cheap so that they are expandable. Any large vehicles would cost too high, and it would be almost impossible to lose a vehicle whenever a UXO explode during the mission.

On the other hand, a small vehicle powered by electrical motor can be mass-produced at much reasonable price. In fact, one of the biggest driving factor for this EOD vehicle is a production cost, and a small vehicle with electrical motor is one of the best way to reduce a production cost.

Since this new EOD concept is not only to improve safety of operations, but also to increase efficiency of operations. It is natural that the EOD vehicle should be fast enough to do operations efficiently. Therefore mobility of the EOD vehicle is important issue and this issue should be addressed in mechanical and electrical design consideration.

1.3.2. Navigation systems

Ability to navigate an unknown terrain is very crucial to success of the mission. There are two major categories in navigation systems. One is an inertial navigation system. Inertial navigation systems are most common technology and have been used extensively starting from the birth of airplane navigation. Most common inertial

navigation systems include gyroscope, compass, and accelerometer. The other one is an absolute positioning system. This technology is more recent, and one of the most common technology is Global Positioning System (GPS). There are also many different methods and techniques to provide an absolute position data to a certain reference.

Inertial navigation systems are often used in dead reckoning navigation. Dead reckoning navigation does not have a closed loop information so that an error from dead reckoning accumulates during its operation. But, for a short time interval, inertial navigation systems provide high bandwidth and accurate data. For the EOD vehicle, dead reckoning is required to navigate and to control on a rough unknown terrain.

On the other hand, absolute positioning systems are also required to reset the accumulated navigation errors from dead reckoning systems. Without absolute positioning systems, repeated and long operations would be impossible. Short comings with GPS are accuracy and bandwidth of data. Some differential GPS provides a higher accuracy at stationary state, but the accuracy degrades as a system is in motion. Also a bandwidth of GPS data is not high enough for a control purpose. But integration of dead reckoning and absolute positioning would solve the navigation and control problem more efficiently.

1.3.3. Hazard avoidance systems

Rough unknown terrain is a big challenge for a relatively small autonomous vehicle. Navigation and control of the EOD vehicle in a known and controlled environment would be a lot easier. A small rock and tree branch can be an obstacle and the EOD vehicle needs a means of detecting these potential obstacles with minimum complexity and cost. It is not very critical to be able to determine a shape or height of obstacles, but it is critical to be able to determine obstacles with sizes or shapes that are impossible to climb.

1.3.4. Communications

The ground station should send commands and location data of UXOs to each EOD vehicles, and each EOD vehicles should send its own position data and all mission critical information to the ground station. All data are formatted in digital signals for easy access to each CPUs of the ground station and EOD vehicles.

Two-way communication is required to complete the mission. A required bandwidth of two-way communication is depend on the data flow rate and amount. Also number of operation EOD vehicles in a mine field is a factor to the limit of the bandwidth. The more EOD vehicles operated, the more communication channels required. It is possible for actual EOD operation to use a military frequency, but it is only possible after the development of final product. Thus a civilian bandwidth or open frequency channel can be only used for the EOD vehicle development.

1.3.5. Power source

Since the EOD vehicle is operated by itself, some kind of independent carry-on power source is required. Batteries are most common power sources for a small robots and

most convenient. For the EOD project, batteries are used for convenience and accessibility. The power source should be easily replaceable on site, easy to carry, and easy to maintain.

1.4. Concepts and Background of the EOD Vehicle

This EOD project is carried in Intelligent Unmanned Vehicle Center (IUVC), C.S. Draper Lab[1], and is supervised under Dr. David Kang[2]. IUVC has produced some autonomous vehicles. MITy-2 is a six-wheeled autonomous vehicle and is capable of autonomous maneuver. Especially mechanical platforms of EOD-1 is based on MITy-2, which has three platforms connected by steel strings. In rough terrain, it has been shown that six-wheeled vehicles are more efficient than caterpillar based vehicles.

Figure 1.4.1. shows a picture of EOD-2. As it mentioned, EOD-2 has three platforms connected with two steel wires and six wheels for better mobility. The front platform is mainly composed of a grappler mechanism, bumper switch, and sonar hazard detection sensor. The middle platform has a main CPU, motor encoder circuit, gyro, wireless modem, LPS transponder, video camera, and video transmitter. The rear platform has a power regulator circuit, motor driver circuit, and battery package. Steering wheel mechanisms are mounted on the front and rear platforms.

[1] 555 Technology Square, Cambridge, MA 02139

[2] 555 Technology Square, MS 27, Cambridge, MA 02139, Phone:(617) 258-2947

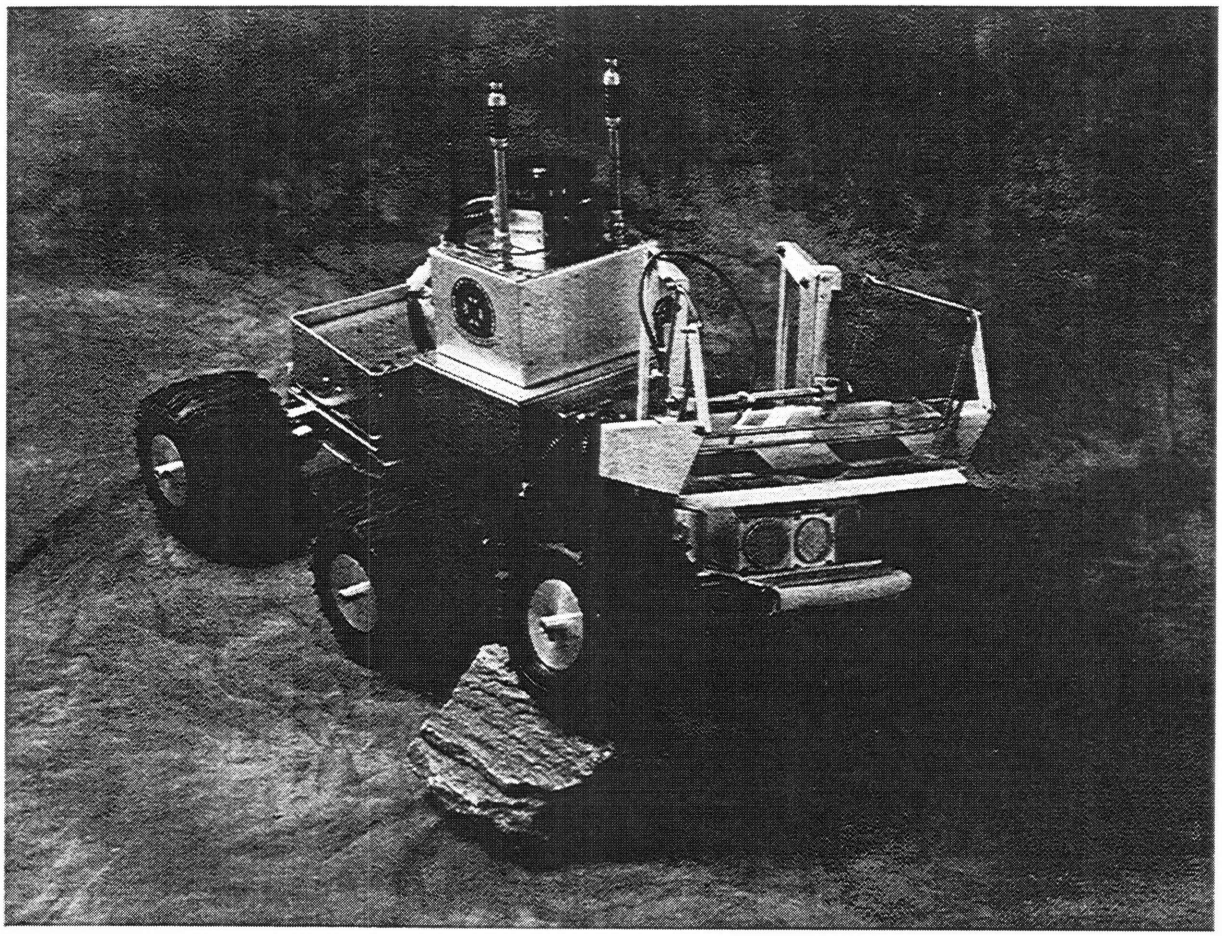

Figure 1.4.1. Picture of EOD-2

CHAPTER 2

Energy Requirement and Batteries

EOD-1 and EOD-2 must provide their own power sources by themselves in part of an independent operation requirement. There are several different forms of storing energy, and each one of them has its strength and weakness. Main concerns in choosing a power source are energy density, cost, accessibility, maintenance, and packaging. Depend on the power source, a whole system design concept can change. One of the most important factor in a system design is a power budget, that is a major driving factor in design and selection of the system components. Often this factor is ignored easily during the initial design stage, and later it is found out that the power budget is not enough to afford all good designs. That is a waste of time and resources. In this chapter, many different power sources are discussed. Particularly many different modern batteries and advantages of using batteries are discussed.

2.1. Energy requirements

Deciding how much power is needed is a design process itself. An initial estimate of deliverable power will give a power budget for electronics, and sensors. Once the a rough design is finished, a recalculation and a possible increase of deliverable power are required to refine a design process. There are many different kinds of power sources and each of them has its advantages and disadvantages. For instance, a gasoline has a very high energy density, but it is more difficult to operate on a small vehicle with limited space and weight than a battery.

EOD vehicles must be able to operate long enough in the mine field. Mobility is also a important factor since increasing an operation efficiency is one of the main objective. It is natural to require a maximum speed of the EOD vehicle is about to equal to the speed of human walking. Its original maximum speed is 5 ft/sec or 1.5 m/sec which is roughly a human walking speed. This speed requirement is relatively fast for the size of the vehicle to be built. The EOD vehicles are about 0.7 m long and weighs 10 kg. The traveled distance at the maximum speed is about twice longer than the length of the vehicle, and kinetic energy at the maximum speed is 11.3 J. Mostly efficiency of the electric vehicle is about 45 - 55 % which suggest about 5.6 W is going to be wasted. On the other word, a power source must be able to supply 5.6 W just to maintain the maximum speed, 1.5 m/s. But it is less likely to operate at the maximum speed of the

vehicle for the normal operation. Most likely the desired operation speed at the normal condition is about a half of the maximum speed, 0.75 m/sec, due to energy conservation, controllability, and operation optimum speed. The power required to maintain the new operating speed, 0.75 m/sec, is now reduced to 2.8 W. Of course this requirement is only for a laboratory conditioned environment. When the operation terrain is rough with many obstacles, the estimated efficiency is much lower. The efficiency of the 45 to 55 % is only for the mechanical efficiency which did not include actual electrical efficiency, either. Therefore much more power is required, and an estimation of the power requirement can be estimated a lot better after selection of the driver motor. A selection of the required motor can be also done more effectively with some mechanical and electrical mathematical models, but it is also a good practice to use somewhat overrated motors for a prototype. It is always possible to degrade motors later after the prototype is working, but it is too late if the prototype does not work adequately for a proof-of-concept demonstration. It is a common mistake to try save cost on a prototype by using barely acceptable components. It is quite common that manufacture's claim is not true for certain conditions, and it is always a good idea to test and/or verify the manufacture's claim before building a prototype. Including a safety factor for a prototype design is a correct procedure. In a timed contract or project, saving time is saving cost.

Above simple calculation is a preliminary estimation of power required solely from the kinetic energy. Electronics and sensors in EOD vehicles also requires power, and it is yet to be determined along the actual development of the system. But an approximate estimation is never a bad idea, especially it helps a designer to guide ones design and to decide what electronics and sensors are affordable. For instance, a main CPU with IO device in a small size usually requires about 15 to 25 W of power. All other electronics should be in the order of 10 to 20 W. Of course all these are preliminary calculation and will be recalculated and justified after a real design procedure.

2.2. Batteries

The first practical battery, the silver zinc voltaic pile, was built by Alessandro Volta nearly 200 years ago. For this accomplishment the unit of electrical force, the volt, was named after Volta. Shortly after Volta's discovery the first rechargeable battery was constructed by Johann Wilihelm Ritter. Unfortunately no practical means existed to recharge it, except from a primary battery. The electric generator was not to come along for another twenty years so the development of rechargeable technology was essentially stalled for the lack of a charger. The next significant step in battery development came 60 years later as George Leclanche introduced his carbon zinc "wet" battery, a technology that paved the way for today's common flashlight battery.

2.2.1. Primary and secondary cells

Batteries are generally classified as either primary or secondary. Primary batteries are the type that may be used only one time since the active chemical reaction is irreversible when the cell discharges. Once the primary battery is discharged completely, it is discarded. Secondary batteries, on the other hand, may be used

repeatedly because the chemical reaction which produces electrical energy can be reversed by recharging the batteries.

Primary cells come in a number of commercial variations to address different markets. The common zinc-carbon has for years formed the basis for the primary battery market and still serves for the low end applications because of its low cost. The Alkaline-Manganese is rapidly replacing the zinc-carbon as the cell of choice for today's advancing electronic market. It's higher energy density makes it strong competitor when the hourly operating cost is considered. Mercury-Zinc and Mercury-Cadmium have been popular in the miniature battery arena where they have been called upon to serve a variety of low power applications ranging from implantable heart pacers to cameras, hearing aids and watches. Because of environmental implications and technology developments they are being replaced by other systems. The Air-Zinc battery is gaining popularity in low power devices. The lithium battery is called upon to power many microelectronics.

Rechargeable cells are manufactured in three basic types. The most common is the open type which is typical of the standard automotive starting battery. The battery is open to the atmosphere and during use gases are emitted and occasional replenishments of the lost water from the electrolyte is required. A variation, the maintenance free battery increases the volume of electrolyte so the battery will not require maintenance during its service life. The second form is the semi-sealed which employs some form of electrolyte immobilization scheme to reduce the possibility of acid leakage. These cells are open to the atmosphere and also release gases during charge and discharge. The third type is the fully sealed cell. During normal operation, a sealed cell does not permit the venting of gas to the atmosphere. The fully sealed cell requires that the gases generated when charging the cell be recombined as part of the process. This recombinant technology is employed in all sealed Ni-Cd and in some sealed lead cell types.

2.2.2. Lead acid battery

There are many technologies for rechargeable batteries. Lead-Acid is by far the least expensive and most popular. Automotive style batteries have very thin plates, and not much lead paste, for very high power. The capacity of an automotive battery is not important in its design use, which is why it is rated in cold cranking amperes (CCA). The automotive battery is not designed to discharge more than 50% of its capacity. On the other hand, deep-cycle batteries are designed to be discharged to 80%. They have thick plates and dense plate, that reduces power but allows a long life. The deep-cycle battery is rated in ampere-hours (AH).

All lead-acid batteries are made up of 2 volt cells. Figure 2.2.1 and Figure 2.2.2 show the voltage curve of lead-acid battery when it is charging and discharging. On Figure 2.2.1 and Figure 2.2.2, add 3.6e-3 V for every 1 °C below 25 °C, and multiply by 6 to get the voltage of 12 V battery. For example, if each cell is 1.95 V, that is about 30 % of discharge at 22 °C. But if the temperature is 0 °C, then the battery is about 45 % discharged instead of 30 %.

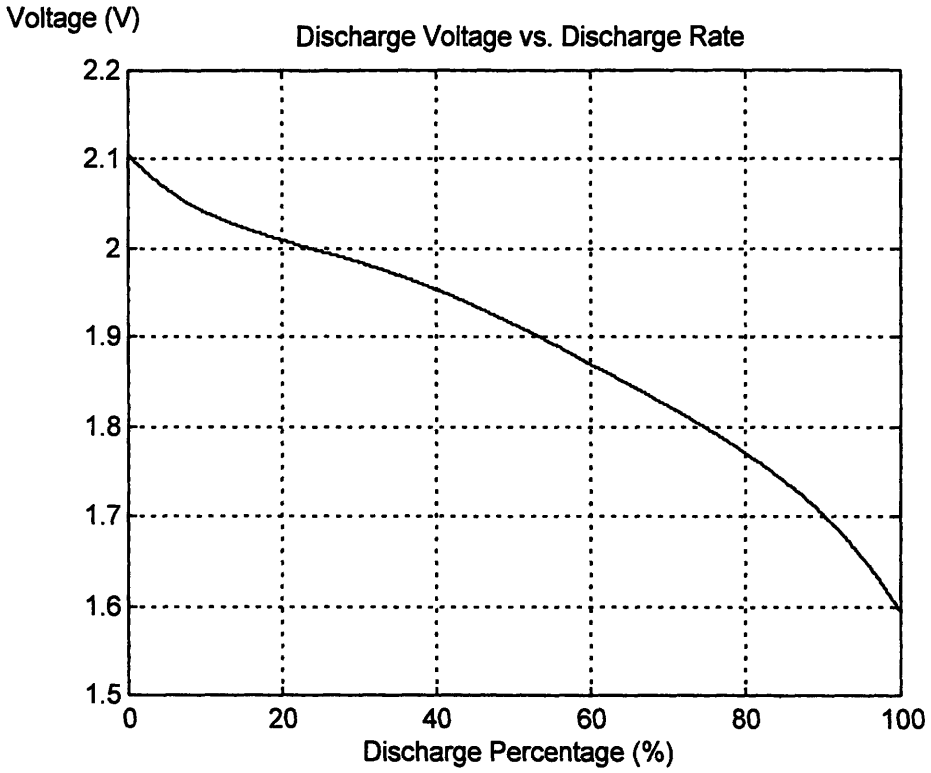

Figure 2.2.1. Lead-acid 2-Volt cell discharge curve

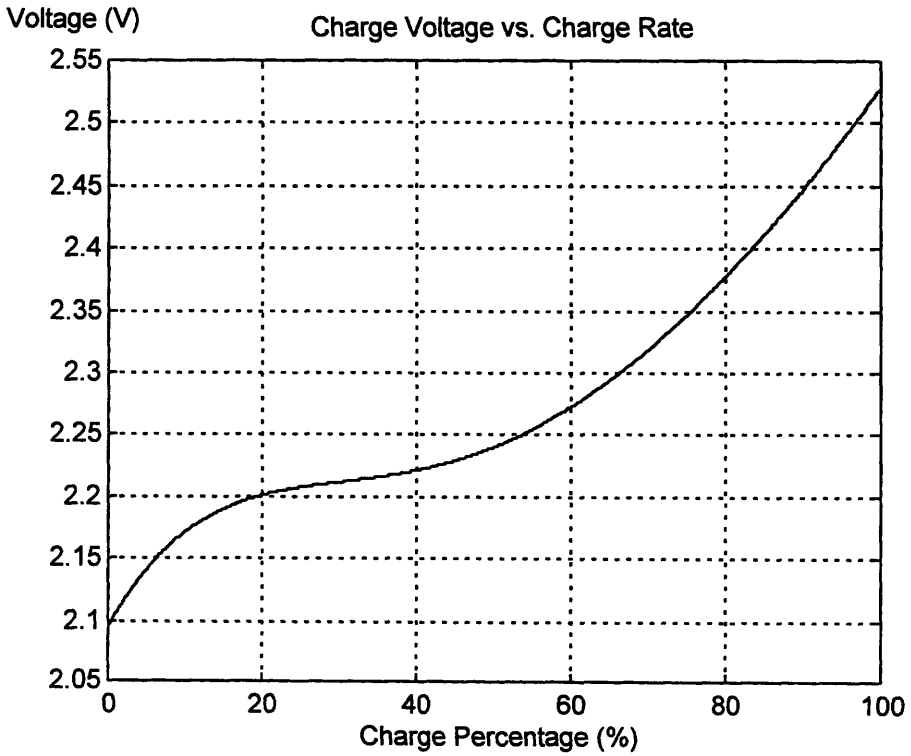

Figure 2.2.2. Lead-acid 2-Volt cell charge curve

The only accurate measurement of open circuit voltage is after the battery has rested for 24 hours, with no charge, recharge, or load of any kind on the battery. Notice that a big drop-off in Figure 2.2.1 after 80 % of discharge. At about 80 % depth of discharge the battery is running out of lead dioxide, so potential voltage drops off very quickly. If the battery is discharged beyond that point, voltage reversals can happen which lead to high heat and essentially self-destructs.

The capacity of a lead-acid battery is the number of amperes-hours until the voltage drops below 10.5 V for a 12 V battery. This is usually specified at a current draw that will discharge the battery in 20 hours. If the battery is discharged faster than that, the actual capacity is lower. For example, 3.7 AH lead-acid battery rated in 20 hours, can draw 0.185 A of current for 20 hours to use 3.7 AH. But if a current is drawn at 3.7 A rate, then the total power supplied is 57 % of 3.7 AH or 2.1 AH. Thus a large current draw in a short time period actually reduces a useable battery capacity. Figure 2.2.3 shows a useable capacity versus a different discharge rate for a battery rated in 20 hours.

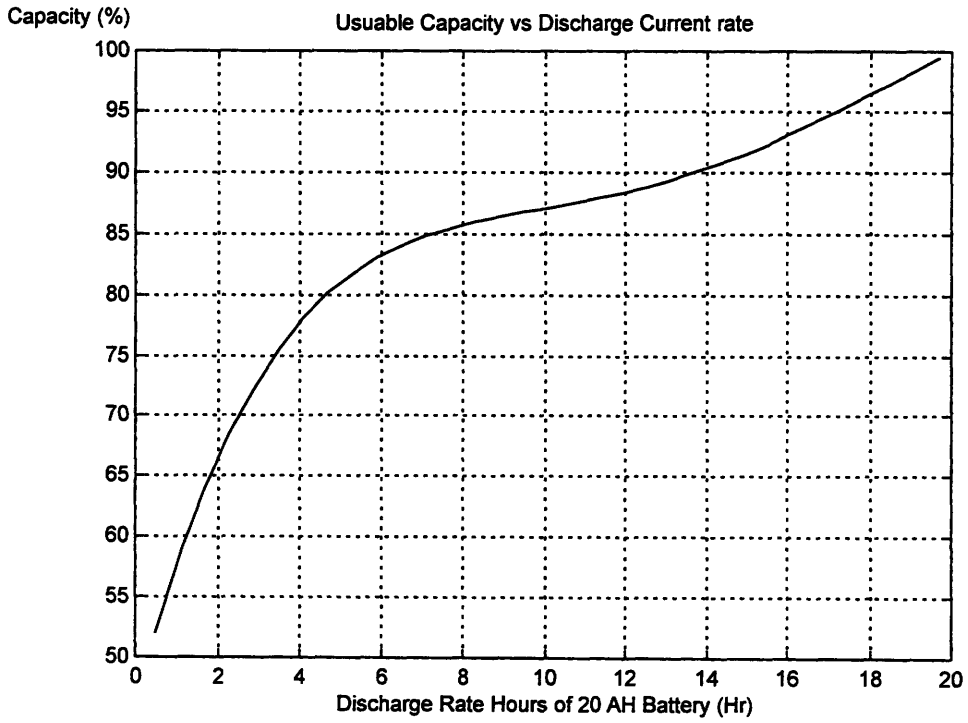

Figure 2.2.3. Useable capacity of 20 hour rated lead-acid battery versus discharge rate for the maximum usage

This limits a maximum usage of the battery when a large load is required for a short time. If a system draws 3.7 A during a normal operation from a 3.7 AH rated in 20 hours lead-acid battery, then it is not 1 hour to be able to operate, it is 57 % of 1 hour or only 34 minutes. Of course if a system is drawing 3.7/20=0.185 A of current, then

a battery life is 20 full hours. It is more desirable to be able to get maximum capacity from a battery without damaging a battery.

The optimum temperature for a battery is 25 °C. For every 8.3 °C below 25 °C, there will be a 10 % loss of capacity. So, at 0 °C, there is only 70 % useable capacity. Also, when the battery is fully charged, to above 1.20 specific gravity, the electrolyte freezes at about -23 °C. But, if the battery is not fully charged, and the specific gravity is 1.10, then the electrolyte freezes at -6.7 °C. This stresses the cases, the plastic gets brittle and may crack. High temperature causes a reduction in life because of the increased corrosion of oxygen and lead, but not of capacity.

If battery cells are connected in parallel to charge, the cells will have different internal resistance and the current will not divide evenly. The good cells (with low internal resistance) will get overcharged and flake off a lot of lead while the weak cells will not get enough current to cause any flaking thus the cells continue to deteriorate. If several batteries are used simultaneously, charge identical batteries in series and discharge in series. This will force the batteries to have equal voltage levels and same current charge rates.

2.2.3. Ni-Cd battery

The nickel electrode and alkaline system lagged the lead acid development by 30 years. Edison's experiments in 1890 resulted in the Nickel hydroxide positive electrode working in conjunction with an iron negative electrode in an alkaline electrolyte to form the first rechargeable alkaline system. In 1910, Waldmar Junger, a Swedish inventor, developed the Nickel Cadmium pocket plate battery. European experimenters designed the first recombinant Nickel-Cadmium battery in the early 1950's that is the basis for today's Ni-Cd industry.

Adding together the potentials for the Cadmium anode and the Nickel cathode yields the predicted cell voltage for a Ni-Cd cell, 1.3 V, and it is close to actual rate of 1.2 V. By convention, a fast charging is for 1 hour or less charging time. A quick charge is for 1 hour to 14 hours of charging time. More than 14 hours of charging time is called trickle charge. This means that charge rates ranging 0.05 C to 0.1 C for trickle charge, 0.2 C to 0.5 C for quick charge, and 1 C or greater for fast charge. Trickle and quick charge are popular because of the relatively low cost and simplicity of implementation. For a fast charge, a monitor circuit is required not to overcharge the Ni-Cd battery. The cell pressure stays low during most of charging time and rises as the cell approaches full charge. The higher pressure is the result of the oxygen generation. The higher the overcharge rate the higher the rate of oxygen generation. The cell temperature increases due to the heat of recombination of the oxygen on the negative, Nickel. This is an almost same phenomenon in the lead-acid battery and is not desirable.

Individual cells are rated at 1.2 V and voltage for batteries are multiples of the individual cell voltage of 1.2 V. However, the discharged voltage will probably exceed 1.2 V for some portion of the discharge period. Most manufacturers rate cell capacity by stating a conservative estimate of the amount of capacity which can be discharged from a relatively new, fully charged cell. The accepted rating practice is to state a cell

rating in AH (or mAH) to a cutoff voltage of 0.9 V at its one-hour discharge rate. Also the rate of self discharge is about 1 % per day at room temperature and doubles for every 10 °C above room temperature.

Under controlled conditions, a Ni-Cd cell can last up to 10 years with minimum cycling. On the other hand, cells have been cycled up to 10,000 times, under controlled conditions. Generally the definition of failure of the cell is the cell fails to yield 80 % of its rated capacity. The primary failure mode is the loss of separator integrity which manifests itself in a cell short.

2.3. Comparison and choice of Batteries

There are many different kinds of battery beside lead-acid and Ni-Cd battery. Table 2.3.1 shows a comparison of different batteries in energy density.

Battery Type	Specific Energy Wh/kg	Specific Power W/kg	Energy Efficiency (%)
Lead-Acid	40	130	65
Aluminum-Air	200	150	35
Lithium-Iron-Disulfide	> 130	> 120	---
Lithium-Polymer	100	100	---
Nickel-Cadmium	56	200	65
Nickel-Iron	55	130	60
Nickel-Metal Hydride	80	200	65
Nickel-Zinc	80	150	65
Sodium-Sulfur	100	120	85
Zinc-Air	120	120	60
Zinc-Bromine	70	100	65

Table 2.3.1.[1] Comparison of different batteries in energy density

The nickel-cadmium battery has 200 W/kg of specific power versus lead-acid's 130 W/kg of specific power. Also a Ni-Cd battery is rated at an 1-hour discharge rate while a lead-acid battery is normally rated at a 20-hour discharge rate. Thus a Ni-Cd battery is desirable for a longer life time, but the cost of Ni-Cd batteries is roughly twice of the cost of lead-acid batteries. For mass production a production cost is also an important part. The current batteries used in the EOD vehicles are lead-acid. It is not because of cost, but it is because of packaging of batteries. Lead-acid batteries come in various size and voltage, and those batteries are readily available for any emergency use. But Ni-Cd batteries have a limited selection of size and shape which makes packaging of Ni-Cd batteries extra works. If a packaging is not a problem, Ni-Cd batteries are desirable.

[1] Robert Q. Riley Enterprises, P.O.Box 12294, Scottsdale, Arizona 85267-2294

CHAPTER 3

Electronic Sensors and Actuators

In mobile robot electronics, compactness, low power consumption, weight, simplicity and yet robustness are required to survive in a rough environment operation. Sensors and actuators are constantly exposed to high operating temperature and vibration while the EOD vehicle is operating on rough terrain. Design and implementation of circuits under this hostile condition must be done carefully. A new approach to a DC brush motor control circuit is designed to improve its performance and compactness over a conventional previous PWM H-bridge motor circuit using a Motorola MC33033 chip and a single specialized IC H-bridge motor circuit using a National Semiconductor LMD18245. Also a sonar obstacle detection sensor circuit, Laser Positioning System (LPS) and a filter network for a micro-mechanical gyro will be discussed.

3.1. EOD-2 Driver Motor and Gearhead

A driver motor and gearhead were chosen based on the maximum speed and weight of the EOD vehicle. A DC servo motor has a higher output power per size than a stepper motor's. A stepper motor control would be easier than a DC servo motor, but it is less efficient and under-powered for a maximum affordable size of the EOD driver motor. Also a DC servo motor is still widely used and has a wide variety of selections.

A MicroMo® DC motor was chosen by Jim Dyess, a former draper fellow at IUVC. This particular DC motor has power output of 15 Watts (25 Watts with appropriate cooling) which is sufficient to power the EOD vehicles up to speed of 5 ft/sec. Its maximum no load speed is 4800 RPM and produces speed of 5 ft/sec with a 25:1 ratio gearhead. The driver motor used in EOD-1 has a nominal voltage of 12 V. The choice of voltage was rather arbitrary since 12 V battery pack was popular. Unfortunately this caused some difficulty in a driver circuit, and power efficiency of driver circuits claimed lower than desired. By moving into a higher voltage, 24 V, efficiency of driver circuits could claim a better efficiency. In fact, a very significant improvement was made, and driver circuit design was a lot easier.

The EOD-2 has a same driver motor with a 24 V nominal voltage. as in the EOD-1. But EOD-1 driver motor has a nominal voltage of 12 V and used 24 V for actual motor voltage rail. Table 3.1.1. shows electrical specifications of the driver motors for 12 V

and 24 V nominal voltage. Also Table 3.3.2. is mechanical specifications of above motors.

	EOD-1 Motor	EOD-2 Motor
Nominal Supply Voltage (Volts)	12	24
Armature Resistance (Ω) ±12%	2.4	10.5
Maximum Power Output (Watts)	15.00	13.71
Maximum Efficiency (%)	75	74
No Load Speed (RPM) ±12%	4800	4800
No Load Current (mA) ±50%	90	45
Friction Torque (@ No Load Speed) (oz-in)	0.297	0.297
Stall Torque (oz-in)	16.30	14.85
Velocity constant (RPM/Volt)	407	204
Back EMF Constant (mV/RPM)	2.455	4.902
Torque Constant (oz-in/Amp)	3.32	6.628
Armature Inductance (mH)	0.23	0.94

Table 3.1.1. Electrical specifications of EOD drive motors

	EOD-1 Motor	EOD-2 Motor
Mechanical Time Constant (mS)	13	13
Armature Inertia ($\times 10^{-4}$ oz-in-Sec^2)	3.6	3.3
Radial Acceleration ($\times 10^3$ Rad/Sec/Sec)	42	42
Bearing Play: Radial (mm)	<0.015	<0.015
Bearing Play: Axial (mm)	0	0
Thermal Resistance: Rotor to Case (°C/W)	1.5	1.5
Thermal Resistance: Case to Ambient (°C/W)	9	9
Maximum Shaft Loading: Radial (oz)	72	72
Maximum Shaft Loading: Axial (oz)	180	180
Weight (oz)	9.8	9.8
Rotor Temperature Range	-55°C to 125°C	-55°C to 125°C

Table 3.1.2. Mechanical specifications of EOD drive motors

Notice that the armature resistance of the EOD-2 motor is 10.5 Ω versus 2.4 Ω of the EOD-2 motor armature resistance. A power loss through H-bridge network is directly proportional to armature current. Thus a H-bridge power loss of the EOD-2 is less than a power loss of the EOD-1. A detailed calculation and discussion is in Chapter 3.2. Driver Motor Circuit.

A gearhead was chosen based on the maximum designed speed of the EOD vehicles. Eq.3.1 shows a simple calculation used to choose a gearhead ratio.

$$n = \frac{4800}{60} \cdot \frac{2\pi r}{v_{max}} = 25.1 \qquad \text{(Eq.3.1)}$$

Where

$r = 0.0762\ m$ = radius of the wheel

$v_{max} = 1.524\ m/s = 5\ ft/\text{sec}$ = desred maximum velocity

The maximum angular velocity is 4800 RPM, but it is true for no load speed. An actual load speed is lower than the no-load speed and varies based on a load. Thus actual maximum EOD vehicle velocity is slower than 5 ft/sec.

3.2. EOD Driver Motor Circuits

Pulse Width Modulation (PWM) motor control circuits are most widely used by industry, hobbyist, school and researchers. Main attraction of this PWM motor control circuit is power efficiency. PWM modulate a signal voltage level proportional to an on-voltage duty cycle, thus PWM uses an effect of averaging voltage. A switching frequency is selected fast enough not to see a chattering motion of motor. Faster switching means a better averaging voltage and better motor response. But a switching frequency is limited by a maximum transistor switching frequency and PWM generator frequency. Also power efficiency drops as a PWM frequency increases.

PWM is extensively used to drive a highly inductive load. If a load is purely resistive, output voltage and current are in phase, which makes a very sudden power delivery. A delivered power will also be in a pulse form and it is not very much desirable. A smooth power delivery is more desirable in many application. In fact, class A amplifier is most desirable in many application due to its high fidelity of amplifying input power. PWM is used mainly to produce an average voltage, that should be equal to the original signal voltage. But the output signal is just a sequence of fast switching. The load should see an average voltage, but the response would be noticeably different than the original signal when the switching frequency is not adequate. PWM cannot be used in a music system, since the output signal is totally different from the input signal. In fact that is why it is called 'modulated'. A speaker will sounds the modulated signal instead of the original signal, even though a speaker is inductive. But a PWM circuit is very useful for motor controller circuit. A DC servo motor with a load naturally demodulates the PWM signal. An armature controlled DC servo motor with a rotational load has a third order dynamics from the PWM control armature voltage. Naturally this third order dynamics is a Low Pass Filter (LPF) which eliminates high frequency contents of the PWM armature voltage signal. This is a natural way of demodulation, but it is not perfect. However this is why a PWM motor controller is most extensively used area while PWM signal cannot be used in a speaker without a demodulation.

A speaker uses the class A or class AB amplifiers, but maximum efficiency is 25 % and 78.5 %, respectably. Since maximum efficiency is 25 % and 78.5 %, usual operation efficiency is about 10% to 20% and 50% to 60%, respectably. For a power

operation amplifier, the class AB is most popular type of output stage. The class A has very low power efficiency, it is rarely used beyond output of 1 Watt. If one uses a power operational amplifier for a motor control circuit, maximum theoretical efficiency is 78.5 % and actual operating efficiency is close to 50 % or lower. The power conversion efficiency of PWM is depends on an impedance of a solid state switch.

Since the nature of PWM does not require a high fidelity signal amplification, the output stage circuit is simple. PWM does not even have any other signal form than a pulse. Therefore the power output stage needs to track an on-off input signal to produce an exact copy of PWM input signal and power amplification. There are several different configurations that implements the power output stage of motors.

High-side switching configuration is a popular switching circuit for one directional motion control. The N-channel MOSFET is used as a source follower. One needs to be careful that the gate voltage must be equal the output voltage plus the gate-source voltage at that specific load current. The gate voltage should be well above the rail voltage since the drain-source voltage should be minimum for a maximum power transfer to the load. Therefore the gate voltage should be $V_G = V_{GS(ON)} + V_S \approx V_{GS(ON)} + V_{CC}$. The gate voltage can be provided by several different techniques, i.e. a separate voltage source, voltage doubler, boost trapping, inductive flyback, pulse transformer, and so on. One must decide which technique is most suitable for the particular application. National Semiconductor makes a built-in boost trapper in their popular H-bridge networks if space and component number are very important. A pulse transformer is an easy solution, but the pulse transformer can be bulk and expansive. A voltage doubler needs a few diode, capacitor and PWM input, and it is cheap. However it can only double the rail voltage. If more than double of the rail voltage is required, cascaded diode-capacitor network can raise this rail voltage even higher. Flyback converter is using a high spark voltage of the inductor. When the power side inductor current is disconnected, the stored energy of the inductor is dumped to the diode-capacitor network. This flyback converter needs a transistor driver for the inductor.

Totem-pole network is also a popular network if bi-directional operations are required for DC motors. Totem-pole has a similar structure of push-pull network. Instead of using a n-channel and p-channel MOSFET, totem-pole use two n-channel MOSFETs. However totem-pole requires $\pm V_{CC}$, which is not much desirable for battery operations. Some might say, there exist a DC polarity inverter and could be used to provide $\pm V_{CC}$. It is true, but this DC polarity inverter is usually intended for low power output. (Usually its maximum output is less than 0.5 W to 1 W). For the EOD's 15 W output motor, no DC polarity inverters can suffice the power requirement.

H-bride is by far the most common DC motor driver network and better performance over other networks. H-bridge is also a bi-direction motor control network and needs only $+ V_{CC}$ instead of two different polarity. This is most charming feature of H-bridge and extensively used in battery powered motors. H-bridge also gives a great flexibility on controlling discharging rate. Noticeable one is that H-bridge has a fastest discharging rate than any other driver networks, which allows a fast motor breaking.

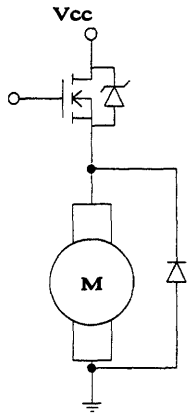

(a) High side switching as a source follower

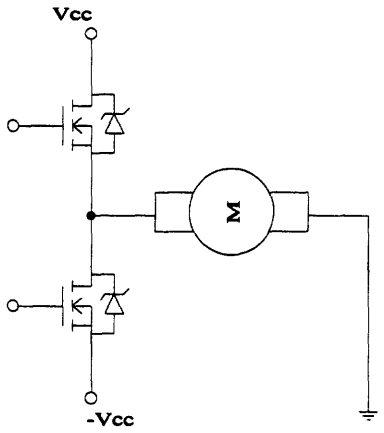

(b) Totem-pole

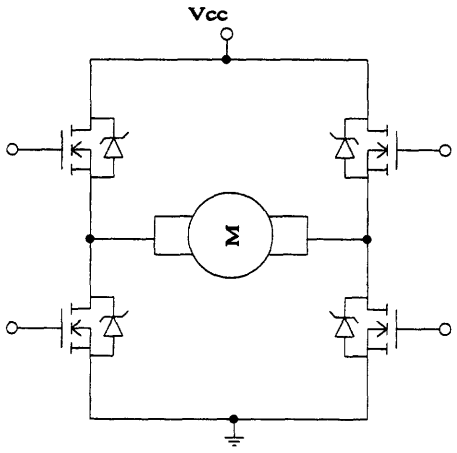

(c) H-bridge

Figure 3.2.1. Various motor driver output stages

(Usually claimed by many semiconductor manufactures, but, in fact, this feature is what most control theorist assumed in their modeling and controller designer for decades). One can notice that H-bridge needs four MOSFETs or BJTs instead of two in totem-pole bi-directional motor driver. Especially when ten motor driver control circuits must be implemented in the rear platform of the EOD vehicle, 40 transistors are need. This is rather undesirable. The original EOD-1 was build by this 40 TMOSFET, but it was changed by other design which essentially used a National Semiconductor's single chip to generate PWM and drive motors. If the EOD motors had similar specification of the National Semiconductor's intended motor, it could have worked better. But the National Semiconductor LMD18245 had inadequate DA converter resolution (it is only 4 bits), which makes any reasonable control algorithms unworkable. In addition LMD18245 was very under-powered compared to the EOD-1's MicroMo motors. A new design for the EOD driver motors was completed and fully simulated with sliding mode control algorithm. This design reduces complexity of the usual motor control circuits to a half. Same time it can use a much better control algorithm, sliding mode control, than a conventional PWM with continuous PID control.

Before a detailed design procedure and thoughts are discussed, it is important to discuss importance of power efficiency of various H-bridge and switching technique. When the PWM signal is on, one source MOSFET and one opposite side sink MOSFET is on. Figure 3.2.2. shows a basic operation of H-bridge.

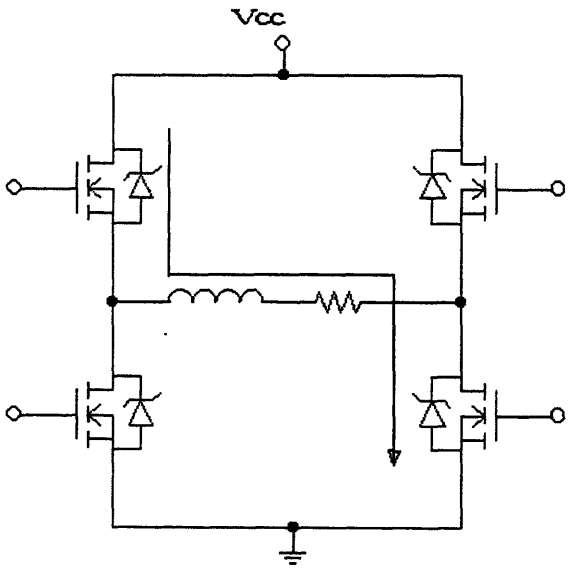

Fi ure 3.2.2. H-bridge Operation

Notice that the diode is already integrated in almost every power MOSFET or BJT to protect the devices damaging from inductive load. Motor is heavily inductive and need to be treated carefully when the power is switched off. PWM is a fast switching signal, and those power MOSFET could be easily damaged if diodes are not connected as in Figure 3.2.2. From Figure 3.2.2., a current route is from S_1, motor and to S_4 when the motor is rotating in forward motion and the PWM signal is on duty-cycle. Now the PWM signal is off-duty-cycle, S_4 is in a cut-off region and the energy stored in the

inductor suddenly accumulates a very high voltage (as high as 500 V). If there were no diode, the inductor current had no where to flow until the break-down voltage of S_4 or S_2 reaches. Then a spark will occur inside of MOSFETs. This break-down is different from regular reversible avalanche of semiconductor. This break-down is irreversible which will cause malfunction. To prevent this, diodes are added to redirect current route to S_2 diode. Thus the motor voltage will not reach to the break-down voltage of semiconductor. Even to enhance the diode function, S_2 will be on during off-duty of PWM signal in forward mode. Table 3.2.1. show a logic truth table of H-bridge operation. This logic could vary in some degree, nonetheless basic logic remains same.

PWM	Direction	Brake	Active Output Drivers
H	H	L	S_1, S_4
H	L	L	S_2, S_3
L	X	L	S_1, S_2
H	H	H	S_1, S_2
H	L	H	S_3, S_4
L	X	H	None

Table 3.2.1.[1] Logic truth table of H-bridge

Now let us look at more detail on the MOSFET characteristic. When the MOSFET is on-state, an equivalent resistance value between source and drain, $r_{DS(ON)}$, should be as small as possible. If $r_{DS(ON)}$ is too large, then there will be a significant power loss through the MOSFET. Maximum power transfer of two networked system has been always very important part of any design, this $r_{DS(ON)}$ should be considered seriously. If a H-bridge design loses a lot of power, then it loses its original purpose of using PWM and H-bridge. For example if one loses more than 30 % than it is better to use class AB output amplifiers. As mentioned earlier class AB amplifiers has a maximum efficiency of 78.5% and usual 50% to 60% power transfer efficiency. And class AB has a very high fidelity signal amplification, while PWM suffers from its averaging voltage by a fast switching.

EOD-1 motor has 2.4 Ω armature resistance and EOD-2 motor has 10.5 Ω armature resistance. A usual 3 to 15 A MOSFET has $r_{DS(ON)} = 0.3\Omega$ which is considerably low $r_{DS(ON)}$ resistance. Also a Motorola MTP50N05 is 50 A MOSFET and has 0.03 Ω of $r_{DS(ON)}$ resistance. While a cost for 3 A MOSFETs and 50 A MOSFETs are almost same, there is no cost advantage for 3 A MOSFETs. Even they share same package size. Assume the motor stalled. The maximum continuous current for both EOD-1 and EOD-2 motors are $24V/2.4\Omega = 10$ A and $24V/10.5\Omega = 2.286$ A, respectably. Notice that even though the EOD-1 motor is rated 12 V, the EOD-1 is using 24 V system. So when the EOD-1 stalls, this is a maximum continuous current. One might argue it is not necessary, since the motor will be current regulated. It is true if the motor is current limited. But one should design a circuit to handle a worst case scenario. What if the current limit is malfunctioning ? That is why still one should consider 10 A stall

[1] Logic table from National Semiconductor data book, LMD18200[1]

current not 5 A. Usual safety factor for MOSFET is 2 to 3 times, which gives 20 to 30 A MOSFETs and 5 to 8 A MOSFETs, respectably. One might think 50A MOSFET is an overkill. Only by looking at the above safety factor calculations, it seems very unreasonable to use 50 A MOSFET versus 20 A and 8 A MOSFETs. But, instead of using smaller current rated MOSFETs, 50 A MOSFET was used in the original EOD-1 motor driver for the following reason. Let's calculate the power conversion efficiency from H-bridge to DC motors. Since only resistance consumes power, a power consumption calculation is somewhat simple.

$$\eta_{eff} = \frac{P_{out}}{P_{in}} = \frac{I^2 R_a}{I^2\left(2r_{DS(ON)} + R_a\right)} = \frac{R_a}{2r_{DS(ON)} + R_a} \qquad \text{(Eq.3.2)}$$

Where R_a is an armature resistance of DC motor.

Thus the power transfer efficiency of each H-bridge is following.

$$\eta_{eff\_3A} = \frac{R_a}{2r_{DS(ON)} + R_a} = \frac{2.4}{0.6 + 2.4} = 0.800$$

$$\eta_{eff\_50A} = \frac{R_a}{2r_{DS(ON)} + R_a} = \frac{2.4}{0.06 + 2.4} = 0.976 \qquad \text{(Eq.3.3)}$$

As one can notice from Eq.3.3, the power efficiency of 3A rated MOSFET has 80 % while the 50 A rated MOSFET has 97.6 % efficiency. This is a significant improvement especially motor driver is spending more than 70 % of whole EOD battery power. This is a saving of 12.3 % of overall battery power improvement. Also notice that the power transfer efficiency is independent of armature current. Thus above argument of whether calculating a stall current at 24 V or 12 V is justified. Only change for a normal run mode will be overall improvement of the power transfer efficiency for both 3 A H-bridge and 50 A H-bridge. This can be explained easily by $r_{DS(ON)}$. The above $r_{DS(ON)}$ is a typical resistance at their maximum current. When the load current of MOSFET lowers, the $r_{DS(ON)}$ also become smaller. This can be seen easily from MOSFET current equation. On the triode region the current-voltage curve is not linear, but rather square-root proportional. Thus the drain-source resistance, $r_{DS(ON)}$, become smaller as the source current become smaller. Therefore using MTP50N05 was a good choice since it improved the power efficiency. Thus it also requires a smaller heat sink compare to 3A rated drivers which can significantly save space and weight. Also when the 3A driver operates at higher temperature than the 50A driver, the power transfer efficiency becomes even worse because of increasing $r_{DS(ON)}$ exponentially. In the worse case condition, the 3A rated driver has a potential to be permanently damaged by thermal-runaway. For EOD-2 the power transfer efficiency for the 3A rated driver is 94.6 %. The 50A driver would have had 99.4 %, but the 50A rated driver was not designed for the EOD-2 motor, anyhow. The 3A rated driver has a good efficiency, and well suitable for the EOD-2 motors. Figure 3.2.3 shows the old motor driver circuit while Figure 3.2.4 shows the new motor driver circuit. LMD 18200 is a single chip H-bridge pack with 3A rating. This package is used to reduce number components in the new circuit.

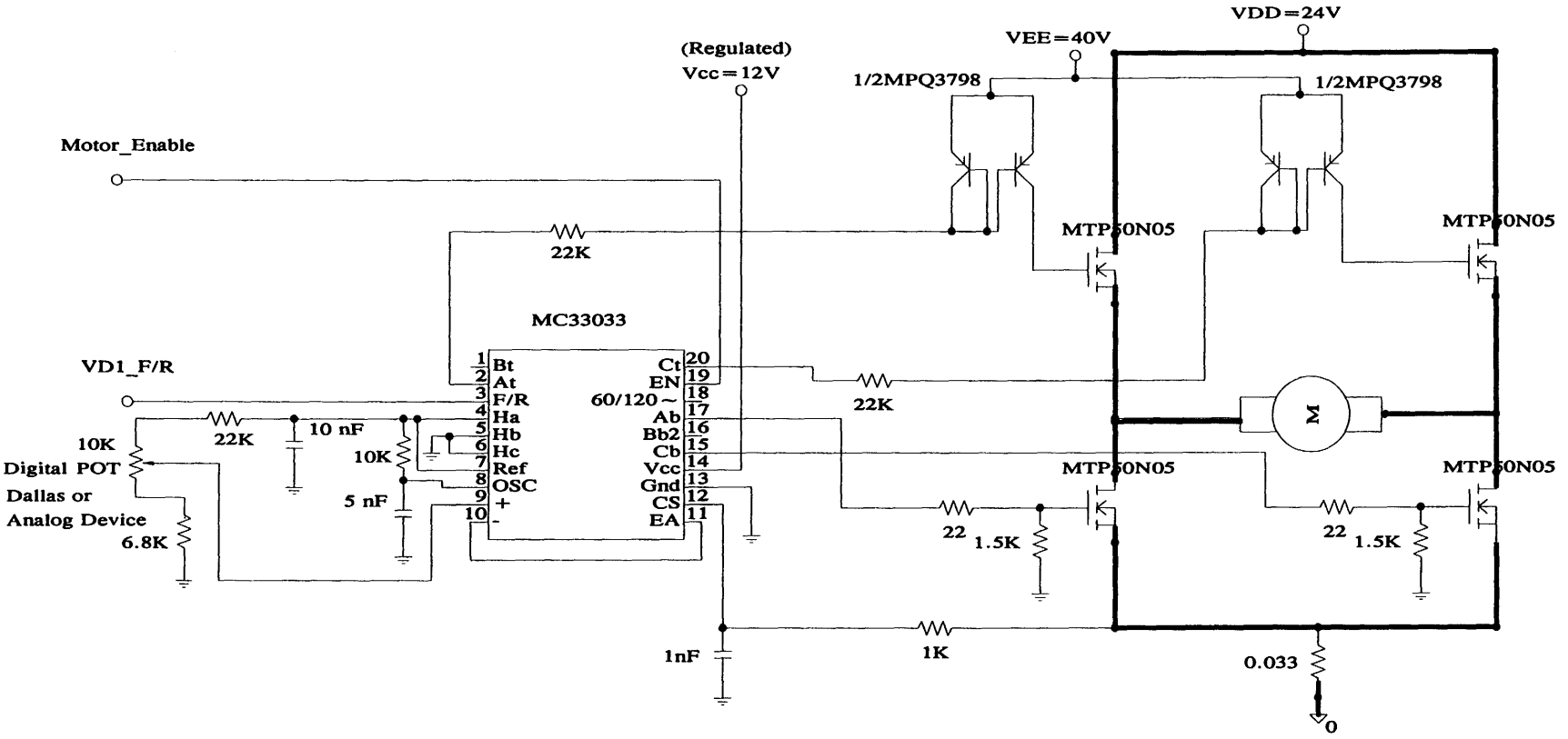

Figure 3.2.3. The original EOD-1 motor control circuit

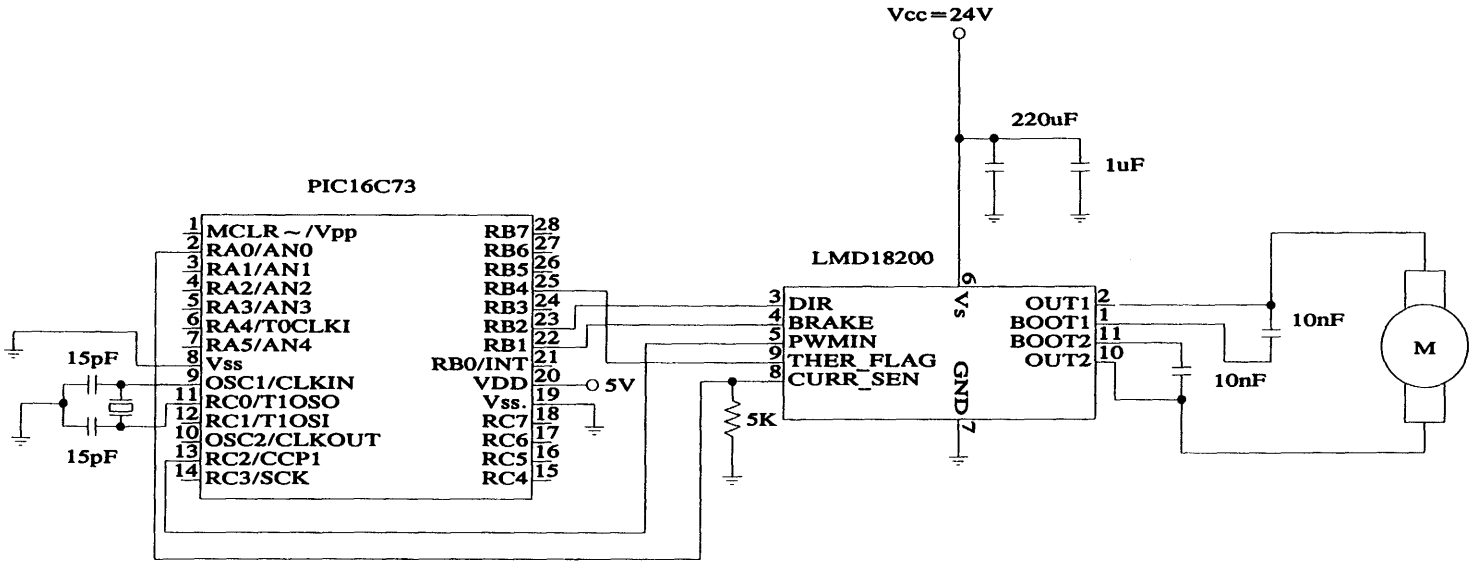

Figure 3.2.4. The new EOD-2 motor control circuit

But it is still desirable to be able to find a 5A rated H-bridge chip. Another possibility is to increase the nominal battery voltage from 24 V to 36 V or 48 V. This way a DC motor with same output power will be 2/3 or 1/2 of the current of 24V motor. Most of MOSFET can handle up to 50 to 60V which has still same range of $r_{DS(ON)}$. If the voltage rating rate of MOSFET rise to 100 V, then $r_{DS(ON)}$ increases up to 3 to 10 Ω.

Figure 3.2.3. shows a conventional H-bridge control circuit. In fact this circuit is already simplified considerable by employing MC33033, a Brussels DC motor controller chip. This MC33033 has several built in features that simplify PWM generation, motor current limit, thermal protection, direction bit, and motor enable, but flexible enough to customize ones design for specific applications. However this was not enough to build 10 controllers in a 4x5 circuit board, which gave us no choice but to use a simple LMD 18245, fully integrated motor driver chip. But this chip could been good for a smaller motor with no real feedback speed control. Lack of output resolution, which is only 4 bits, is a serious problem with several different speed mode control design.

The new motor control circuit solves problems by using a 8 bit microprocessor, PIC16C73, to control the H-bridge. Output voltage can be again used in a PWM format, but it is not necessary to do so. Sliding mode control uses a switching output with no variable output voltage. The controller itself calculate the output in a switching form, which eliminates PWM of a continuous control voltage. This way there is no need for PWM generation by either calculation by 8 bit microprocessor or dedicated PWM chips. Already the control output from is in a very convenient form, such a system that does not need a PWM generator nor a DA converter. This is a significant improvement in performance, simplicity and robustness of the motor controller area. In addition, many sliding mode controller applied in motor controller dose not employ a simple switching control law if the controller must be a servo system. When the controller is a servo system, the sliding mode controller tends to be a fast switching plus a nominal time varying servo command. If the output of the sliding mode controller is in such a form, it is impossible using a simple switching law. That kind of sliding mode controller requires a class AB output stage to be able to vary output voltage and a fast switching capability. A new sliding mode controller used in Chapter 5 is a pure switching output even though it is a servo controller.

3.3. Sonar Sensors

When the EOD vehicles are navigating to the destination along its path, it must be able to detect an obstacle. The EOD vehicle must know its obstacles in the unknown terrain condition to navigate. There are many techniques available to detect an obstacle. Radar could be a very good solution as far as obstacle detection is concerned, but a radiowave radar is too big and expensive for this particular vehicle. If the vehicle were a size of a regular passenger car with high price tag, then the radiowave radar would been a very good choice. Instead a small, inexpensive and simple sonar radar is a good alternative. For a simple obstacle detection, a sonar circuit detects a reflected sonar signal fired by a ultrasonic transducer and measure the time traveled. Then distance from the vehicle to the obstacle can be calculated. It is possible to measure the reflected sonar signal, and, by using a usual signal condition, distance, size and speed of the obstacle can be

determined. But, for the EOD vehicle's simple obstacle detection avoidance algorithm, only distance of the obstacle from the vehicle is need.

This sonar sensors are composed of three parts: Polaroid ultrasonic transducers, the range board and timing & control circuit. Polaroid ultrasonic transducers are the same unit used in Polaroid cameras. The range board is a pre-assembled and introduced in "Electronics Now" September 1993 issue. This range board does firing the ultrasonic transducers and set a flag when the reflected sonar signal is detected. Timing & control board control the firing sequence, measure the time traveled, and interface data to the main processor board, Zilog.

Theory of operation is simple. Three Polaroid sonar transducers are mounted in the front of the EOD-2. These transducers are pitched up a little where anything that is higher than the sonar path will be determined as obstacles. Each transducers have 20 ° of beam angle so that three sonar transducers are angled 20 ° to each other. This gives a frontal obstacle sweep angle of 60 °. Firing sequence and control of the range board is done by the timing & control board. Data collected is then transferred to the main processor for its navigation and obstacle avoidance algorithm. Figure 3.3.1. shows the firing sequence of the sonar sensor.

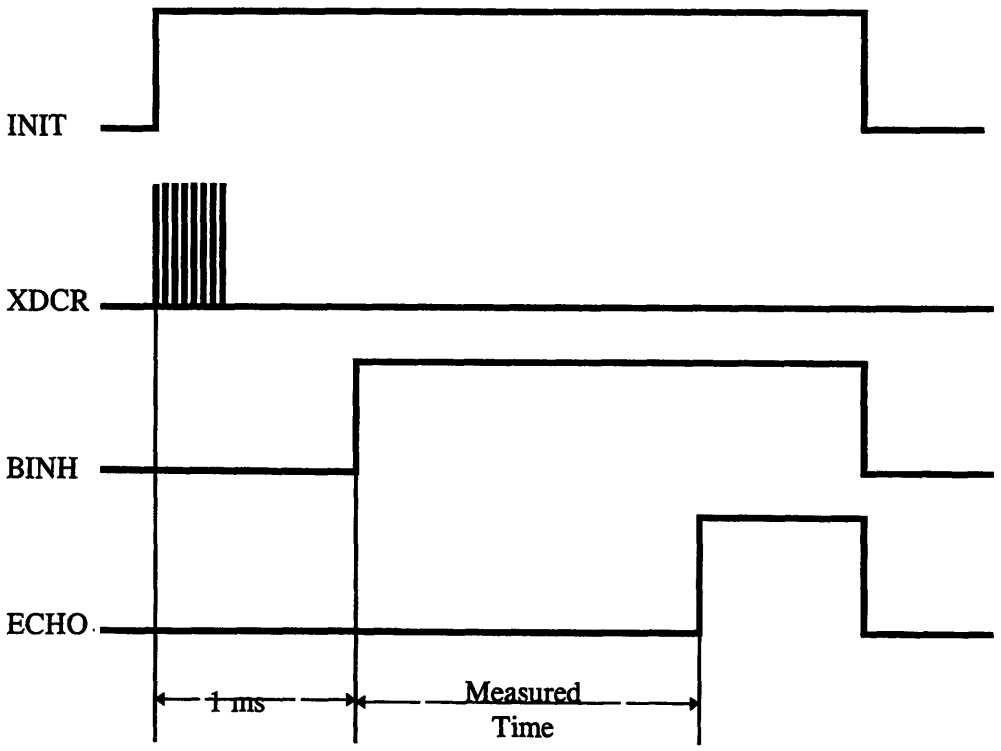

Fi ure 3.3.1. Timing diagram of the range board[1]

When the timing board sets INIT high, then the range board fires the sonar transducer. Then the timing board sets BINH high to let the range board starts its receiving mode

[1] Courtesy of Electronics Now, September 1993

for an echo. This sequence should be done 1 ms after INIT goes high to allow the pulse transmission and for the transducer to settle down. When an echo is detected by the range board, the ECHO goes high. Then the time traveled is measured and thus distance can be calculated by the following formula.

$$d = \frac{t}{2} \cdot (340 + 0.6 \cdot \Delta T) \qquad \text{(Eq.3.4)}$$

Where d is distance in meters, $t = 0.001 +$ measured time in seconds and $\Delta T = (15 -$ ambient temperature) in Celsius.

The timing board is consist of PIC16C61 microprocessor embedded in STAMP™-II microprocessor board, signal delay circuit for 1 ms time delay and MM54HC595 8-bit shift register for parallel data output. STAMP™-II microprocessor board is a convenient PIC16C61 power board and has a own BASIC program language. However for future design it is better to use the PIC assembly instead of STAMP™-II BASIC to solve some problems and have more reliable operation. The PIC assembly code will also make interface to main processor easy. Figure 3.3.2. shows a schematic of the timing & control board for three sonar transducers and 8-bit parallel data output.

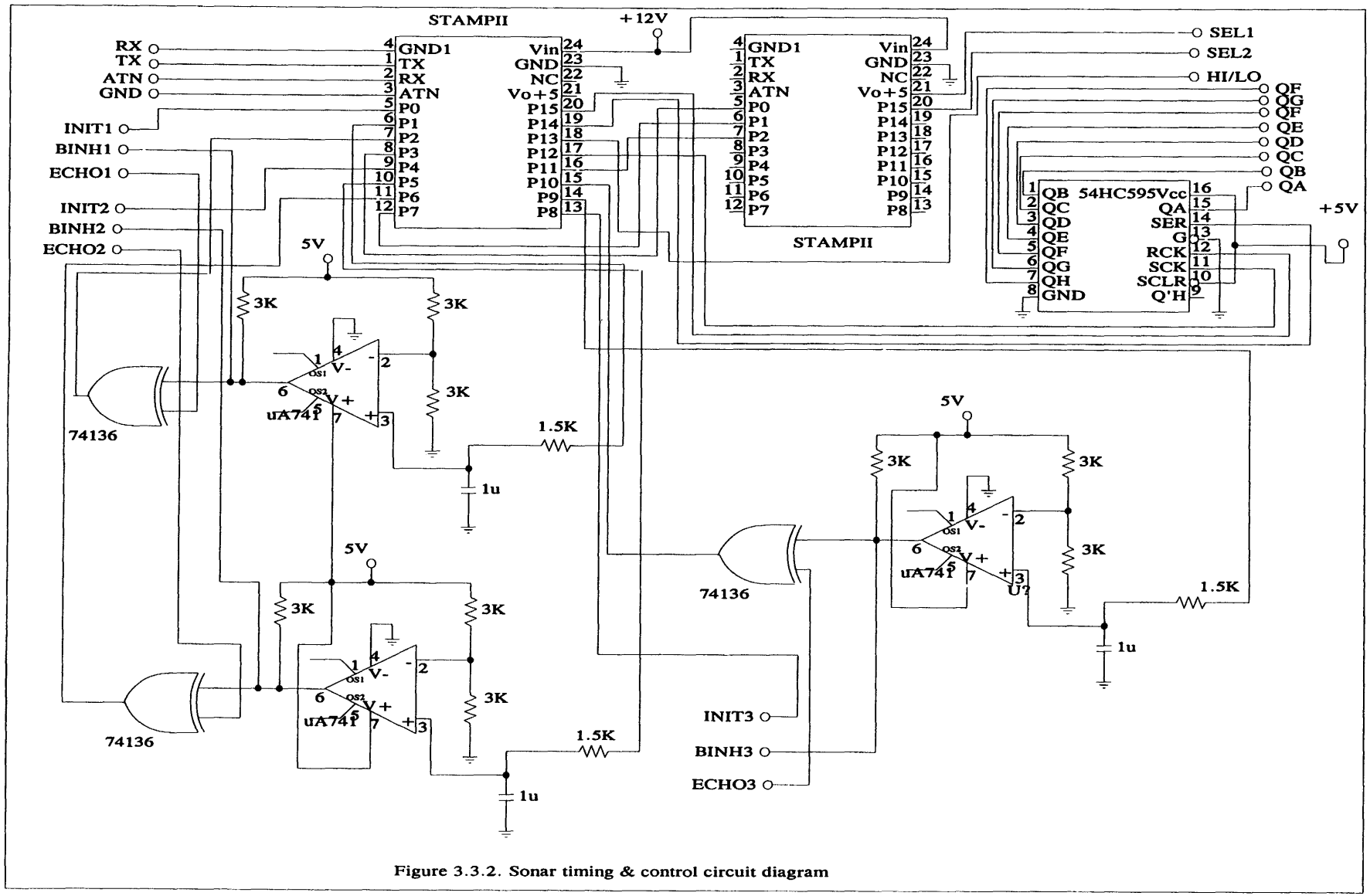

Figure 3.3.2. Sonar timing & control circuit diagram

3.4. Laser Positionin System (LPS)

For the EOD vehicle navigation, an absolute positioning system is required beside INS. Differential GPS is a good candidate but it still does has limitation like accuracy degradation under fast differential GPS antenna movement and weak signal on a cloudy day. LPS is a tracker as its alias implies, a laser positioning system. The LPS consists of two laser beacons (a.k.a. STROABS) and one or more transponders, and the system is supposed to track the transponders, i.e. give the positions of the transponders relative to the beacons.

The two beacons contain laser diodes (beacon1 has one laser and beacon2 has two lasers). The beacons are positioned a distance apart. An operation range is from 10 to 200 feet. The lasers in each beacon sweep around in a circle. Each beacons contain a sensor to detect a laser hit. Using this sensor, the angular velocity of beacon2 is to be synchronized with beacon1.

The system operates in the following manner. A cycle begins when beacon2 detects a laser hit. This causes five clocks (r, r2, xy1, xy2 and z) on board a remote computer to be activated. When beacon2 detects another hit, clock r is stopped. Hence, r measures the time required for beacon1's laser to go one full revolution. Clock r2 is stopped when beacon1 detects a laser hit. Hence r2 measures the phase lag of the leading beacon2 laser. The clocks xy1, xy2 and z2 are stopped each time the transponder detects a laser hit. Notice that the transponder cannot distinguish between the lasers from beacon1 and beacon2. Also, if the system contains more than one transponder, there are multiple xy1, xy2 and z clocks. Base on the geometry of the system, the order of the hits is known. Using the times r, r2, xy1 and xy2, the position of the transponder can be computed. Figure 3.4.1. shows a geometry of the system.

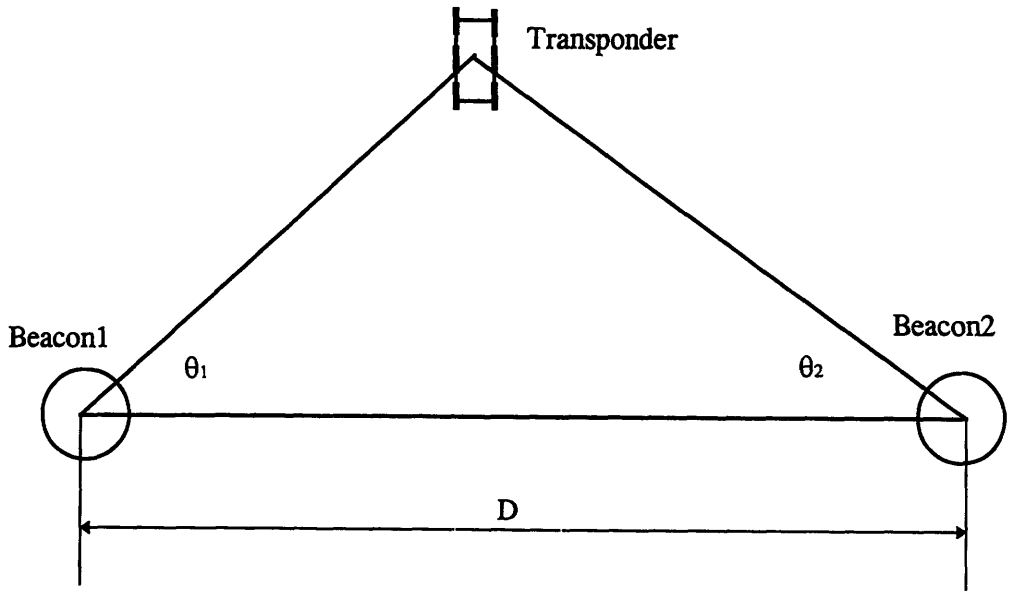

Fi ure 3.4.1. LPS geometrical configuration.

This LPS was provided by MTI© system with significant engineering design faults. Provided electronics were not properly functioning to successfully track transponders. There were three major design faults.

First, beacon2 must be synchronized to beacon1 with a small phase lag angle. This phase angle value can be anywhere in between 30 to 60 degrees, but the phase angle must be stable once it is fixed at certain angle. A simple PLL is employed in the beacon synchronization, but its stabilization range is too narrow to synchronize. In fact beacon2 fails to synchronized to beacon1 for most of time. After several painful trial beacon2 finally synchronizes if one is very lucky. When a line of sight between two beacon is blocked for a short period of time, beacon2 is already asynchronized. This is a major design flaw. Thus to solve this problem, a new synchronization circuit must be designed and implemented. The design of such circuit has been done and its hardware is completed. Simulation of the new synchronization circuit is done in Chapter 6. Actual 8-bit microprocessor assembly programming has yet to be completed.

Second, the transponder's radio communication system was not reliable. A CB frequency are used with a 6 transistor superheterodyne AM transmitter and receiver. A CB frequency in between 27 MHz to 30 MHz is extremely busy range, which caused a problem for outdoor operations. The best way to eliminates this interference is to get a frequency allocation from FCC, but it is still limited in locations and the process takes more than 1 to 2 years. Alternative was to use a better AM CB receiver. A 6 transistor superheterodyne AM receiver did not have high Q number and squelching mode. A armature HAM radio receiver, which is very popular and accessible from market, is a good alternative for high Q number receiver. This essentially solved communication linkage problem. Since the receiver is in the ground station, size of the receiver is not much bounded as in the transmitter. Also the transmitter in the EOD vehicle is adequate for the proper operation. Its output power is 300 mW which is powerful enough to operate within the EOD operation site.

Third, the choice of synchronization beacon was poor engineering decision. Beacon1 is a free spinning laser while beacon2 is a synchronization laser. Fact is the spinning inertia of beacon2 is much larger than one in beacon1. And both beacon motors were powered by same power source without each individual power regulation. This mean when the power supply voltage is 12 V, then beacon1 laser is spinning with smaller load than beacon2's load. To be able to control beacon2 to synchronize free spinning beacon1, beacon2 must have more control authority. The original setup by MTI was opposite. The controlled beacon2 had a heavier load than beacon1's and beacon1 and beacon2 uses same voltage to power motors. To solve this problem, the supply voltage should be regulated separately. Now the beacon1 is regulated by LM2931CT, low voltage drop-out variable regulator. The regulated voltage is set to 8 V from 12 V power source. Then beacon2 is regulated to 9 V. This is a current setup for LPS and seems to be best voltage level for the current PLL circuit to synchronize. This will soon be changed due to addition of the new synchronization circuit. The new synchronization circuit will use 12 V and will not be regulated to lower voltage. A LQR control or its variation will be implemented, and its design and computer simulation will be shown in Chapter 5 and 6, respectably. Figure 3.4.2. shows the low drop-out voltage regulator circuit and Figure 3.4.3. shows the new synchronization circuit.

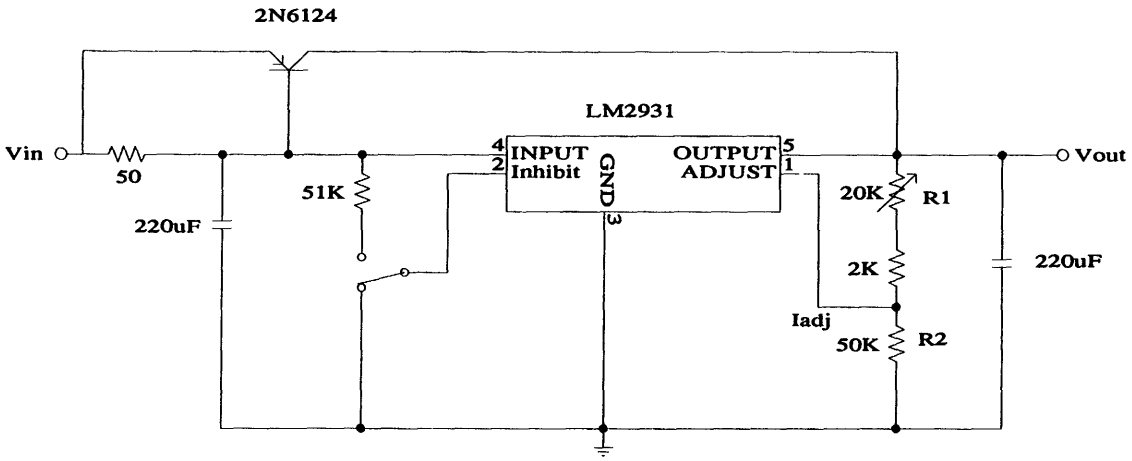

Vour = Vref(1 + R2/R1) + IadjR2 Iadj = 0.2uA (Typical)

Figure 3.4.2. Low drop-out 3A voltage regulator

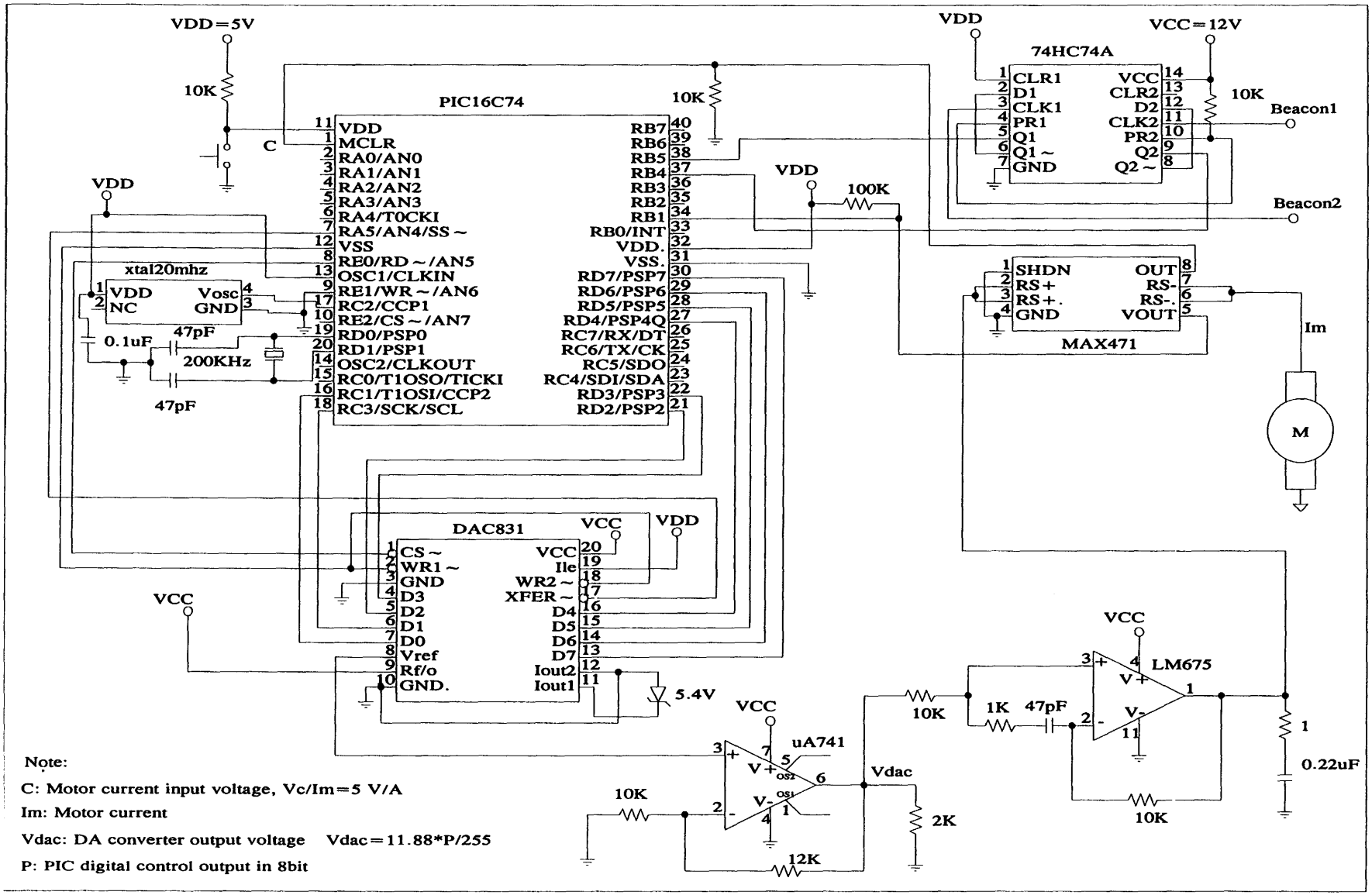

Figure 3.4.3. New synchronization circuit

Note that the new synchronization circuit is using an operational amplifier, LM675, for motor control. Unlike the EOD-2 motor driver circuit, this LPS is not a mobile system. Once positions of beacons are set up, each beacons are fixed during the EOD operation. Thus a size of synchronization circuit is not as important as in one of the EOD motor driver circuit. The synchronization circuit in Figure 3.4.3. gives flexibility of implementing almost any kind of control algorithm. This would serve as an interesting test bed for many different motor control algorithm. If more power is required, LM12, 80W operational amplifier, can substitute LM675 in the above circuit. However it makes me wonder now that why this synchronization circuit is needed if the simpler EOD motor control circuit get the job done with sliding mode control. Only one reason in my mind justifies reason of the LPS synchronization circuit being different from the EOD motor control circuit. The LPS synchronization circuit is more flexible to implement different control algorithm when sliding mode control fails to control.

3.5. Gyro Low Pass Filter/Anti-Aliasin Circuit

A micro-mechanical gyro is used to estimate an EOD vehicle heading angle. By integrating the gyro output, angle estimation can be derived. Integration is done by a local microprocessor and AD converter. Since the output of the gyro is sampled, it is a good idea to use an anti-aliasing filter. Also it can change estimation performance which will be discussed in more detail in Chapter 4.3. Eq.3.5 shows a desired transfer function of the LPS/anti-aliasing filter.

$$T(S) = \frac{10\pi}{S + 10\pi} \qquad \text{(Eq.3.5)}$$

This filter can be implemented by an RC network. A passive RC network is not desirable since the output impedance is too high for an AD converter. Usually more than 10 KΩ source resistance will cause a problem in most AD converter. Therefore an active LPF is more desirable since its output impedance is nearly 0.1 Ω or less. Figure 3.5.1. shows an active LPF/anti-aliasing filter.

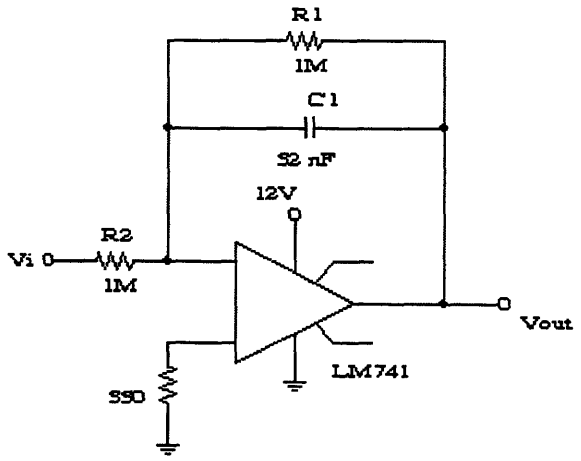

Fi ure 3.5.1. LPF/anti-aliasing filter for AD converter

CHAPTER 4

Mathematical Modeling of EOD Vehicle Dynamics

For system analysis and control, a mathematical model of system is a basis and starting point. In other words, modeling of the system is essential for a system analysis, controller deign and simulation. Also each design stage may not necessarily use a same model. For instance a linear model can be used to design a controller, and a nonlinear model with noise can be used in simulation and verification of the controller. There exist many results in linear control theory, so it is advantageous to use a linear model for controller design. Any system is hardly linear, but it is possible to linearize the system around its nominal trajectory. Once a linear controller is designed, a nonlinear model can be used to verify and simulate the whole system with the linear controller. One can also to design a nonlinear controller based on a Lyapunov function, but it is harder to analyze and design a controller and whole system. Many nonlinear control theories have been developed, but most of them are still based upon a Lyapunov function method. Depend on a situation, a nonlinear controller could be more advantageous than a linear controller. It is controller engineer's responsibility to be able to choose an optimum controller based on case by case. Thus providing a linear and nonlinear model of system is important in control and analysis.

4.1. Models of Motor, Gear and Wheels

A modeling of a DC motor is very common and important in practical situation. A complete model of a DC motor has been available in academia for a long time, but in an industry it has been hardly used in controller design. Main reason was complete trust on a PID controller in industries. In many industrial practices, no model of DC motor nor system is used to design a controller. In most of DC motor control design, a PID controller with unknown parameters is actually implemented and parameters of a PID are tweaked until the response of the DC motor is satisfactory in some degree. This was most common practice, and actually it is still practiced among industries. But it is not a efficient way to design an optimum controller. Many cases response of system can be improved significantly. In addition a control force can be reduced to achieve a similar or better system response. Also in our EOD vehicle case, it is more desirable to predict and design a controller using a computer simulation than actually to build a controller and tweak control gains until a speed and position of the EOD is acceptable.

Since a six-wheeled vehicle has been proven to be most maneuverable in rough terrain, the EOD vehicle is also a six-wheeled vehicle with three separate platforms connected with two flexible steel wires. Also most of the time, the reference command is a position command with a fixed speed. This implies that the reference command will be a first order polynomial. Since the EOD vehicle will operate in rough terrain, each motors are controlled independently. This will give more flexibility in operation. i.e. A rock can block only the left front wheel while other wheels are at flat surface, and the left front wheel needs more torque than others. Thus six DC motors are required for the drivers.

The DC brush motor used for a drive motor has 15 atts of output. (or 25 atts with adequate cooling). Also its gear ratio is 25:1. Desired maximum velocity of the vehicle on a flat surface is 1.5 m/s. A gear train has a dynamics, but for all practical purpose it is assumed to have friction force, damping force and inertial force which leads to a second order linear dynamics. A backlash is ignored in controller design as it mentioned in Chapter 3.1. Drive Motor and Gear. A backlash of the gear is less than 2.5 degrees or equivalently less than 0.0436 rad. This is also equal to 3.32 mm in translation motion. But a backlash will be included in a simulation and verification of the controller. Figure 4.1.1. shows a drawing of an internal system of DC motor without load.

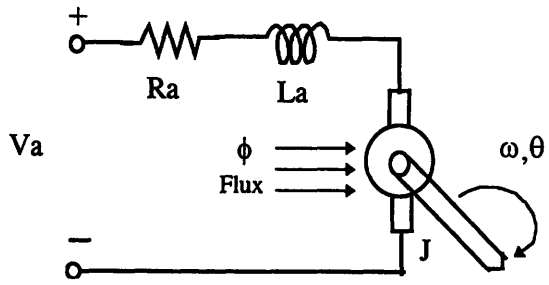

Figure 4.1.1. DC motor with a load

First a block diagram of a DC motor without a load will be derived. Then a gear and load will be modeled. A load has two different mode which are a wheel without slipping and a wheel with slipping.

An armature dynamics is determined by a simple Kirchoff's law.

$$V_a(t) = i_a(t)R_a + L_a \frac{di_a(t)}{dt} + V_{bemf}(\omega(t)) \qquad \text{(Eq.4.1)}$$

here V_{bemf} is a back electro motive force and linear function of $\omega(t)$. This back EMF limits a torque applied at a higher speed.

$$V_{bemf}(t) = K_{emf} \cdot \omega(t) \qquad \text{(Eq.4.2)}$$

Where K_{bemf} is a back EMF constant of the DC motor.

The motor torque $\tau_m(t)$ is linearl proportional to a armature current, $i_a(t)$. It is assumed that the motor torque is related linearl to the air-gap flux, ϕ.

$$\tau_m(t) = K_\tau i_a(t) \qquad \text{(Eq.4.3)}$$

Also the motor torque $\tau_m(t)$ is equal to the load torque of the motor, $\tau_L(t)$, and the disturbance torque, $\tau_d(t)$.

$$\tau_m(t) = \tau_L(t) + \tau_d(t) \qquad \text{(Eq.4.4)}$$

The disturbance torque is composed of internal and external forces such as gravit gradient force in a hill, small obstacles i.e. rocks, and so on. Thus the disturbance torque is unknown b its nature, but sometimes it is possible a least to predict its waveform. The load torque for rotating mass is written as

$$\tau_L(t) = J\frac{d^2\theta(t)}{dt^2} + f\frac{d\theta(t)}{dt} + \tau_f \qquad \text{(Eq.4.5)}$$

Where,

J = Armature Inertia +Load Inertia

f = Rotational Damping Friction Coefficient

τ_f = Rotational Frictional Torque

Therefore if Eq.4.2, 4.3, 4.4 and 4.5 are substituted in Eq.4.1, the load angle, $\theta(t)$, is a function of the armature voltage, $V_a(t)$. Or equivalentl a block diagram can be obtained. Take Laplace transformations of Eq. 4.1, 4.2, 4.3, 4.4 and 4.5 then the armature voltage, $V_a(s^1)$, is a function of the armature current, $I_a(s)$.

$$V_a(s) = (R_a + L_a s)I_a(s) + V_{bemf}(s) \qquad \text{(Eq.4.6)}$$

Then the armature current is

$$I_a(s) = \frac{V_a(s) - K_{bemf}s\theta(s)}{R_a + L_a s} \qquad \text{(Eq.4.7)}$$

And the load torque, $\tau_L(s)$, is

$$\tau_L(s) = Js^2\theta(s) + fs\theta(s) + \tau_f = \tau_m(s) - \tau_d(s) \qquad \text{(Eq.4.8)}$$

Figure 4.1.2. shows a block diagram of a DC motor with a rotational load. A gear and wheel on the ground require more complicated model which will be derived later.

[1] "s" is a Laplace operator.

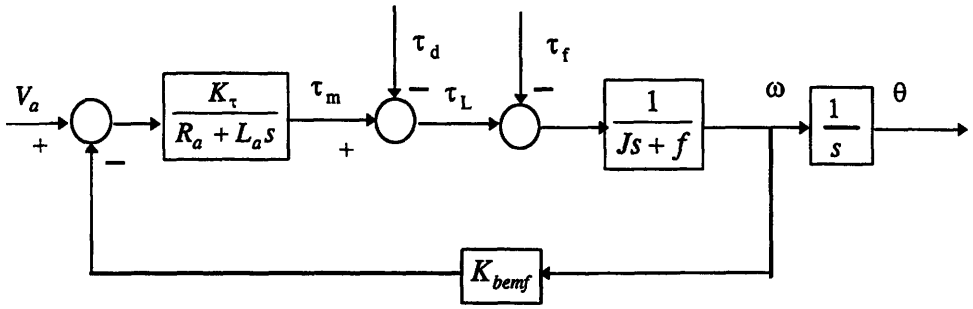

Figure 4.1.2. Block diagram of an armature controlled DC motor

From the above block diagram, the transfer function of $\theta(s)/V_a(s)$ is obtained.

$$\frac{\theta(s)}{V_a(s)} = \frac{K_\tau}{s\left[(R_a + L_a s)(Js + f) + K_{bemf}K_\tau\right]} \qquad \text{(Eq.4.9)}$$

However, the armature time constant, $\tau_a = L_a / R_a$, is much faster than other eigen-modes for many DC motors, thus the armature time constant is negligible for practical simulation. But the armature time constant is still important for a direct P M control and sliding mode control. For a simulation and verification of sliding mode control, the armature time constant must be included.

Notice that K_τ is equal to K_{bemf}. This equality may be shown by considering the steady state motor operation and the power balance when the rotor resistance is neglected. The power input to the rotor is $K_{bemf}\omega i_a$ and the power delivered to shaft is $\tau\omega$. In the steady state condition, the power input is equal to the power delivered to the shaft. Thus $K_{bemf}\omega i_a = \tau\omega = K_\tau i_a \omega$, which implies that $K_{bemf} = K_\tau$.

Now let's consider a gear and a wheel load. For simplicity assume a gear head with a simple gear ratio, n, and a frictional torque loss. Of course a rotational damping coefficient exists, but it can be absorbed in a motor damping coefficient, *f*. Same goes to the gear moment of inertia. A wheel on the ground has a different effect on a load dynamics. Figure 4.1.3. shows a free body diagram of a wheel on the ground with and without slipping. hen the wheel is slipping, frictional force, F, becomes a constant kinetic frictional force. It is expected that the mass of vehicle is directly related to the wheel load dynamics, but it is acting differently based on the wheel slipping condition. By definition, the wheel is not slipping when the contact point of the wheel and ground has a same velocity which means the contact point has zero velocity in a local earth gravitational inertial frame. In this paper, a local earth inertial frame is assumed rather than an absolute frame. Thus it is implying that Newton's law apply in this local inertial frame. An observer on the surface of the earth cannot be an inertial frame since the sum of all accelerations and gravitational attractions are not zero. In the other words, the acceleration is not transformed away. However general relativity admits local inertial frame, where the laws of physics apply in a local region. This local earth inertial frame is assumed in deriving all dynamic equations in this paper with exception of Inertial Navigation System (INS).

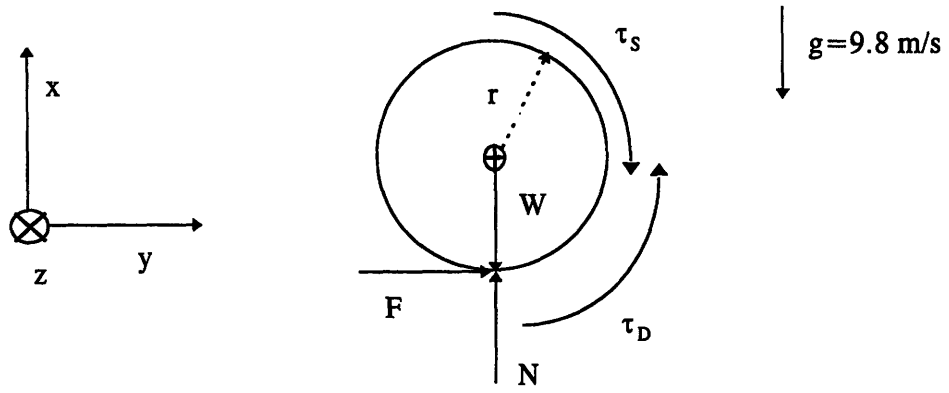

Figure 4.1.3. Free body diagram of a wheel on the ground

First let's assume the wheel is rotating without slipping. A moment of inertia of the wheel is Jw. A mass of one wheel is mw, and a mass of a platform without wheels is mp. Let's define $m_L = m_W + 1/2 \cdot m_P$.

$$\sum_X | \quad N - m_L g = 0 \qquad \text{(Eq.4.10)}$$

$$\sum_y | \quad F = m_L \ddot{y} \qquad \text{(Eq.4.11)}$$

$$\ddot{y} = r\ddot{\theta}_L \qquad \text{(Eq.4.12)}$$

$$\sum_M | \quad \tau_S - \tau_D - Fr = J_W \ddot{\theta}_L + f_W \dot{\theta}_L \qquad \text{(Eq.4.13)}$$

Where r is a radius of the wheel. Since the wheel is not slipping, Eq.4.12 can be used. Thus F can be solved and is substituted in Eq.4.13. Also notice that τ_S is a torque applied to a load shaft after a gearhead. A shaft torque is amplified by the gearhead and a simple model of a gearhead can derive an equation between the motor torque, τ_m, and the shaft torque, τ_S. Since a gearhead is used, an inter disturbance and external disturbance will have different effect directly related to the gear ratio, n. Following derivation ignores an internal disturbance, thus $\tau_m = \tau_L$, $\tau_d = 0$.

$$\tau_m = J\ddot{\theta} + f\dot{\theta} + \tau_f + \tau_x \qquad \text{(Eq.4.14)}$$

$$n\tau_x = (J_W + m_L r^2)\ddot{\theta}_L + f_W \dot{\theta}_L + \tau_D \qquad \text{(Eq.4.15)}$$

$$\theta = n\theta_L \qquad \text{(Eq.4.16)}$$

Then if Eq.4.15 and 4.16 is substituted to Eq.4.14, a famous n^2 relationship appears.

$$\tau_m = (J + \frac{1}{n^2}(J_W + m_L r^2))\ddot{\theta} + (f + \frac{f_W}{n^2})\dot{\theta} + \tau_f + \frac{\tau_D}{n} \qquad \text{(Eq.4.17)}$$

hen the wheel is rotating with slipping, a kinetic friction will replace a static friction. But a static friction is not a constant function and is a direct function of an angular velocity. On the other hand, a kinetic friction is not a function of an angular velocity and a constant assuming a constant kinetic friction coefficient and a normal force. Thus a translation velocity is not directly proportional to an angular velocity. Thus if the wheel is rotating with slipping, sums of forces and torques are following.

$$\sum_x | \quad N - m_L g = 0 \qquad \text{(Eq.4.18)}$$

$$\sum_y | \quad F = \mu_k N \qquad \text{(Eq.4.19)}$$

$$\sum M | \quad \tau_S - \tau_D - Fr = J_W \ddot{\theta}_L + f_W \dot{\theta}_L \qquad \text{(Eq.4.20)}$$

Thus a kinetic friction, F, is a just a constant force assuming a constant μ_k and N. hen the EOD is operating on rough terrain, μ_k and N will change. But μ_k and N are not known and/or predictable in real time. Eq.4.21 shows a motor torque as a function of θ.

$$\tau_m = (J + \frac{J_W}{n^2})\ddot{\theta} + (f + \frac{f_W}{n^2})\dot{\theta} + \tau_f + \frac{1}{n}(\tau_D + \mu_k m_L g r) \qquad \text{(Eq.4.21)}$$

From above equations, Math Flow Diagrams (MFD) are obtained. Figure 4.1.3. shows a MFD of a wheel without slipping. Also Figure 4.1.4. shows a MFD of a wheel with slipping.

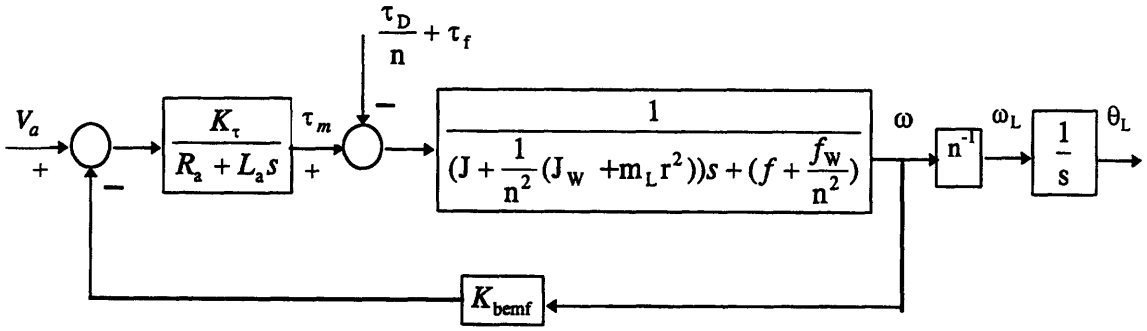

Figure 4.1.3. MFD of a wheel without slipping

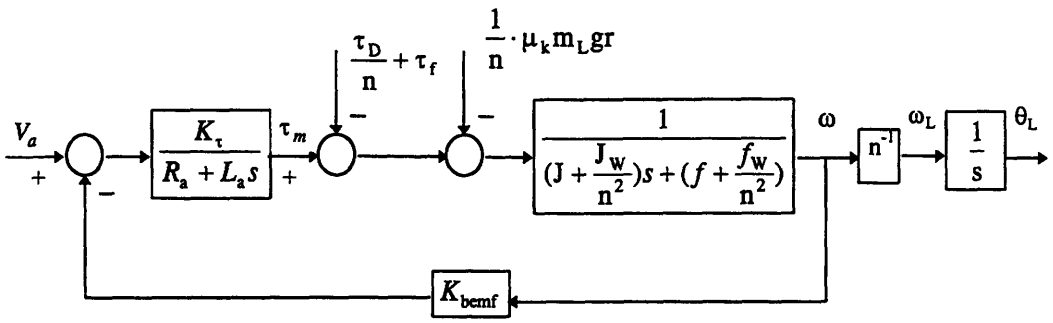

Figure 4.1.4. MFD of a wheel with slipping

A kinetic frictional torque is a constant while a static friction torque is a direct function of a translation acceleration assuming μ_k and N are constant. When the EOD vehicle is operating on rough terrain, a kinetic friction coefficient, μ_k, a normal force, N, will change due to change of terrain conditions. When the EOD vehicle is climbing a normal force, N, is reduced with proportional to $\sin(\theta_{slope})$. A wheel starts to slip when an applied torque to a wheel is exceeding a maximum static friction. A more accurate description is in Eq.4.22 for a wheel on the ground.

$$\text{Slipping if } \tau_S - \tau_D - J_W\ddot{\theta}_L - f_W\dot{\theta}_L \geq Fr \qquad \text{(Eq.4.22)}$$

Table 4.1.1. shows some coefficients of friction on different materials. Most of time a kinetic friction coefficient is smaller than a static frictional coefficient for a same material.

Materials	μ_s	μ_k
Steel on steel	0.74	0.57
Aluminum on steel	0.61	0.47
Copper on steel	0.53	0.36
Rubber on concrete	1.0	0.8
Wood on wood	0.25-0.5	0.2
Glass on glass	0.94	0.4
Waxed wood on wet snow	0.14	0.1
Waxed wood on dr snow	-	0.04
Metal on metal (lubricated)	0.15	0.06
Ice on ice	0.1	0.03
Teflon on Teflon	0.04	0.04
S novial joints in humans	0.01	0.003

Table 4.1.1. Coefficients of Friction[1]

[1] All values are approximate. Ra mond A. Serwa , "Ph sics for Scientist & Engineers," Third edition, HBJ, 1990.

From Figure 4.1.3. and 4.1.4. MFD, state variable representation can be derived. Define $x_1 = \theta_L$, $x_2 = \omega$, $x_3 = \tau_m$. Also measured outputs are load angle and angular velocity. The motor torque, τ_m, can be indirectly measured by measuring the armature current. As mentioned earlier, a measurement of an armature current by Kelvin mirror current is linear at room temperature, but is nonlinear at higher operating temperature. Eq.4.23 shows a state variable matrix for a motor dynamics with a no slipping wheel.

$$\begin{bmatrix} \dot{x}_1 \\ \dot{x}_2 \\ \dot{x}_3 \end{bmatrix} = \begin{bmatrix} 0 & n^{-1} & 0 \\ 0 & -\dfrac{n^2 f + f_W}{n^2 J + J_W + m_L r} & \dfrac{n^2}{n^2 J + J_W + m_L r} \\ 0 & -\dfrac{K_\tau K_{bemf}}{L_a} & -\dfrac{R_a}{L_a} \end{bmatrix} \begin{bmatrix} x_1 \\ x_2 \\ x_3 \end{bmatrix} + \begin{bmatrix} 0 \\ 0 \\ \dfrac{K_\tau}{L_a} \end{bmatrix} [V_a] + \begin{bmatrix} 0 \\ \dfrac{n^2}{n^2 J + J_W + m_L r} \\ 0 \end{bmatrix} \left[\tau_f + \frac{\tau_D}{n} \right]$$

$$y = \begin{bmatrix} 1 & 0 & 0 \end{bmatrix} \begin{bmatrix} x_1 \\ x_2 \\ x_3 \end{bmatrix} \qquad \text{(Eq.4.23)}$$

Now form Figure 4.1.4., a state variable representation of a motor dynamics with a slipping wheel. Eq.4.24 shows a state variable matrix for a motor dynamics with a slipping wheel.

$$\begin{bmatrix} \dot{x}_1 \\ \dot{x}_2 \\ \dot{x}_3 \end{bmatrix} = \begin{bmatrix} 0 & n^{-1} & 0 \\ 0 & -\dfrac{n^2 f + f_W}{n^2 J + J_W} & \dfrac{n^2}{n^2 J + J_W} \\ 0 & -\dfrac{K_\tau K_{bemf}}{L_a} & -\dfrac{R_a}{L_a} \end{bmatrix} \begin{bmatrix} x_1 \\ x_2 \\ x_3 \end{bmatrix} + \begin{bmatrix} 0 \\ 0 \\ \dfrac{K_\tau}{L_a} \end{bmatrix} [V_a] + \begin{bmatrix} 0 \\ \dfrac{n^2}{n^2 J + J_W} \\ 0 \end{bmatrix} \left[\tau_f + \frac{\tau_D}{n} + \frac{\mu_k m_L g r}{n} \right]$$

$$y = \begin{bmatrix} 1 & 0 & 0 \end{bmatrix} \begin{bmatrix} x_1 \\ x_2 \\ x_3 \end{bmatrix} \qquad \text{(Eq.4.24)}$$

4.2. Models of Three Platform Dynamics

EOD vehicle has three separated platforms which are connected by two steel wires. That means, three platforms could have rocking motion due to separate control of 6 wheels. The rocking motion can be eliminated (or reduced substantially) by studying the vehicle dynamics and design an overall controller. The reason that two steel wires are used to connect each platforms is to provide flexibility and maneuverability in

rough terrain. Following figures show the advantage of using 6 wheeled vehicle connected by steel wires.

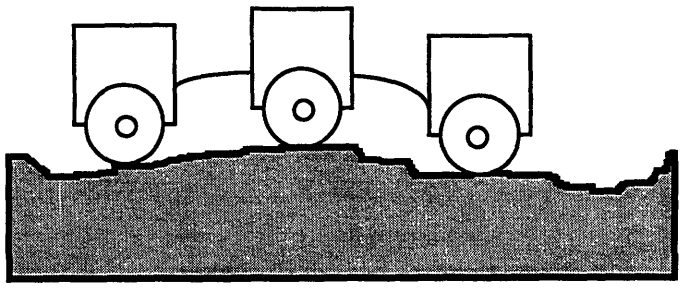

(a)

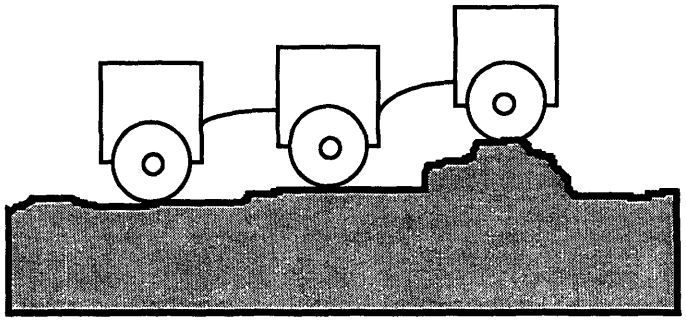

(b)

Figure 4.2.1. Flexible three platforms add advantage in maneuvering on rough terrain

But when its wheels are controlled locally with same desired velocity, the EOD vehicle started rocking motion while it is traveling. If the rear wheel try to go faster than the middle wheel, then two steel wires bend instead just pushing the middle platform. Then the middle platform gained its speed while the rear wheel slows down. Once those connecting wires are straight, then same process repeats provided the vehicle is still in transient mode. Unfortunately when the vehicle travels slow with a low resolution in the control voltage, the above rocking motion is preventing the vehicle to travel in a steady speed. Thus a constant rocking motion continues on instead of dying out. One possible solution is to use stiffer wires to reduce the undesired rocking motion. But stiffer wires provide less flexibility, which was the main reason using flexible wires instead of rigid beams. Also we can shorten wires, but some minimum distance required to preventing each platforms are not heating to each other during rocking motion. It may be possible to find a optimal wire gage and length, but the current settings for the wire gage and length are pretty much optimized. A better solution is to make sure the front wheel spins faster than the middle wheel and the middle wheel spins faster the rear wheel during a transient. This can be done by different bandwidth

filters for desired speed reference on each platforms. hen the vehicle is accelerating the front platform has a highest bandwidth reference input filter. On the other hand, if the vehicle is decelerating, the front platform has a lowest bandwidth reference input filter. Bandwidths of each input filter are design parameters and could be determined roughly from the modeled vehicle dynamics.

Main purpose of controller design is to have a virtual stiff compression spring constant while the flexibility of the wires provides a better mobility on rough terrain. A closed loop controller will be eventually designed, but how to measure the distance of the platform is remained as an open question. For the implementation an open loop control be implemented to solve the above problem, but a close loop controller will be much better for the performance. But a close loop control idea can be applied other similar problems with more room and budget to build a sensor (i.e. trains, multi-cargo trucks).

In modeling of two steel wires connecting platforms, it is assumed a steel wire obeys Hook's law. Since two wires are oriented in horizontal to the ground, even a small force applied to steel wires induce a buckling. In other words, a buckling load required for steel wires are relatively small thus will be assumed to be zero. In fact steel wires are already buckled. Thus a steel wire is modeled by a spring with two different region of spring coefficient. Figure 4.2.2. shows a steel wire with both ends fixed.

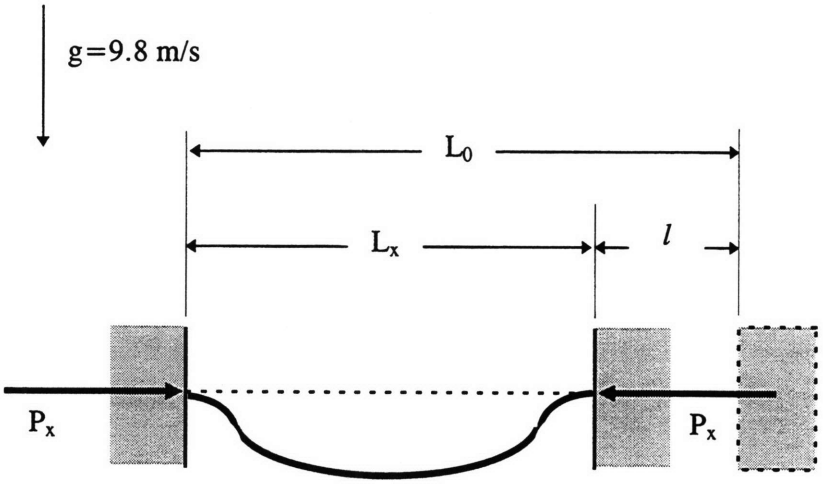

Figure 4.2.2. Fixed-fixed steel wire

here L_0 is a relaxed length when P_x is zero. The moment and vertical force do exist, but they are ignored due to a small effect on rocking motion of platforms. Vertical force do effect on the normal force of each platform, but it is small compare to a weight of each platform. This essentially leads to a =(n)/7Vspring obeying a Hook's law. Notice that a spring constant when it is stretched is much larger than one when it is compressed. It is very much possible to derive a spring constant when it is compressed but is much easier to actually measure it. hen steel wires are stretched, a same spring model is valid with a much higher spring constant, until it reaches a yield strength. Driver motors for the EOD vehicle does not have enough power to reach the yield

strength of the steel wire used. Thus Young's modulus, which is the slope of the stress-strain curve in elastic region, is applied.

$$E = \frac{\sigma}{\varepsilon} \qquad \text{(Eq.4.25)}$$

here E is a modulus of elasticity, or Young's modulus. Also σ is a engineering stress and ε is an engineering strain.

$$\sigma = \frac{P}{A_0} \qquad \text{(Eq.4.26)}$$

$$\varepsilon = \frac{l_x - l_0}{l_0} \qquad \text{(Eq.4.27)}$$

here P is an applied tension force, A_0 is the original cross-section area, l_x is the distance between the gage marks after force P is applied, and l_0 is the original distance between the gage marks. Therefore a steel wire can be modeled by a spring with two different spring constants for compression and tension regime. Eq.4.28 and Eq.4.29 are mathematical descriptions for a steel wire with above simplification.

$$F = \begin{cases} -k_1 l & \text{where } l < 0 \\ -k_2 l & \text{where } l > 0 \end{cases} \qquad \text{(Eq.4.28)}$$

here

$$k_1 = 122\ N/m$$

$$k_2 = \frac{A_0 E}{l_0} = \frac{\left(3.14 \times 10^{-6}\right)\left(2 \times 10^{11}\right)}{0.1} = 6.3 \times 10^6\ N/m \qquad \text{(Eq.4.29)}$$

F is a compression force which in same direction with an engineering stress σ and ε is a strain.

Now let's examine a dynamics of one platform assuming a force F as an arbitrary force. An interaction between platforms will be studied later. Each platforms are mounted on an outside shaft of wheels. Thus a platform cannot rotate about its mounting point as long as tires are not rotating on the ground and there is no tire deformation. But a tire deforms when a rotational torque is applied. A tire returns to an original shape when a rotational torque is removed. This is true for a elastic region of a tire material, and a tire will have a permanent deformation beyond a elastic region, i.e. plastic deformation region. If the tires are twisted into a plastic deformation region, those tires should be replaced which is not a desirable situation. But the EOD motor drivers do not have enough torsion power to push tires beyond a elastic region. Also a tire comes back to its original shape quickly which suggest an existence of a strong damping force. hile actual tire torsion dynamics is high order nonlinear dynamics, a simplification of dynamics to a linear first order is sufficient for all practical purpose.

It is assumed that a tire torsion dynamics can be modeled by a spring force and a damping force. A first order model will not exhibit an oscillatory damping motion which exists on a real tire dynamics. It is possible to model to a high order nonlinear dynamics, but it is not necessary to obtain a high fidelity model to approximate and study dynamics of this vehicle rocking motion which is not a dominant dynamics. It is just to study dynamic behavior and possible future problems for a bigger vehicle with more power.

Figure 4.2.3. on next page shows free body diagrams of a platform assuming a force F exerted by two steel wires as an arbitrary force. Eq.4.30 is a simplified mathematical equation of tire torsion dynamics.

$$M_t = -k_t\delta - f_t\dot{\delta} \qquad \text{(Eq.4.30)}$$

By summing a moment about a point P, a relationship of θ and F can be determined.

$$-2k_t\delta - 2f_t\dot{\delta} + F\frac{d_2}{\cos(\delta_0)}\cos(\delta_0 - \delta) + m_p g d_1 \sin(\delta) = J_P\ddot{\delta}$$

or

$$J_P\ddot{\delta} + 2f_t\dot{\delta} + 2k_t\delta - m_p g d_1 \sin(\delta) = Fd_2\frac{\cos(\delta_0 - \delta)}{\cos(\delta_0)} \qquad \text{(Eq.4.31)}$$

here J_P is a moment of inertia of a platform about a point P. Notice that for the real system M_t is a sum of two tire torsion torques, and F is a sum of force exerted by two steel wires. These compensation must be included to accommodate an actual platform's 3D shape and two wheels attached. Now the above equation is a second order nonlinear ODE. For a dynamic simulation, this Eq.4.31 simulates closer to an actual platform dynamics than a linealized second order ODE. Still a linealized second order ODE is useful for a simple system analysis and control. Since the deflected angle γ is small and the offset angle $\delta_0 = 1.2$, following assumptions can be made.

$$\sin(\delta) \cong \delta$$

$$\cos(\delta_0 - \delta) = \sin(\delta_0)\sin(\delta) + \cos(\delta_0)\cos(\delta) \cong \sin(\delta_0)(\delta) + \cos(\delta_0) \qquad \text{(Eq.4.32)}$$

The deflected angle δ will not exceed π/6 rad for above operation since two platform will hit to each other at the deflection angle δ of π/6 rad. In fact, this is the main reason studying the rocking motion to ensure each platforms not hitting to each other. Especially the middle and front platform are tall relative to their distance which they may hit to each other with a small angle deflection δ. Then a linearized second order ODE can be obtained. Notice that the error of $\cos(\delta_0 - \delta)$ at $\delta = \pi/6, \delta_0 = 1.2$ is 0.09.

$$J_P\ddot{\delta} + 2f_t\dot{\delta} + (2k_t - m_p g d_1)\delta = Fd_2\left(\frac{\sin(\delta_0)}{\cos(\delta_0)}(\delta) + 1\right) \qquad \text{(Eq.4.33)}$$

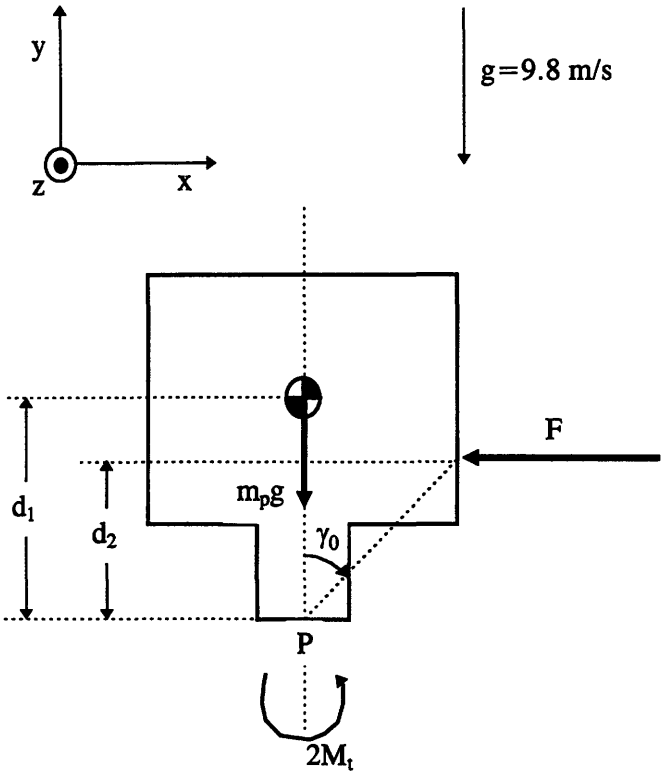

(a)

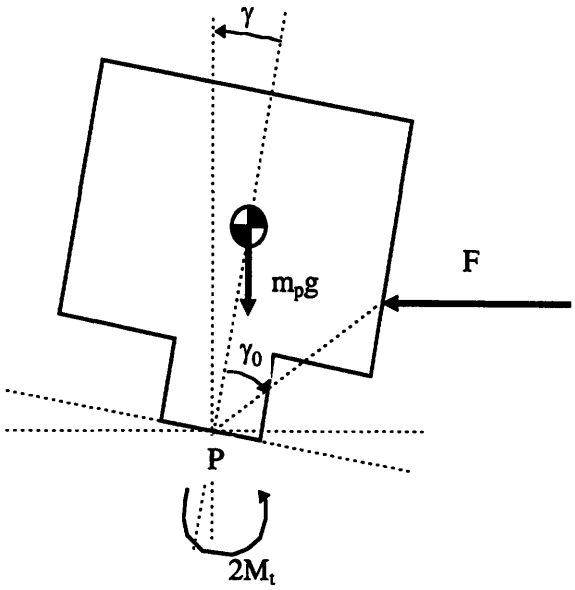

(b)

Figure 4.2.3. Free body diagrams of a platform

The rocking motion of platforms is also a first mode dynamics. A twisting motion in sideways does occur due to uneven terrain. But when one tire is in higher position than the other one in same platform due to an unknown rough terrain condition, there is very little left to do. This twisting motion is also stable and a second mode dynamics, thus it does not occur on a flat surface.

The compression force F applied by the two steel wires is a function of distance l and modeled as a spring with two different spring constant regimes. This distance l is also a function of motor torque τ_m. Since all three platforms are interconnected, a relationship of l and τ_m must be expressed with all three platform motor torques. Figure 4.2.4. shows a model of three platforms connected by two steel wires and applied motor torques.

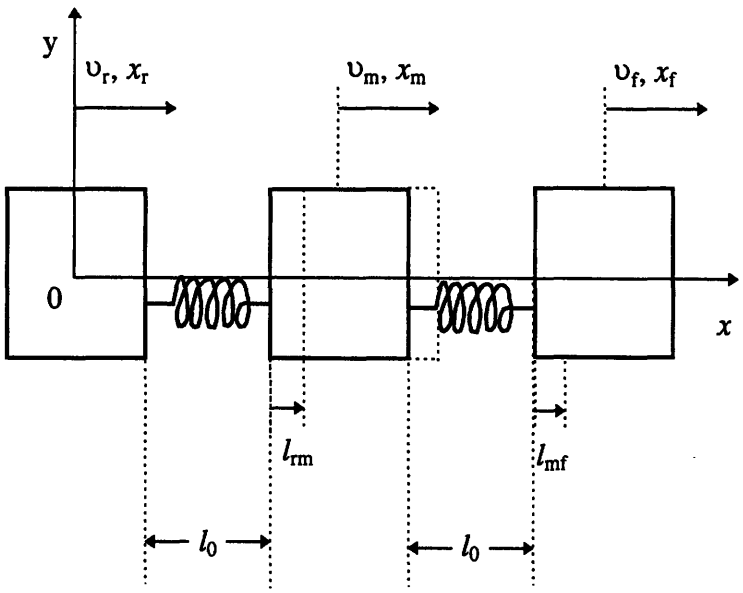

Figure 4.2.4. Model of three platforms connected by two steel wires

Translation velocities of each platforms are directly related to the derivatives of l_{rm} and l_{mf}. Let's assume the wheels are rotating without slipping. If the wheels are slipping, it is not controllable. It is intuitively obvious that no frictional force can be added to compress or stretch steel wires when wheels are slipping. Thus rocking motion of platforms is stable due to no applied force.

$$F_1 = -2kl_{rm} = -2k(x_m - x_r - l_0) \qquad \text{(Eq.4.34)}$$

$$F_2 = -2kl_{mf} = -2k(x_f - x_m - l_0) \qquad \text{(Eq.4.35)}$$

here l_0 is a nominal distance between platforms, and k is k_1 where $\varepsilon < 0$ and k_2 where $\varepsilon > 0$ from Eq.4.28. Finally the deflected angle δ can be related to a function of the motor torque τ_m or armature voltage V_a. Since the armature voltage V_a could be only ±24 V and 0 V, a continuous voltage cannot be implemented beside applying an

average voltage. Actually what is happening on averaging voltage is averaging an armature current which is a directly proportional to a motor torque τ_m.

Definition of variables. Each platforms shares same motor and wheel parameters except platform mass m_P and external disturbance τ_D. Front, middle and rear platform m_P and τ_D will be noted by f, m and r suffix, respectably. Let us define state variables of above systems.

$$x_1 = \delta_r, x_2 = \dot{\delta}_r, x_3 = \delta_m, x_4 = \dot{\delta}_m, x_5 = \delta_f, x_6 = \dot{\delta}_f$$

$$x_7 = \theta_{Lr}, x_8 = \omega_r, x_9 = \tau_{mt}, x_{10} = \theta_{Lm}, x_{11} = \omega_m, x_{12} = \tau_{mm}, x_{13} = \theta_{Lf}, x_{14} = \omega_f, x_{15} = \tau_{mf}$$

$$y_1 = \delta_r, y_2 = \delta_m, y_3 = \delta_f, y_4 = \theta_{Lr}, y_5 = \theta_{Lm}, y_6 = \theta_{Lf}$$

where r, m, f suffix refers rear, middle and front platforms.

For simplicity, left and right motors in a same platform have 50:50 weight distribution, thus both motors have virtually same responses for practical purpose. In reality each motor will be controlled independently which will provide better maneuverability on rough terrain. Eq.4.36 is a nonlinear dynamic system of the platforms with Eq.4.31 and $\gamma(t, V_a)$. Also Eq.4.37 is a linearized dynamic system of the platforms with Eq.4.33 and $\gamma(t, V_a)$.

$$\begin{bmatrix}\dot{x}_1\\ \dot{x}_2\\ \dot{x}_3\\ \dot{x}_4\\ \dot{x}_5\\ \dot{x}_6\end{bmatrix}=\begin{bmatrix} x_2 \\ \frac{1}{J_P}\left(-2k_t x_1-2f_t x_2+m_{pr}gd_{1r}\sin x_1-2kd_2\frac{\cos(\delta_0-x_1)}{\cos(\delta_0)}\left(r(x_{10}-x_7)-l_0\right)\right) \\ x_4 \\ \frac{1}{J_P}\left(-2k_t x_3-2f_t x_4+m_{pm}gd_{1m}\sin x_3-2kd_2\frac{\cos(\delta_0-x_3)}{\cos(\delta_0)}\left(r(x_{13}-2x_{10}+x_7)-l_0\right)\right) \\ x_6 \\ \frac{1}{J_P}\left(-2k_t x_5-2f_t x_6+m_{pf}gd_{1f}\sin x_5+2kd_2\frac{\cos(\delta_0-x_5)}{\cos(\delta_0)}\left(r(x_{13}-x_{10})-l_0\right)\right)\end{bmatrix}$$

$$\begin{bmatrix}\dot{x}_7\\ \dot{x}_8\\ \dot{x}_9\end{bmatrix}=\begin{bmatrix}0 & n^{-1} & 0\\ 0 & -\frac{n^2f+f_W}{n^2J+J_W+m_{Lr}r^2} & \frac{n^2}{n^2J+J_W+m_{Lr}r^2}\\ 0 & -\frac{K_\tau K_{bemf}}{L_a} & -\frac{R_a}{L_a}\end{bmatrix}\begin{bmatrix}x_7\\ x_8\\ x_9\end{bmatrix}+\begin{bmatrix}0\\ 0\\ \frac{K_\tau}{L_a}\end{bmatrix}\left[V_{ar}\right]+\begin{bmatrix}0\\ \frac{n^2}{n^2J+J_W+m_{Lr}r^2}\\ 0\end{bmatrix}\left[\tau_f+\frac{\tau_{Dr}}{n}\right]$$

$$\begin{bmatrix}\dot{x}_{10}\\ \dot{x}_{11}\\ \dot{x}_{12}\end{bmatrix}=\begin{bmatrix}0 & n^{-1} & 0\\ 0 & -\frac{n^2f+f_W}{n^2J+J_W+m_{Lm}r^2} & \frac{n^2}{n^2J+J_W+m_{Lm}r^2}\\ 0 & -\frac{K_\tau K_{bemf}}{L_a} & -\frac{R_a}{L_a}\end{bmatrix}\begin{bmatrix}x_{10}\\ x_{11}\\ x_{12}\end{bmatrix}+\begin{bmatrix}0\\ 0\\ \frac{K_\tau}{L_a}\end{bmatrix}\left[V_{am}\right]+\begin{bmatrix}0\\ \frac{n^2}{n^2J+J_W+m_{Lm}r^2}\\ 0\end{bmatrix}\left[\tau_f+\frac{\tau_{Dm}}{n}\right]$$

$$\begin{bmatrix}\dot{x}_{13}\\ \dot{x}_{14}\\ \dot{x}_{15}\end{bmatrix}=\begin{bmatrix}0 & n^{-1} & 0\\ 0 & -\frac{n^2f+f_W}{n^2J+J_W+m_{Lf}r^2} & \frac{n^2}{n^2J+J_W+m_{Lf}r^2}\\ 0 & -\frac{K_\tau K_{bemf}}{L_a} & -\frac{R_a}{L_a}\end{bmatrix}\begin{bmatrix}x_{13}\\ x_{14}\\ x_{15}\end{bmatrix}+\begin{bmatrix}0\\ 0\\ \frac{K_\tau}{L_a}\end{bmatrix}\left[V_{af}\right]+\begin{bmatrix}0\\ \frac{n^2}{n^2J+J_W+m_{Lf}r^2}\\ 0\end{bmatrix}\left[\tau_f+\frac{\tau_{Df}}{n}\right]$$

$$\begin{bmatrix}y_1\\ y_2\\ y_3\\ y_4\\ y_5\\ y_6\end{bmatrix}=\begin{bmatrix}x_1\\ x_3\\ x_5\\ x_7\\ x_{10}\\ x_{13}\end{bmatrix}$$

(Eq.4.36)

$$\begin{bmatrix}\dot{x}_1\\ \dot{x}_2\\ \dot{x}_3\\ \dot{x}_4\\ \dot{x}_5\\ \dot{x}_6\end{bmatrix}=\begin{bmatrix} x_2 \\ \frac{1}{J_P}\left((-2k_t+m_{pr}gd_{1r})x_1-2f_tx_2-2kd_2\left(\frac{\sin\delta_0}{\cos\delta_0}\cdot x_1+1\right)\left(r(x_{10}-x_7)-l_0\right)\right) \\ x_4 \\ \frac{1}{J_P}\left((-2k_t+m_{pm}gd_{1m})x_3-2f_tx_4-2kd_2\left(\frac{\sin\delta_0}{\cos\delta_0}\cdot x_3+1\right)\left(r(x_{13}-2x_{10}+x_7)-l_0\right)\right) \\ x_6 \\ \frac{1}{J_P}\left((-2k_t+m_{pf}gd_{1f})x_5-2f_tx_6+2kd_2\left(\frac{\sin\delta_0}{\cos\delta_0}\cdot x_5+1\right)\left(r(x_{13}-x_{10})-l_0\right)\right)\end{bmatrix}$$

$$\begin{bmatrix}\dot{x}_7\\ \dot{x}_8\\ \dot{x}_9\end{bmatrix}=\begin{bmatrix}0 & n^{-1} & 0\\ 0 & -\frac{n^2f+f_W}{n^2J+J_W+m_{Lr}r^2} & \frac{n^2}{n^2J+J_W+m_{Lr}r^2}\\ 0 & -\frac{K_\tau K_{bemf}}{L_a} & -\frac{R_a}{L_a}\end{bmatrix}\begin{bmatrix}x_7\\ x_8\\ x_9\end{bmatrix}+\begin{bmatrix}0\\ 0\\ \frac{K_\tau}{L_a}\end{bmatrix}[V_{ar}]+\begin{bmatrix}0\\ \frac{n^2}{n^2J+J_W+m_{Lr}r^2}\\ 0\end{bmatrix}\left[\tau_f+\frac{\tau_{Dr}}{n}\right]$$

$$\begin{bmatrix}\dot{x}_{10}\\ \dot{x}_{11}\\ \dot{x}_{12}\end{bmatrix}=\begin{bmatrix}0 & n^{-1} & 0\\ 0 & -\frac{n^2f+f_W}{n^2J+J_W+m_{Lm}r^2} & \frac{n^2}{n^2J+J_W+m_{Lm}r^2}\\ 0 & -\frac{K_\tau K_{bemf}}{L_a} & -\frac{R_a}{L_a}\end{bmatrix}\begin{bmatrix}x_{10}\\ x_{11}\\ x_{12}\end{bmatrix}+\begin{bmatrix}0\\ 0\\ \frac{K_\tau}{L_a}\end{bmatrix}[V_{am}]+\begin{bmatrix}0\\ \frac{n^2}{n^2J+J_W+m_{Lm}r^2}\\ 0\end{bmatrix}\left[\tau_f+\frac{\tau_{Dm}}{n}\right]$$

$$\begin{bmatrix}\dot{x}_{13}\\ \dot{x}_{14}\\ \dot{x}_{15}\end{bmatrix}=\begin{bmatrix}0 & n^{-1} & 0\\ 0 & -\frac{n^2f+f_W}{n^2J+J_W+m_{Lf}r^2} & \frac{n^2}{n^2J+J_W+m_{Lf}r^2}\\ 0 & -\frac{K_\tau K_{bemf}}{L_a} & -\frac{R_a}{L_a}\end{bmatrix}\begin{bmatrix}x_{13}\\ x_{14}\\ x_{15}\end{bmatrix}+\begin{bmatrix}0\\ 0\\ \frac{K_\tau}{L_a}\end{bmatrix}[V_{af}]+\begin{bmatrix}0\\ \frac{n^2}{n^2J+J_W+m_{Lf}r^2}\\ 0\end{bmatrix}\left[\tau_f+\frac{\tau_{Df}}{n}\right]$$

$$\begin{bmatrix}y_1\\ y_2\\ y_3\\ y_4\\ y_5\\ y_6\end{bmatrix}=\begin{bmatrix}x_1\\ x_3\\ x_5\\ x_7\\ x_{10}\\ x_{13}\end{bmatrix}$$

(Eq.4.37)

4.3. Model of a Single Axis Micro-mechanical Gyro

This mechanical gyro uses a vibrating quartz tuning fork instead of a spinning wheel to sense angular velocity. The use of a vibrating quartz tuning fork enables this gyro to be small, light, compact and reliable. ith minimum mechanical parts, minimum wear and power consumption could be achieved.

By the Coriolis effect, a rotational motion about the sensor's longitudinal axis produces an analog DC voltage proportional to the rate of rotation. Figure 4.3.1. shows a block diagram of the GyroChip™ II solid-state rate sensor.

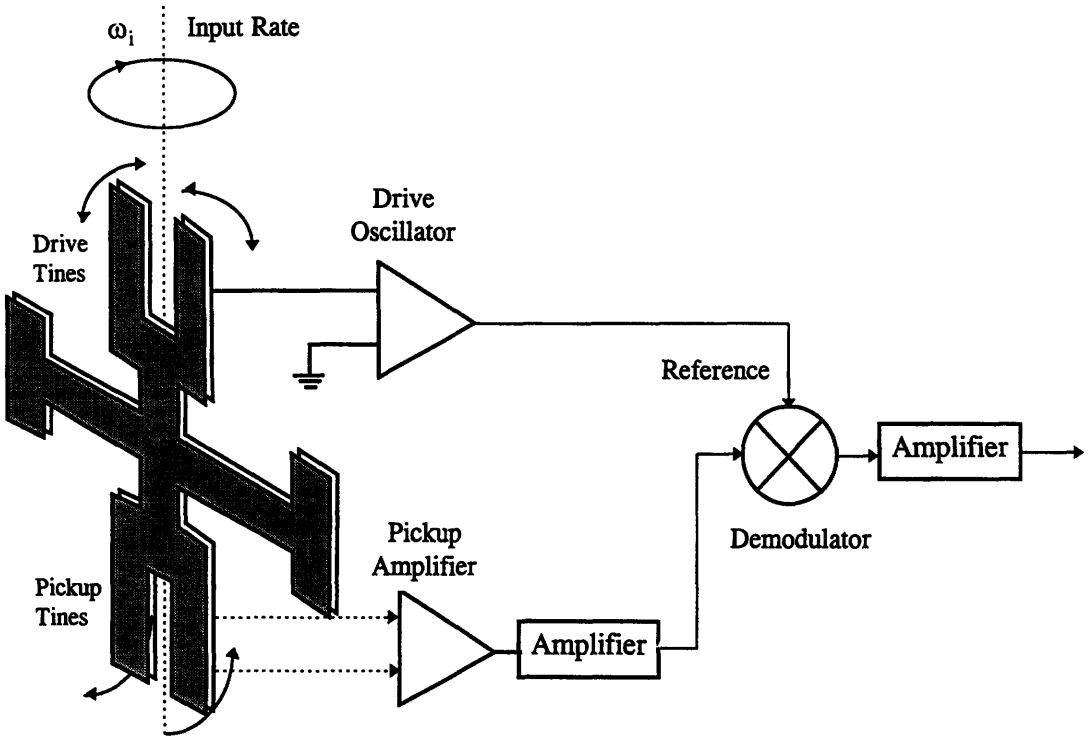

Figure 4.3.1.[1] Block diagram of the GyroChip™ II solid-state rate sensor.

Each tine have a Coriolis force acting on it. The two drive tines move in opposite directions, and the resultant forces are perpendicular to the plane of the fork assemble and in opposite directions. This produces a torque which is proportional to the input rotational rate. Since the radial velocity is sinusoidal, the torque produced is also sinusoidal at the same frequency and in-phase of the drive tines.

This gyro has a corner frequency at 50 Hz with a signal roll-off of -40 dB per decade with a natural sinusoidal tone in the region of 325 ±1 Hz which is due to the driver op-amp oscillation for the quartz element. The bandwidth is defined as a frequency, where -90 degree phase shift occurs, in the manufacture's specifications. It is not a 3dB point,

[1] Figure 4.3.1. is from GyroChip™ II Solid-State Rate Sensor Operational Manual.

but a knee or corner frequency. Therefore the gyro can be modeled as a second order system with some nonlinearities. Figure 4.3.2. shows a block diagram of the gyro.

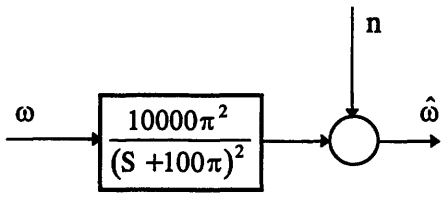

Figure 4.3.2. Block diagram of a linear gyro model

The noise n is composed of a first order Markov process and a sinusoid at 325 Hz. To model the noise n more in detail, the following specifications are necessary. Table 4.3.1. shows a detailed specifications of the gyro.

Performance	
Range	± 100 °/sec
Scale Factor(SF)	± 2 %
SF over Operating Temperature	< 4 % from Ambient
Bias	+2.5 ±0.045 VDC
Bias Stability	
Short Term (100 sec constant temp)	< 0.05 °/sec
Long Term (1 yr.)	< 1.0 °/sec
Linear Acceleration Sensitivity	< 0.06 °/sec/g
Over Operating Environments	< ± 3.0 °/sec
Linearity	< 0.05 % of Full Range
Output Noise (to 100 Hz)	< 0.05 °/sec/√Hz
Bandwidth (-90° phase shift at 50 Hz)	DC to 50 Hz
Resolution and Threshold	< 0.004 °/sec
Alignment (sensitive axis to mounting surface)	<1°
Start-Up Time	< 1.0 sec
Operating Life	> 5 Years
Operating Temperature	-40 °C to +85 °C
Storage Temperature	-55 °C to +100 °C
Operating Vibration (20 to 2000 Hz, Random)	4 g RMS
Survival Vibration (20 to 2000 Hz, Random)	10 g RMS
Shock-Survival (2ms, 1/2 sine)	200g

Table 4.3.1. Specifications of the gyro, GyroChip™ II

From Table 4.3.1. the maximum RMS noise of the device can be derived, and the noise is a first order Markov process with a corner frequency of 100 Hz and a white noise injection. Therefore a fictitious dynamics of noise can be derived and shown in Eq.4.37, and Eq.4.38 shows a composite state variable representations.

Let's define $\xi(t)$ as a unit intensity, zero mean white noise. The RMS values of noise is $\sigma_n = \sqrt{100\ \text{Hz}} \cdot 0.05\ °/\text{sec}/\sqrt{\text{Hz}} = 0.5\ °/\text{sec} = \frac{\pi}{360}\ \text{rad}/\text{sec}$. Then the noise process is

$$\begin{aligned}\dot{n}(t) &= -200\pi \cdot n(t) + 20\sqrt{\pi} \cdot \frac{\pi}{360}\xi(t) \\ &= -200\pi \cdot n(t) + \frac{\pi\sqrt{\pi}}{18}\xi(t)\end{aligned} \qquad \text{(Eq.4.38)}$$

Then the composite state variable equation can be derived.

$$\begin{bmatrix}\dot{x}_1(t)\\ \dot{x}_2(t)\\ \dot{x}_3(t)\end{bmatrix} = \begin{bmatrix}-100\pi & 1 & 0\\ 0 & -100\pi & 0\\ 0 & 0 & -200\pi\end{bmatrix} \cdot \begin{bmatrix}x_1(t)\\ x_2(t)\\ x_3(t)\end{bmatrix} + \begin{bmatrix}0\\ 100^2\pi^2\\ 0\end{bmatrix} \cdot \omega(t) + \begin{bmatrix}0\\ 0\\ \pi^{3/2}/18\end{bmatrix} \cdot \xi(t)$$

$$y(t) = \hat{\omega}(t) = \begin{bmatrix}1 & 0 & 1\end{bmatrix} \cdot \begin{bmatrix}x_1(t)\\ x_2(t)\\ x_3(t)\end{bmatrix} \qquad \text{(Eq.4.39)}$$

4.4. Model of Laser Positioning System (LPS)

This laser positioning device also employees a DC servo motor to spin a cylindrical mass in which a Laser Diode (LD) is mounted. The cylindrical mass is directly driven by a DC motor, thus a gear ratio is 1:1. A mathematical description is thus similar to one of driver wheel motors. Eq.4.40 describes the LPS motor system.

$$\begin{bmatrix}\dot{x}_1\\ \dot{x}_2\\ \dot{x}_3\end{bmatrix} = \begin{bmatrix}0 & \frac{1}{J_{LPS}} & \frac{0}{J_{LPS}}\\ 0 & -\frac{f_{LPS}}{J_{LPS}} & \frac{1}{J_{LPS}}\\ 0 & -\frac{K_\tau K_{bemf}}{L_a} & -\frac{R_a}{L_a}\end{bmatrix}\begin{bmatrix}x_1\\ x_2\\ x_3\end{bmatrix} + \begin{bmatrix}0\\ 0\\ \frac{K_\tau}{L_a}\end{bmatrix}\begin{bmatrix}V_a\end{bmatrix} + \begin{bmatrix}0\\ \tau_f\\ J_{LPS}\\ 0\end{bmatrix} \qquad \text{(Eq.4.40)}$$

$$\begin{bmatrix}y_1\\ y_2\end{bmatrix} = \begin{bmatrix}1 & 0 & 0\\ 0 & 1 & 0\end{bmatrix}\begin{bmatrix}x_1\\ x_2\\ x_3\end{bmatrix}$$

here $x_1(t) = \theta_L(t), x_2(t) = \omega_L(t), x_3(t) = V_a(t)$.

CHAPTER 5

Controller Design for the EOD Vehicle

There are many control theories that work well in theory, but some controllers do not work well in practical applications. Output measurements of a desired accuracy could be difficult under tight time and cost constraint. Or measurements of some outputs make a whole system more complicated and heavy. Also disturbances, a modeling uncertainty and a fast computing time requirement are another obstacles to implement a controller. Control input forms can also be restricted for simplicity or by the nature of control input. For the EOD vehicle, simplicity and robustness are very important attributes. Normally an operational amplifier armature voltage driver and a PWM motor driver are most common. But, in this chapter, a new motor driver circuit with H-bridge configurations will be cooperated with a sliding mode controller, which eliminates a need of heavy-duty op-amps and AD converters. The EOD vehicle has a unique six-wheeled configuration with three platforms connected by steel wires. This configuration helps the EOD vehicle to maneuver better on rough terrain. But it induces another interesting motion, a rocking motion of each platforms during a transient response. This rocking motion will also be studied, and a novel design of reducing the rocking motion will be introduced. Finally a filter design for the micro-mechanical gyro and a phase lock controller for the LPS are derived.

5.1. Sliding Mode Control of Motor Drivers

Variable Structure Control (VSC) was developed from Russia, and it is often called sliding mode control. In general, sliding mode control is a fast switching discontinuous control. Theoretically the switching frequency should be infinitely fast, but the switching frequency is bandwidth-limited. The switching input term can be switching between two fixed values or switching with continuously variable values. The following sliding mode controller is a simple switching control law with two fixed values. As mentioned in Chapter 3.2. Driver Motor Electronics, the control input can be $\pm$ 24 V or 0 V.

Sliding mode control is a robust nonlinear control and needs a simple actuator. Sliding mode control drive a nonlinear plant to the desired trajectory or surface, which is called the sliding surface. When the plant trajectory is not on the sliding surface, sliding mode control drives to the sliding surface and keep on the sliding surface there

after. To maintain the nonlinear plant trajectory on the sliding surface, the sliding condition should be met, that is guaranteed by a Lyapunov function of the sliding surface. For simplicity on the notations, a Single Input Single Output (SISO) system will be considered. A Multiple Input Multiple Output (MIMO) system has essentially same derivations.

Define $\varepsilon(t)$ is an output error, $\varepsilon(t) = y^*(t) - y(t)$, where $y^*(t)$ is a desired output and $y(t)$ is an output. Let's assume a system in the following state model.

$$\begin{aligned} \dot{x}(t) &= f(t, x) + B(t, x)u(t) + F(t,x)d(t) \\ y(t) &= C(t)x(t) \end{aligned} \qquad \text{(Eq.5.1)}$$

Where $x(t) \in R^n$, $u(t) \in R^1$, $f(t,x) = R^n$, $B(t,x) \in R^{n\times 1}$, $F(t,x) \in R^{n\times 1}$, $d(t) \in R^1$, and $C(t) \in R^{1\times n}$. An existence and uniqueness of the system require $f(t,x)$, $B(t,x)$ and $F(t,x)$ to be continuous with respect to t and x, and smooth with respect to x.

Assume Eq.5.1 is in a normal form with no internal dynamics without loss of generality. Thus $y(t) = x_1(t)$. Then sliding surface, $\sigma(t, x)$, can be defined in the following form.

$$\sigma(t,x) = \sum_{i=0}^{n-1} a_i \left(\frac{d}{dt}\right)^i \cdot \varepsilon(t,x) \qquad \text{(Eq.5.2)}$$

Where the sliding surface is a linear stable trajectory. Define the following Lyapunov function.

$$V(t,x) = \frac{1}{2}\sigma^2(t,x) \qquad \text{(Eq.5.3)}$$

Then if $V(t,x)$ is differentiated with respect to t, the control term u(t) appears.

$$\begin{aligned} \dot{V}(t,x) &= \sigma(t,x)\dot{\sigma}(t,x) \\ &= \sigma(t,x)\left[\sum_{i=0}^{n-2} a_i \left(\frac{d}{dt}\right)^{i+1} \left(y^*(t) - x_1(t)\right) + a_n \left(\frac{d}{dt}\right)^n \left(y^*(t) - x_1(t)\right)\right] \qquad \text{(Eq.5.4)} \\ &= \sigma(t,x)\left[\begin{array}{l} \sum_{i=0}^{n-2} a_i \left(\frac{d}{dt}\right)^{i+1} \left(y^*(t) - x_1(t)\right) + a_n \left(\frac{d}{dt}\right)^n \left(y^*(t)\right) \\ -a_n\left(f^{T<n>T}(t,x) + F^{T<n>T}(t,x)d(t)\right) - a_n B^{T<n>T} u(t) \end{array}\right] \end{aligned}$$

For simplicity, define $\Psi(t,x)$ as following.

$$\Psi(t,x) = \sum_{i=0}^{n-2} a_i \left(\frac{d}{dt}\right)^{i+1} \left(y^*(t) - x_1(t)\right) + a_n \left(\frac{d}{dt}\right)^n \left(y^*(t)\right) - a_n \left(f^{T<n>T}(t,x) + F^{T<n>T}(t,x)d(t)\right) \quad \text{(Eq.5.5)}$$

Then Eq.5.4 becomes

$$\begin{aligned} \dot{V}(t,x) &= \sigma(t,x)\dot{\sigma}(t,x) \\ &= \sigma(t,x)\left[\Psi(t,x) - a_n B^{T<n>T} u(t)\right] \end{aligned} \quad \text{(Eq.5.6)}$$

If the control u(t) is defined as following, $\dot{V}(t,x) < 0$.

$$u(t) = \frac{1}{a_n B^{T<n>T}} (\Psi(t,x) + \rho \cdot \text{sign}(\sigma(t,x))) \quad \text{(Eq.5.7)}$$

Then the Lyapunov function $\dot{V}(t,x)$ becomes

$$\begin{aligned} \dot{V}(t,x) &= \sigma(t,x) \cdot \left(-\rho \cdot \text{sign}(\sigma(t,x))\right) \\ &= -\rho \cdot \sigma(t,x) \cdot \text{sign}(\sigma(t,x)) \\ &= -\rho \cdot |\sigma(t,x)| \end{aligned} \quad \text{(Eq.5.8)}$$

Therefore the sliding surface $\sigma(t,x) \to 0$. Also this method is called a equivalent control method, and $u_{eq}(t,x) = \frac{\Psi(t,x)}{a_n B^{T<n>T}}$ is called the equivalent control. This control output is a switching law with a varying actuator input values. The EOD vehicle motor controller can only switch between ± 24 V. Thus another controller form is required to implement to the EOD vehicle. If the following conditions are met, then the pure switching control law can be derived.

1. $\left| u_{eq}(t,x) = \frac{\Psi(t,x)}{a_n B^{T<n>T}} \right| < U_m$, U_m is a constant. For motor driver, $U_m = 24$ V.
2. $|u_{eq}(t,x)| + \eta < U_m$ where $\eta > 0$.

Then $\dot{V}(t,x) < 0$ if $u(t,x) = U_m \cdot \text{sign}(\sigma(t,x))$. (Eq.5.9)

Notice that the reaching time for $\sigma(t,x) = 0$ is finite. The Lyapunov function can be used to find the reaching time.

For the equivalent control law, the sliding surface has the following dynamics.

$$\dot{V}(t,x) = -\rho \cdot |\sigma(t,x)| \quad \Rightarrow \quad \sigma(t,x)\dot{\sigma}(t,x) = -\rho \cdot |\sigma(t,x)|$$
$$\sigma(t,x) = \sigma(t_0,x_0) - \text{sign}(\sigma(t,x)) \cdot \rho t \qquad \text{(Eq.5.10)}$$

Therefore the reaching time t_{req} is

$$t_{req} = \frac{\sigma(t_0,x_0)}{\rho} \qquad \text{(Eq.5.11)}$$

Then for the sliding mode control in Eq.5.9 has the reaching time t_r of $t_r < \frac{\sigma(t_0,x_0)}{\eta}$.

Now the EOD motor controller can be designed as followings. The state model of the motor with a wheel load was derived in Eq.4.22. Let's rewrite the state model.

$$\begin{bmatrix} \dot{x}_1 \\ \dot{x}_2 \\ \dot{x}_3 \end{bmatrix} = \begin{bmatrix} 0 & n^{-1} & 0 \\ 0 & -\frac{n^2 f + f_W}{n^2 J + J_W + m_L r^2} & \frac{n^2}{n^2 J + J_W + m_L r^2} \\ 0 & -\frac{K_\tau K_{bemf}}{L_a} & -\frac{R_a}{L_a} \end{bmatrix} \begin{bmatrix} x_1 \\ x_2 \\ x_3 \end{bmatrix} + \begin{bmatrix} 0 \\ 0 \\ \frac{K_\tau}{L_a} \end{bmatrix} [V_a] + \begin{bmatrix} 0 \\ \frac{n^2}{n^2 J + J_W + m_L r^2} \\ 0 \end{bmatrix} \left[\tau_f + \frac{\tau_D}{n} \right]$$

$$y = \begin{bmatrix} 1 & 0 & 0 \end{bmatrix} \begin{bmatrix} x_1 \\ x_2 \\ x_3 \end{bmatrix} \qquad \text{(Eq.5.12)}$$

Above model is when the wheel is rotation on the ground without slipping. Let's define an error $\varepsilon(t) = y^*(t) - y(t) = \theta^*_L(t) - \theta_L(t)$. Then the sliding surface should be a second order dynamics. Define the sliding surface $\sigma(t,x)$.

$$\sigma(t,x) = \ddot{\varepsilon} + \alpha\dot{\varepsilon} + \beta\varepsilon = 0 \qquad \text{(Eq.5.13)}$$

Where $\alpha, \beta > 0$ which implying $\sigma(t,x) = \ddot{\varepsilon} + \alpha\dot{\varepsilon} + \beta\varepsilon = 0$ is stable. Choosing α,β is purely depend upon the specific application. If the armature voltage is high or the motor torque is very high, then the faster system response can be achieved. Same time if the disturbance is expected and significantly large, then by reducing the system response time the disturbance rejection can is achieved much better. For the EOD vehicle the disturbance torque is very much so expected due to rough terrain condition and hills. Thus a some amount of robustness is desired. This is an typical engineering trade-off problem, and the optimal performance of the EOD vehicle is very subjective. this can be viewed similarly in a linear control system. In a linear system, the gain margin decreases as the control gain increases, in general. A higher control gain means a faster response, but it could go unstable under some uncertainty.

If the Lyapunov function is defined as $V(t,x)=\frac{1}{2}\sigma^2(t,x)$, then $\dot{V}(t,x)$ is following. Define Eq.5.12 as following.

$$\dot{x} = Ax + BV_a + F\left(\tau_f + \frac{\tau_D}{n}\right) \qquad \text{(Eq.5.14)}$$

Then

Let's define an error $\varepsilon(t) = y^*(t) - y(t) = \theta^*_L(t) - \theta_L(t)$. (Eq.5.15)

Where

$$\begin{aligned}\Psi(t,x) = \dddot{y}^* + \alpha\ddot{y}^* + \beta\dot{y}^* + \left(-A_{12}A_{22}{}^2 - A_{12}A_{23}A_{32} + \alpha A_{12}A_{22} - \beta A_{12}\right)\cdot x_2 \\ +\left(A_{12}A_{22}A_{23} - A_{12}A_{23}A_{33} - \alpha A_{12}A_{23}\right)x_3 + \left(A_{12}A_{22}F_2 - \alpha A_{12}F_2\right)\cdot\left(\tau_f + \frac{\tau_D}{n}\right) \\ -A_{12}F_2\left(\dot{\tau}_f + \frac{\dot{\tau}_D}{n}\right)\end{aligned} \qquad \text{(Eq.5.16)}$$

ow $V_a(t)$ must meet the following sliding condition.

$$|\Psi(t,x)| = \left|\begin{aligned}&\dddot{y}^* + \alpha\ddot{y}^* + \beta\dot{y}^* + \left(-A_{12}A_{22}{}^2 - A_{12}A_{23}A_{32} + \alpha A_{12}A_{22} - \beta A_{12}\right)\cdot x_2 \\ &+\left(A_{12}A_{22}A_{23} - A_{12}A_{23}A_{33} - \alpha A_{12}A_{23}\right)x_3 \\ &+\left(A_{12}A_{22}F_2 - \alpha A_{12}F_2\right)\cdot\left(\tau_f + \frac{\tau_D}{n}\right) - A_{12}F_2\left(\dot{\tau}_f + \frac{\dot{\tau}_D}{n}\right)\end{aligned}\right| < A_{12}A_{23}B_3V_{amax} \qquad \text{(Eq5.17)}$$

Where $V_{amax} = +24$ V for the EOD vehicle.

Then the sliding mode control law follows.

$$V_a(t,x) = V_{amax}\cdot \text{sign}(\sigma(t,x)) \qquad \text{(Eq.5.18)}$$

Where

$$\begin{aligned}\sigma(t,x) &= \ddot{\varepsilon} + \alpha\dot{\varepsilon} + \beta\varepsilon \\ &= \dddot{y}^* + \alpha\ddot{y}^* + \beta\dot{y}^* - \beta\dot{x}_1 + \left(A_{12}A_{22} - \alpha A_{12}\right)\dot{x}_2 - A_{12}A_{23}\dot{x}_3 - A_{12}F_2\left(\dot{\tau}_f + \frac{\dot{\tau}_D}{n}\right)\end{aligned} \qquad \text{(Eq.5.19)}$$

otice that the sliding surface $\sigma(t,x)$ includes the disturbance torque τ_D. This disturbance torque τ_D would not appear in the sliding surface $\sigma(t,x)$, if the

disturbance torque τ_D enters to the system same way to the control input does. In other words, if B and F vectors were colinear, i.e. $R[F] \subseteq R[B]$, the disturbance term will not appear on the sliding surface. If $R[F] \subseteq R[B]$, then the disturbance can be canceled out perfectly if the disturbance can be estimated or measured.

The disturbance torque is not measurable, which is anyhow difficult to measure. If the disturbance torque were negligible due to the gear ratio, the calculation of the sliding surface can be done without measuring the disturbance. But if the EOD vehicle is on a hill, the disturbance is not negligible, which cause a problem on the sliding surface calculation. Two different solutions will be suggested to incorporate the disturbance issue. One method is to treat the motor torque as an input. The armature dynamics is much faster than the wheel dynamics in which the armature dynamics could be neglected. Nonetheless overall stability should be proved to ensure the stability of the inter-connected system. Second method is applying an estimation algorithm called disturbance accommodating control to estimate the disturbance in real time. This is an effective algorithm for known waveforms of disturbances.. Either a Lyapunov function or passivity of system can be used to analyze the overall stability.

5.2. Simplification of the Motor Dynamics: Fast Armature Dynamics

The armature dynamics of the EOD driver motor is much faster than the wheel dynamics. Time constant of the armature current is $L_a/R_a = 89.5\ \mu\text{sec}$ or 1.1170e4 Hz. The eigenvalues of Eq.5.12 are 0, -11.13 and -1.1160e4. The wheel dynamics has its natural frequency at 9.2251 Hz where the natural frequency of the armature current is 1.1161e4 Hz. This is a ratio of 1:1002 which can be easily neglected. Also notice that the back EMF of the angular velocity did not change much on the armature natural frequency, where the natural frequency without the back EMF is 1.1170e4 Hz, and the natural frequency with the back EMF is 1.1160e4 Hz. Therefore the armature dynamics will be neglected without changing the original dynamics significantly. Figure 5.2.1. shows the simplified motor dynamics.

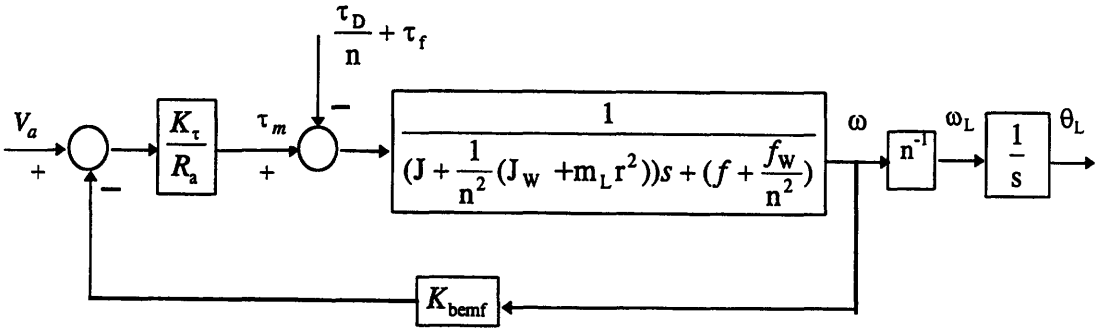

Figure 5.2.1. Simplified motor dynamics: motor torque is considered as a control input Then the simplified state model can be derived and the motor torque is a control input.

$$\begin{bmatrix}\dot{x}_1\\ \dot{x}_2\end{bmatrix}=\begin{bmatrix}0 & n^{-1}\\ 0 & -\dfrac{n^2 f+f_W}{n^2J+J_W+m_L r^2}\end{bmatrix}\begin{bmatrix}x_1\\ x_2\end{bmatrix}+\begin{bmatrix}0\\ \dfrac{n^2}{n^2J+J_W+m_L r^2}\end{bmatrix}\begin{bmatrix}\tau_m\end{bmatrix}+\begin{bmatrix}0\\ \dfrac{-n^2}{n^2J+J_W+m_L r^2}\end{bmatrix}\begin{bmatrix}\tau_f+\dfrac{\tau_D}{n}\end{bmatrix}$$

$$y=\begin{bmatrix}1 & 0\end{bmatrix}\begin{bmatrix}x_1\\ x_2\end{bmatrix} \qquad \text{(Eq.5.20)}$$

Where the control input is the motor torque which can be determined by the following algebraic relationship. otice that the motor angular velocity x_2 is treated as a constant for the following equation. This was justified in the previous page by the small impact of the back E F on the armature current dynamics.

$$\tau_m(t)=\frac{K_\tau}{R_a}\left(V_a(t)-K_{bemf}x_2(t)\right) \qquad \text{(Eq.5.21)}$$

ow let us define a sliding surface and a Lyapunov function. Same definition in Chapter 5.1. applies on the error term, $\varepsilon(t)=y^*(t)-y(t)=\theta^*_L(t)-\theta_L(t)$.

$$\sigma(t,x)=\dot{\varepsilon}+\gamma\varepsilon=0 \qquad \text{(Eq.5.22)}$$

Where $\gamma>0$ and an inverse of a desired time constant. Then the same Lyapunov function is

$$V(t,x)=\frac{1}{2}\sigma(t)^2$$

$$\dot{V}(t,x)=\sigma(t)\cdot\left(\dddot{y}^*+\gamma\ddot{y}^*+\left(\frac{nf+f_W/n}{n^2J+J_W+m_L r^2}-\frac{\gamma}{n}\right)\cdot x_2+\frac{n}{n^2J+J_W+m_L r^2}\left(\tau_f+\frac{\tau_D}{n}-\tau_m\right)\right)$$

(Eq.5.23)

The sliding condition must be met. The sliding condition is

$$\left|\dddot{y}^*+\gamma\ddot{y}^*+\left(\frac{nf+f_W/n}{n^2J+J_W+m_L r^2}-\frac{\gamma}{n}\right)\cdot x_2+\frac{n\tau_f+\tau_D}{n^2J+J_W+m_L r^2}\right|<\frac{n}{n^2J+J_W+m_L r^2}\cdot\tau_m(t)$$

(Eq.5.24)

The sliding condition should be met all time to ensure the existence of the sliding surface. If the above condition is not met, the sliding surface does not exist. The system could go unstable or stable that is depend on the open loop characteristic. The EOD motor driver system has a stable open loop poles. But it does not guarantees the stability of the overall system. Either phase portrait and a Lyapunov function should be studied to ensure the stability of the system when the sliding condition is not met.
If the sliding condition is met, then the sliding mode control is determined with the motor torque as a control input.

$$\tau_m(t) = \tau_{mmax}(t) \cdot \text{sign}(\sigma(t,x)) \qquad \text{(Eq.5.25)}$$

Where

$$\begin{aligned} \sigma(t,x) &= \dot{\varepsilon}(t,x) + \gamma\varepsilon(t,x) \\ &= \dot{y}^* + \gamma y^* - \gamma x_1 - n^{-1}x_2 \end{aligned} \qquad \text{(Eq.5.26)}$$

Or if the armature voltage is found as a control input, then the complete control algorithm for the EOD is found.

$$\begin{aligned} V_a(t) &= \frac{R_a}{K_\tau}\tau_{mmax}(t) \cdot \text{sign}(\sigma(t,x)) + K_{bemf}x_2 \\ &= V_{amax} \cdot \text{sign}(\sigma(t,x)) \\ &= V_{amax} \cdot \text{sign}(\dot{y}(t)^* + \gamma y(t)^* - \gamma x_1(t) - n^{-1}x_2(t)) \end{aligned} \qquad \text{(Eq.5.27)}$$

Now this is much simpler controller algorithm than one in Chapter 5.1. and does not involve with the disturbance measurement requirement. In Eq.5.27, $V_a(t)$ can only be ± 24 V, implying that $\tau_{mmax}(t)$ is varying to make $\left|\frac{R_a}{K_\tau}\tau_{mmax}(t)\right| + |K_{bemf}x_2| = 24$ V. Also notice that the above true since $|K_{bemf}x_2| < V_{amax}$, $\forall t \geq 0$ which cannot change the sign of the armature voltage. when the motor torque must be negative, the armature voltage must be negative, and the back EMF voltage cannot change the direction of the armature voltage to positive to generate the negative motor torque. The role of the back EMF will change the magnitude of the maximum motor torque applied based upon the speed of the motor shaft. This controller is much simpler and can be easily implemented without requiring a fast microprocessor to compute.

5.3. Disturbance Estimation of the Full Motor Driver Model

In Chapter 5.1., the sliding surface contains disturbance torque which is not measurable directly. The sliding mode control suggested in Eq.5.18 and Eq.5.19 is more complicated than one in the simplified model. However the load dynamics is comparably fast or equal to the motor armature dynamics, the assumption of motor torque as a control input is not valid. In that case, the motor armature dynamics should be included for controller design and analysis. Luckily the EOD vehicle dynamics is much slower than the motor armature dynamics, which enables us to simplify the whole motor dynamics. Thus it is not necessary to use more complicated control law in Chapter 5.1.

However several suggestions are made in this paper to estimate the disturbance and to control the fast system dynamics. In many cases motor speed is measured by a tachometer. If the output of the tachometer is differentiated in real time, $\dot{\omega}(t)$ is obtained and is used to find motor disturbance torque. If the output of the tachometer is

noisy, a band limited differentiator can be used to eliminate high frequency noises. This can be an effective algorithm and hardware associated is simple and can be implemented with low power passive components and one op-amp.

There exist many different estimation algorithms, and it is possible to imply disturbance estimation algorithm for the sliding surface in Chapter 5.1. But most of the estimation algorithms are nonlinear high order systems that requires a fast computing power. For the EOD motor control that is not desirable at all and will not be implemented. These disturbance estimation algorithm can be used in more expensive and bigger system with at least a 32 bit dedicated microprocessor for estimation algorithms.

One interesting linear disturbance detection algorithm will be shown for the sake of different options. Consider the following linear system.

$$\begin{aligned} \dot{x} &= Ax + Bu + Fw \\ y &= Cx \end{aligned} \qquad \text{(Eq.5.28)}$$

Where $x \in R^n, y \in R^m, u \in R^r, w \in R^p, A \in R^{n\times n}, B \in R^{n\times r}, F \in R^{n\times p}$ and $C \in R^{m\times n}$. Assuming w is disturbance and each element w_i has waveform structure. Then one can find a fictitious disturbance dynamic model that contains waveform of w_i. Let's consider the following dynamic process for the p-tuple disturbance.

$$\begin{aligned} w &= Hz \\ \dot{z} &= Dz + \begin{bmatrix} \delta_1 \\ \vdots \\ \delta_\rho \end{bmatrix} \end{aligned} \qquad \text{(Eq.5.29)}$$

Where $z \in R^\rho, H \in R^{p\times\rho}$ and $\delta_i, i = 1,\cdots,\rho$ is a time sequence of the Dirac delta function. The above fictitious disturbance dynamic process can be chosen to optimally estimate the actual disturbance functional forms. Now if one rewrite the system, Eq.5.28, with Eq.5.29, then one can find a composite system model.

$$\begin{aligned} &\begin{bmatrix} \dot{x} \\ \dot{z} \end{bmatrix} = \left[\begin{array}{c|c} A & FH \\ \hline 0 & D \end{array}\right] \begin{bmatrix} x \\ z \end{bmatrix} + \begin{bmatrix} B \\ 0 \end{bmatrix} [u] + \begin{bmatrix} 0 \\ \delta(t) \end{bmatrix} \\ &y = [C \mid 0] \begin{bmatrix} x \\ z \end{bmatrix} \\ &\Leftrightarrow \\ &\tilde{x} = \mathbf{A}\tilde{x} + \mathbf{B}u + \tilde{\delta} \\ &y = \mathbf{C}\tilde{x} \end{aligned} \qquad \text{(Eq.5.30)}$$

If the pair $(\mathbf{A},\mathbf{C})$ is completely observable then one can accurately estimate $x(t)$ and $z(t)$ by a conventional state observer, i.e. either full order observer or reduced order observer. A full order observer has a following generic form.

$$\dot{\hat{x}} = \mathbf{A}\hat{x} + \mathbf{B}u - \mathbf{K}_0\left(y - \mathbf{C}\hat{x}\right) \qquad \text{(Eq.5.31)}$$

Define $\varepsilon_{\vec{x}} = \tilde{x} - \hat{x}$. Then the error dynamics is

$$\begin{aligned} \dot{\varepsilon}_{\vec{x}} &= \dot{\tilde{x}} - \dot{\hat{x}} \\ &= \left(\mathbf{A} + \mathbf{K}_0\mathbf{C}\right)\varepsilon_{\vec{x}} + \delta \end{aligned} \qquad \text{(Eq.5.32)}$$

Thus one can choose $\mathbf{K_0}$ to make the error dynamics stable if the pair $(\mathbf{A},\mathbf{C})$ is completely observable. This is evident by transposing $\left(\mathbf{A} + \mathbf{K}_0\mathbf{C}\right)$. More detailed discussion can be found in C.D. Johnson's papers.

Let's consider Eq.5.12 and Eq.5.14 for disturbance estimation. Rewrite the motor dynamic model as following.

$$\dot{x} = Ax + BV_a + F\left(\tau_f + \frac{\tau_D}{n}\right) \qquad \text{(Eq.5.33)}$$

Where

$$A = \begin{bmatrix} 0 & n^{-1} & 0 \\ 0 & -\dfrac{n^2 f + f_W}{n^2 J + J_W + m_L r^2} & \dfrac{n^2}{n^2 J + J_W + m_L r^2} \\ 0 & -\dfrac{K_\tau K_{bemf}}{L_a} & -\dfrac{R_a}{L_a} \end{bmatrix} \qquad \text{(Eq.5.34)}$$

$$B = \begin{bmatrix} 0 \\ 0 \\ \dfrac{K_\tau}{L_a} \end{bmatrix} \qquad F = \begin{bmatrix} 0 \\ \dfrac{n^2}{n^2 J + J_W + m_L r^2} \\ 0 \end{bmatrix}$$

Now τ_f is a simple kinetic friction force which has a stepwise constant waveform. Actual disturbance torque τ_D can be approximated by second order polynomial. Finding a proper base function is important part, and more base functions will perform better to estimate closely actual disturbance. However small bump and hill can be estimated well with even simple second order polynomials. Therefore a fictitious dynamic process of disturbance torque can be modeled as following.

$$\tau_f + \frac{\tau_D}{n} = Hz \quad \Leftrightarrow \quad \tau_f + \frac{\tau_D}{n} = \begin{bmatrix} 1 & 0 & 0 \end{bmatrix} \begin{bmatrix} z_1 \\ z_2 \\ z_3 \end{bmatrix}$$

$$\dot{z} = Dz + \delta \quad \Leftrightarrow \quad \begin{bmatrix} \dot{z}_1 \\ \dot{z}_2 \\ \dot{z}_3 \end{bmatrix} = \begin{bmatrix} 0 & 1 & 0 \\ 0 & 0 & 1 \\ 0 & 0 & 0 \end{bmatrix} \begin{bmatrix} z_1 \\ z_2 \\ z_3 \end{bmatrix} + \begin{bmatrix} \delta_1 \\ \delta_2 \\ \delta_3 \end{bmatrix} \qquad \text{(Eq.5.35)}$$

Solution of z will be a second order polynomial, $z(t) = c_1 t^2 + c_2 t + c_3$. A composite system model is then follows.

$$\begin{bmatrix} \dot{x} \\ \dot{z} \end{bmatrix} = \left[\begin{array}{c|c} A & FH \\ \hline 0 & D \end{array}\right] \begin{bmatrix} x \\ z \end{bmatrix} + \begin{bmatrix} B \\ 0 \end{bmatrix} [u] + \begin{bmatrix} 0 \\ \delta(t) \end{bmatrix}$$

$$y = [C \mid 0] \begin{bmatrix} x \\ z \end{bmatrix}$$

$$\Leftrightarrow \qquad \text{(eq.5.36)}$$

$$\tilde{x} = \mathbf{A}\tilde{x} + \mathbf{B}u + \tilde{\delta}$$

$$y = \mathbf{C}\tilde{x}$$

Where

$$A = \begin{bmatrix} 0 & 4.0000e-2 & 0 \\ 0 & -7.2746e-1 & 4.9826e4 \\ 0 & -2.3305 & -1.1170e4 \end{bmatrix} \qquad B = \begin{bmatrix} 0 \\ 0 \\ 49.787 \end{bmatrix} \qquad F = \begin{bmatrix} 0 \\ 4.9826e4 \\ 0 \end{bmatrix}$$

$$H = \begin{bmatrix} 1 & 0 & 0 \end{bmatrix} \qquad D = \begin{bmatrix} 0 & 1 & 0 \\ 0 & 0 & 1 \\ 0 & 0 & 0 \end{bmatrix} \qquad \text{(Eq.5.37)}$$

$$C = \begin{bmatrix} 1 & 0 & 0 \\ 0 & 1 & 0 \\ 0 & 0 & 1 \end{bmatrix}$$

Since angle, angular velocity and motor torque are measurable, all three state variables can be used to estimate disturbance torque. The pair $(\mathbf{A},\mathbf{C})$ is completely observable by checking the observability Gramian. i.e. rank($G(\mathbf{A},\mathbf{C})$) = 6. Then a full state observer can be implemented by simple pole placement method.

Unfortunately this method requires 6th order dynamics to simulate in a real time and not very much desirable. Even a reduced order observer will require 3rd order observer. If the computing power is available, this method is recommended for a good disturbance accommodation.

5.4. System Analysis of Three Platform Dynamics

This rocking motion of the EOD vehicle was much ignored during mechanical design and was not a major problem for open loop control, i.e. torque control instead of speed control. For a closed loop control this rocking motion could be observed during a transient response and damped out providing the closed loop control sampling frequency is high enough. When the closed loop control sampling frequency was low, i.e. the EOD-2 has 25 Hz of update due to the Zilog main process load, the rocking motion of the EOD-2 became evident. This was also mainly contributed by very low phase margin of the motor controller in EOD-2. A simple PD controller with very low sampling frequency sometimes caused instability of wheels. In addition quantization of output voltage to 4 bit was simply not enough to control. In other words, lack of AD resolution and high sampling frequency contributed to a small gain and phase margin, which caused casual instability of wheel dynamics.

If applied force by connecting steel wires were zero, the rocking motion decays out very quickly due to a strong damping force of a tire. When some of wheels are rotating different speed, compression force will be created by wires. This was the main problem of the EOD-2 motor control. The improved motor controller, sliding mode controller, essentially eliminate the above problems, therefore reducing the rocking motion during the vehicle's acceleration. Nonetheless analysis of the rocking motion would help to design a better mechanical mount and design.

When all three platforms are accelerating or decelerating at a same rate even during a transient, the rocking motion will not occur. A feedback control could reduce the rocking motion, but what it is essentially doing is keeping three platforms at same speed throughout transient and steady state. Major drawback of this feedback control with the EOD vehicles would be an extra sensors and signal conditioning electronics to measure either a rotational angle of each platform or distance between platforms. This feedback control could be used in bigger systems like trains and trucks.

Still there is a passive open loop solution. Since three platforms have different mass, an acceleration of each platform is different. If a desired command input has a different bandwidth but same gain, then each platform will response accordingly. If the input of fastest platform goes through a Low Pass Filter (LPF) to match a transient response of a slowest platform, a speed difference of two platforms during a transient will be minimum. This is also only an input filter which can be done easily on microprocessor without extra electronics.

Let's consider the simplified motor dynamics in Eq.5.20 for implementation above idea. As one can notice easily, the lightest platform will have a fastest maximum acceleration. Therefore by filtering the input of the lightest platform motor to the open loop bandwidth of the slowest platform, an acceleration and speed difference is minimized. In return the rocking motion platforms will be minimized. The rocking motion due to rough terrain, i.e. climbing rocks, is not subject to concern. In fact providing most possible tire contact point is a main design consideration to improve maneuverability of the vehicle. By making connection materials of platforms flexible, all three platforms are in contact with ground all the time, thus providing most normal force. Eq.5.38 is a three driver motor model derived from Eq.5.20, a reduced model.

$$\begin{bmatrix}\dot{x}_1\\ \dot{x}_2\end{bmatrix}=\begin{bmatrix}0 & n^{-1}\\ 0 & -\dfrac{n^2 f+f_W}{n^2J+J_W+m_{Lr}r^2}\end{bmatrix}\begin{bmatrix}x_1\\ x_2\end{bmatrix}+\begin{bmatrix}0\\ \dfrac{n^2}{n^2J+J_W+m_{Lr}r^2}\end{bmatrix}[\tau_m]+\begin{bmatrix}0\\ \dfrac{-n^2}{n^2J+J_W+m_{Lr}r^2}\end{bmatrix}\left[\tau_f+\frac{\tau_{Dr}}{n}\right]$$

$$\begin{bmatrix}\dot{x}_3\\ \dot{x}_4\end{bmatrix}=\begin{bmatrix}0 & n^{-1}\\ 0 & -\dfrac{n^2 f+f_W}{n^2J+J_W+m_{Lm}r^2}\end{bmatrix}\begin{bmatrix}x_3\\ x_4\end{bmatrix}+\begin{bmatrix}0\\ \dfrac{n^2}{n^2J+J_W+m_{Lm}r^2}\end{bmatrix}[\tau_m]+\begin{bmatrix}0\\ \dfrac{-n^2}{n^2J+J_W+m_{Lm}r^2}\end{bmatrix}\left[\tau_f+\frac{\tau_{Dm}}{n}\right]$$

$$\begin{bmatrix}\dot{x}_5\\ \dot{x}_6\end{bmatrix}=\begin{bmatrix}0 & n^{-1}\\ 0 & -\dfrac{n^2 f+f_W}{n^2J+J_W+m_{Lf}r^2}\end{bmatrix}\begin{bmatrix}x_5\\ x_6\end{bmatrix}+\begin{bmatrix}0\\ \dfrac{n^2}{n^2J+J_W+m_{Lf}r^2}\end{bmatrix}[\tau_m]+\begin{bmatrix}0\\ \dfrac{-n^2}{n^2J+J_W+m_{Lf}r^2}\end{bmatrix}\left[\tau_f+\frac{\tau_{Df}}{n}\right]$$

(Eq.5.38)

From a sliding mode control in Eq.5.27, three separate sliding mode control are found.

$$\begin{bmatrix}V_{ar}\\ V_{am}\\ V_{af}\end{bmatrix}=\begin{bmatrix}V_{amax}\cdot\text{sign}\left(\dot{y}_r(t)^*+\gamma y_r(t)^*-\gamma x_1(t)-n^{-1}x_2(t)\right)\\ V_{amax}\cdot\text{sign}\left(\dot{y}_m(t)^*+\gamma y_m(t)^*-\gamma x_3(t)-n^{-1}x_4(t)\right)\\ V_{amax}\cdot\text{sign}\left(\dot{y}_f(t)^*+\gamma y_f(t)^*-\gamma x_5(t)-n^{-1}x_6(t)\right)\end{bmatrix} \qquad \text{(Eq.5.39)}$$

One key to design an open loop filter is keeping the tension of wires during transient. When the EOD vehicle is accelerating, the front platform should have a faster dynamics than the middle platform dynamics. This will ensure the middle platform not pushing the front platform, thus there is no compression force of wires. A same relationship goes to the middle and rear platform. On the contrary, the front platform should decelerate slow than the middle platform. Therefore a filter should change it's bandwidth higher or lower based on whether the EOD vehicle is accelerating or decelerating. A first order filter should be sufficient for the input filter.

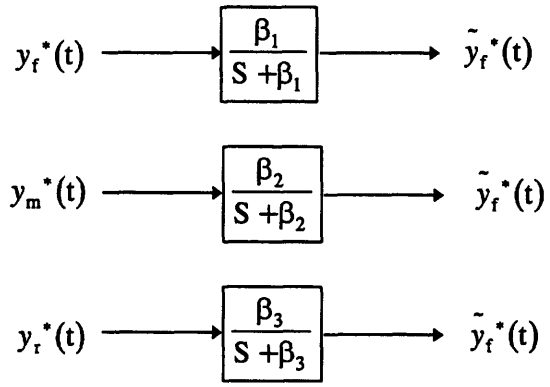

Figure 5.4.1. Input filter bank

Where $\beta_i=\begin{cases}\beta_i^a\\ \beta_i^d\end{cases}$, for i = 1,2,3 $\quad \beta_1^a>\beta_2^a>\beta_3^a, \quad \beta_1^d<\beta_2^d<\beta_3^d$.

5.5. Heading Angle Estimation by Micro-Mechanical Gyro

A heading angle of the EOD-2 is estimated by a single axis gyro. A simple integration of a gyro angular velocity measurement will give a heading angle. This is so called dead-reckoning navigation system or Inertial Navigation System (INS). Main problem with INS is accumulation of error. Heading angle measurement is often obtained by integrating angular velocity, that cause even a small DC bias of angular velocity measurement causes instability on the integration. Also an additive noise is causing correct estimation of a heading angle. To improve a heading angle estimation, a Kalman filter could be used. But a Kalman filter requires a complete linear steering wheel dynamics with a steering wheel armature voltage as an input. Steering motor has 3rd order dynamics, and a steering wheel angle of front and rear wheels is coupled with translation velocity of the EOD vehicle. Then angular velocity is proportional to the steering wheel angle and translation velocity of the EOD vehicle. Total system will be 6th order even ignoring a dynamics of the gyro. This high order is not very much desirable, and a Kalman filter cannot solve a problem of a DC drift bias. One can estimate the a DC drift bias assuming the DC drift bias is stable. But from the gyro specification, short term (100 second constant temperature) bias stability is < 0.05 °/sec or 5 ° of heading angle drift in 100 seconds even with a cancellation of nominal drift bias.

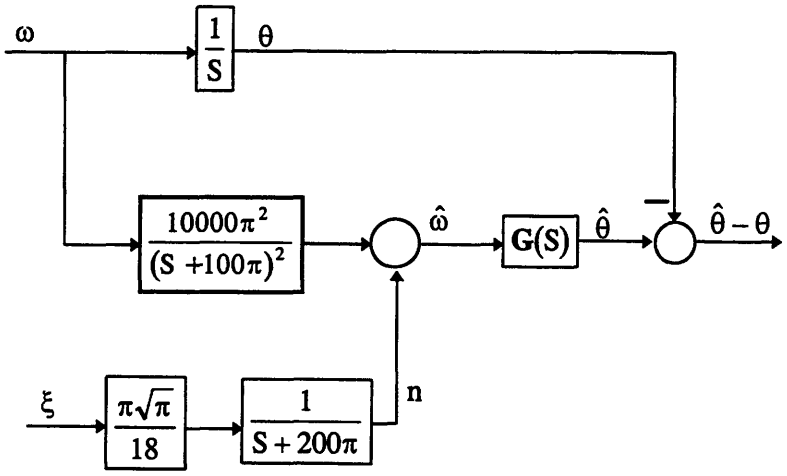

Figure 5.5.1. Heading angle estimation with a gyro dynamics

Normally a input of system is available to design a Kalman filter, but in this case the angular velocity ω is a quantity to be estimated and is not accessible. Thus from the above model it is not possible to design a Kalman filter to estimate the heading angle θ. But as mentioned earlier, ω is coupled by a steering wheel dynamics and translation velocity. Figure 5.5.2. shows a coupled heading angle estimation model with a steering wheel model. Notice that for $\hat{\theta}$, G(S) is not specified yet instead of simple integrator, $\frac{1}{S}$. G(S) will be a passive filter network to reduce a noise effect and to compensate a drift bias and its time variation of a drift bias.

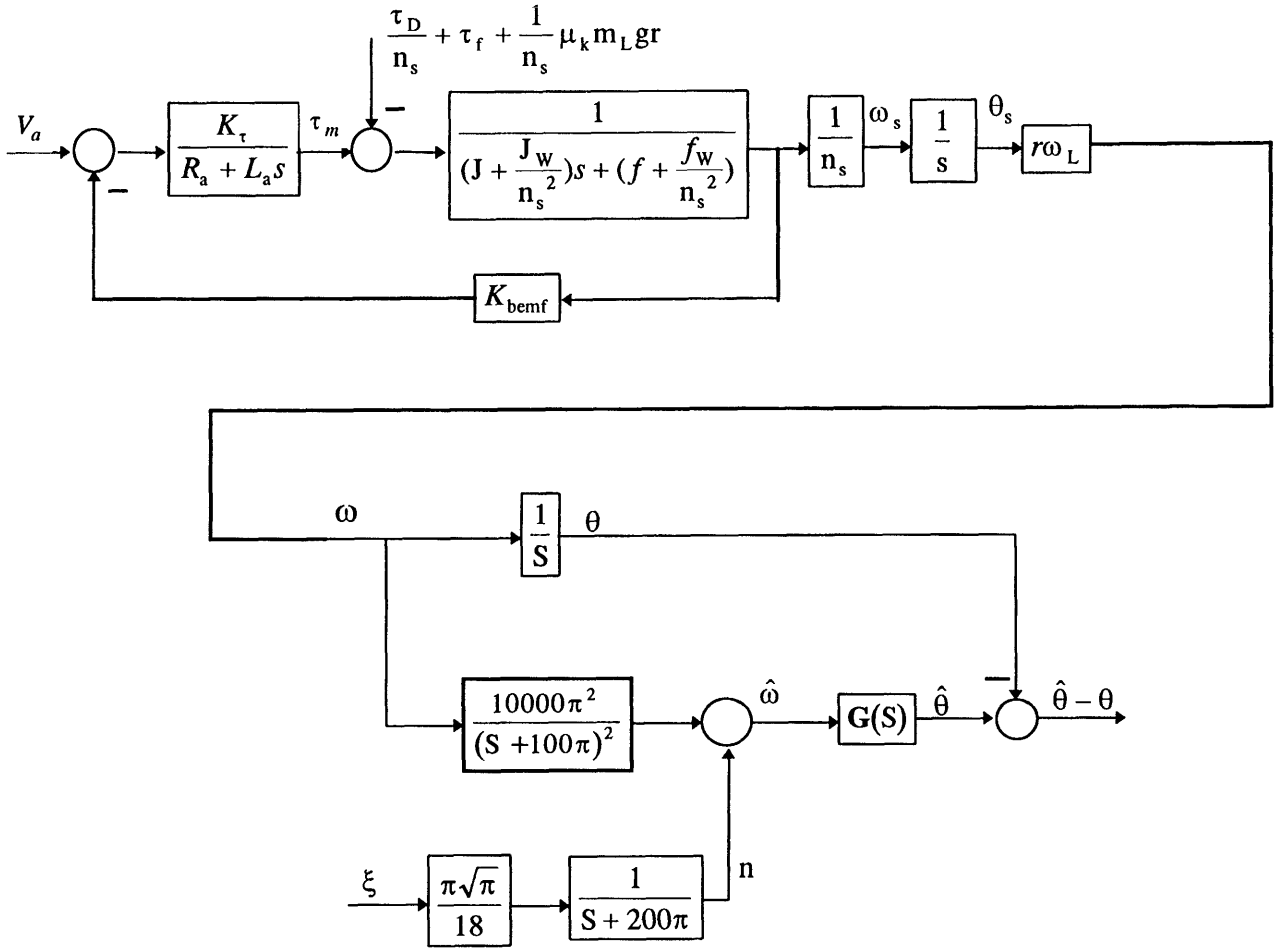

Figure 5.5.2. Coupled heading angle estimation model with a steering wheel model

Define $\varepsilon = \hat{\theta} - \theta$. From Figure 5.5.1., a transfer function can be found.

$$\varepsilon(S) = \left(G(S) \cdot \frac{10000\pi^2}{(S+100\pi)^2} - \frac{1}{S} \right) \cdot \omega(S) + G(S) \cdot \frac{\pi\sqrt{\pi}}{18(S+200\pi)} \cdot \xi(S) \qquad \text{(Eq.5.40)}$$

If G(S) is a simple integrator which is logical, then an angular velocity measurement has a bandwidth at 50 Hz=100π rad/sec. Also a bandwidth of the unit intensity white noise is 100 Hz=200π rad/sec. Figure 5.5.3. shows bode plots of the above transfer function when G(S) is a simple integrator. But a bandwidth of the EOD vehicle is lower than 50 Hz. Maximum angular velocity of the EOD vehicle can not usually exceed 1 Hz. A turning radius of the EOD-2 is 0.5 m and maximum velocity is 1.53 m/s. Therefore a maximum turning angular velocity is 0.49 Hz. For a fast settling time or transient response of the gyro, it is generally required 5 to 10 times of the maximum system angular velocity. Therefore an actual measurement bandwidth is 2.5 to 5 Hz. Thus G(S) can be implemented as a LPF at a cutoff frequency at 5 Hz or 10π rad/sec. Then the LPF G(S) is shown in Eq.5.41 and is a first order LPF with an integrator.

$$G(S) = \frac{10\pi}{S+10\pi} \cdot \frac{1}{S} \qquad \text{(Eq.5.41)}$$

This LPF can be implemented with a passive elements or a discrete LPF in a 8 bit local microprocessor. Figure 5.5.4. shows bode plots of Eq.5.40 with a LPF with a 10π rad/sec bandwidth. As one can notice easily, this low pass filter network will reduce an effect of white noise and a jitter due the EOD vehicle's high frequency vibration. But estimation error at a low frequency is higher than the pure integrator. This is a trade-off. Reducing a jitter noise error and system vibration error by adding a LPF increase a low frequency estimation error.

Still a small DC drift bias will eventually offset a heading angle as time pass. Reducing this effect requires an exact estimation of a slow DC drift bias that short term (100 sec constant temperature) bias stability is <0.05 °/sec and long term (1 year) bias stability is <1.0 °/sec. But real problem is accurate measurement of the gyro output voltage. The voltage to angular velocity conversion ration is 15 mV/(°/sec) and initial offset is $+2.5 \pm 0.045$ V. Now if the AD converter has 8 bit of resolution, then a voltage resolution is 9.69 mV. Initial offset can be measured with 3 1/2 digit accuracy, but the long term bias stability is 15 mV. If one build a dead-band around nominal bias voltage, this DC drift bias could be eliminated. Only one drawback with this dead-band is that an actual angular velocity, that is less than a dead band, cannot be measured. But if main navigation system of the EOD vehicle drive above the dead-band all time, then the drift bias problem can be solved. In fact the EOD vehicle will never rotate at a lower rate of 2.0 °/sec or 30 mV. Thus a 8 bit local processor can ignore its first one bit, which means it is sufficient to use its 7 bits.

Thus a LPF at cutoff frequency of 5 Hz and 1 bit dead-band will improve a heading angle estimation. It is a mistake not to use a filter network before AD converter, which can isolate high frequency noise and vibration.

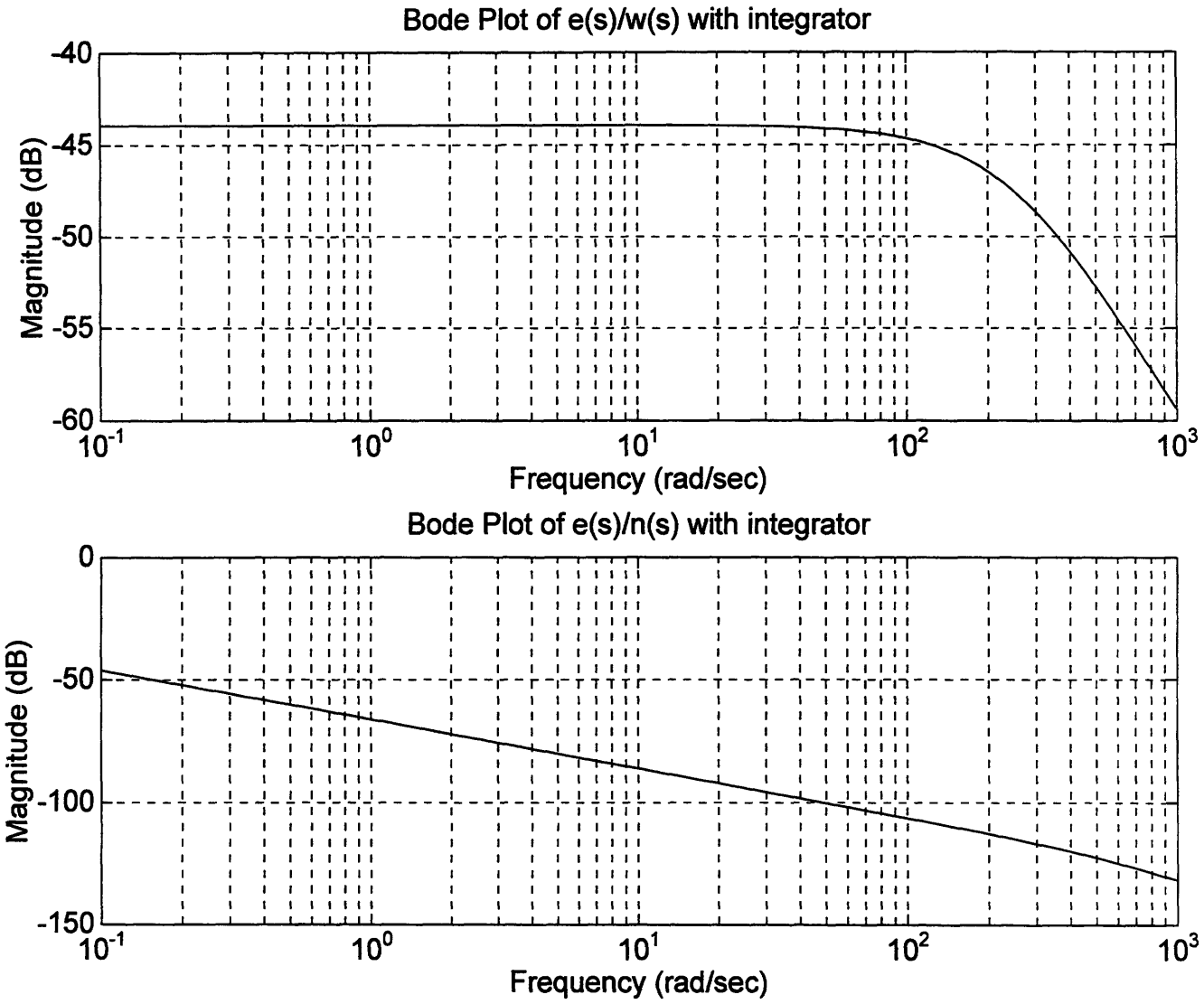

Figure 5.5.3. Bode plot of a heading angle estimation error with a pure integrator

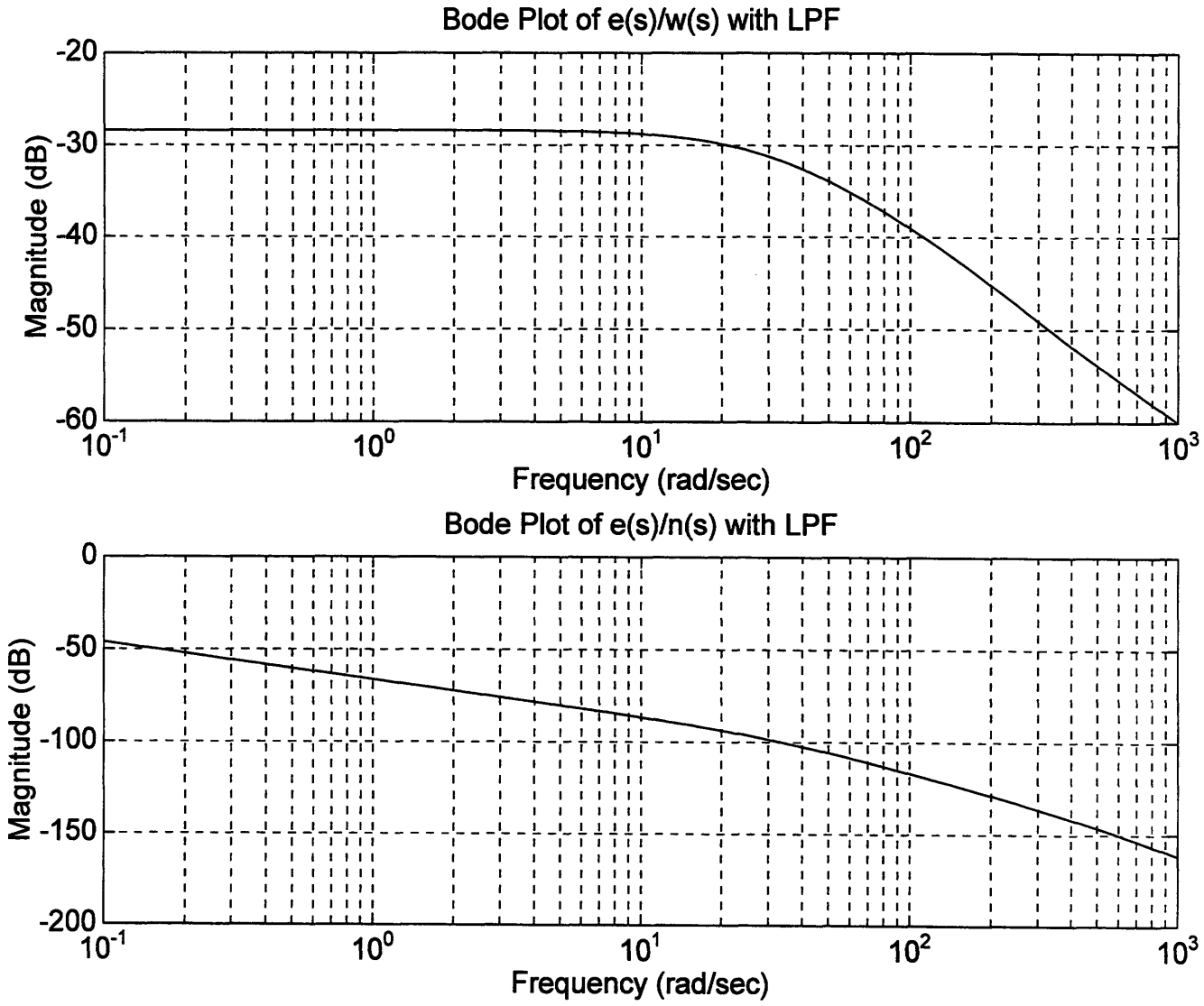

Figure 5.5.4. Bode plot of a heading angle estimation error with a LPF and integrator

5.6. LPS Speed Control and Synchronization of Phase Angle

Most of problems with original LPS has been solved except synchronization of two spinning laser beam at a fixed phase angle. This involves with a phase angle and angular speed of two rotating beacons. A Phase Lock Loop (PLL) has been used in an original system, but it has a limited stabilization region. It is known fact that PLL has a small region of stability for an accurate phase locking. If a wider region of stability is required, an accuracy of phase locking must be reduced or no phase locking.

Two PLL can solve the above synchronization problem. A first PLL is a general stabilization PLL that will drive LPS to a stable region of a second PLL. Once LPS is in a stable region of a second PLL, the second PLL will lock on a desired phase. Even though this approach will increase a chance of stabilization, but still this method will not cover all operation region of LPS. Also a switching of two PLL must occur at a proper region, in which a switching surface must be designed and implemented. This might work but there is a better solution.

As in Chapter 3.4. Laser Positioning System, a motor controller circuit is implemented. This motor controller circuit is different from the EOD vehicle driver motor circuit, i.e. control input voltage varies between 0 V to 12 V instead of a switching voltage. This means a regular linear control algorithm can be used. A LQR controller will be implemented. A measurement of angle is not continuous, and a phase angle is in between to measurement. Thus an angle measurement cannot be used in a continuous fashion, which is a unique situation. First a LQR controller is designed and an estimation technique of angle and velocity will be discussed later.

Let's rewrite a system model.

$$\begin{bmatrix} \dot{x}_1 \\ \dot{x}_2 \\ \dot{x}_3 \end{bmatrix} = \begin{bmatrix} 0 & 1 & 0 \\ 0 & -\frac{f_{LPS}}{J_{LPS}} & \frac{1}{J_{LPS}} \\ 0 & -\frac{K_\tau K_{bemf}}{L_a} & -\frac{R_a}{L_a} \end{bmatrix} \begin{bmatrix} x_1 \\ x_2 \\ x_3 \end{bmatrix} + \begin{bmatrix} 0 \\ 0 \\ \frac{K_\tau}{L_a} \end{bmatrix} [V_a] + \begin{bmatrix} 0 \\ \frac{\tau_f}{J_{LPS}} \\ 0 \end{bmatrix}$$

$$y = \begin{bmatrix} 1 & 0 & 0 \end{bmatrix} \begin{bmatrix} x_1 \\ x_2 \\ x_3 \end{bmatrix}$$

$$\Leftrightarrow \qquad \text{(Eq.5.42)}$$

$$\dot{x} = Ax + Bu + F$$

$$y = Cx$$

Where

$$A=\begin{bmatrix}0 & 1 & 0\\ 0 & -0.30 & 1.97e5\\ 0 & -1.40 & -2.67e4\end{bmatrix},\quad B=\begin{bmatrix}0\\ 0\\ 30.6\end{bmatrix},\quad F=\begin{bmatrix}0\\ 12.2\\ 0\end{bmatrix},\quad C=\begin{bmatrix}1 & 0 & 0\end{bmatrix} \qquad \text{(Eq.5.43)}$$

Now define a quadratic cost function, $J(\mathrm{t},x)$.

$$J(\mathrm{t},x)=\int_0^\infty\left[y(\mathrm{t})^2+V_a(\mathrm{t})^2\right]d\mathrm{t} \qquad \text{(Eq.5.44)}$$

Then a LQR controller can be found by solving Control Algebraic Riccati Equation (CARE).

$$u(x)=-\left(x_1-y^*\right)-0.0580x_2-0.429x_3 \qquad \text{(Eq.5.45)}$$

Where y^* is a reference angle of beacons.

Open loop poles of the system are $0, -1.23$ and $-2.70e4$, where closed loop poles are $-2.70e4$ and $-11.9 \pm j9.2$. Therefore the closed loop system is stable.

A torque is measured by measuring an armature current directly. Thus angular velocity can be estimated by using a standard state observer. By the separation principle, an overall system is stable. An angle measurement is done discretely, but it can be interpolated by using angular velocity information. Thus this system is stable, but LPS with a LQR controller still shows a steady state error for its angle. A PID controller also would have same kind of steady state error since the reference is a ramp input.

5.7. Control Simulations for the EOD Driver Motor and LPS

Sliding mode control for the EOD motor is simulated under various condition. Two different types of sliding mode controller are simulated. One is using ± 24 V switching control and the other is using either + 24 V and 0 V, or - 24 V and 0 V. Difference is energy efficiency of the later is better than one of the first. This is evident since the later control has less duty cycle than the first control. For an energy conservation, the later sliding control algorithm is better. In fact the later control has less chattering. The switching frequency for all simulations is 1 KHz, which is reasonable for PIC16C74 with 20 MHz of clock frequency. Thus this switching frequency is much lower than usual PWM frequency. This is very desirable feature and performance is much better than conventional PWM control's.

When the desired position is more exotic, which is sine wave, with a considerably large disturbance torque, switching control with ± 24 V performs better than on-off switching control. Mainly it is due to the amplitude of disturbance torque with very high frequency, and EOD driver motors have more torque to compensate disturbances with ± 24 V switching. However this trajectory is very unlikely for a vehicle motion. Also notice that the desired oscillation frequency is 2 Hz with 32 Hz sinusoid disturbance. Even though this condition switching to ± 24 V performs better, but it is not necessary for a normal EOD vehicle trajectory. On-off switching control still tracks the desired position with some steady state error. For typical trajectory like ramp input for the vehicle position, this new on-off sliding mode control works better and more importantly has very good power efficiency.

LPS synchronization is done very nicely with LQR servo control. Beacon2 speed is tracking beacon1's speed, which is regulated by voltage regulator circuit. Main concern was whether motor controller has enough control authority to synchronize. Beacon2 should be powered by 12 V or higher voltage to ensure its synchronization.

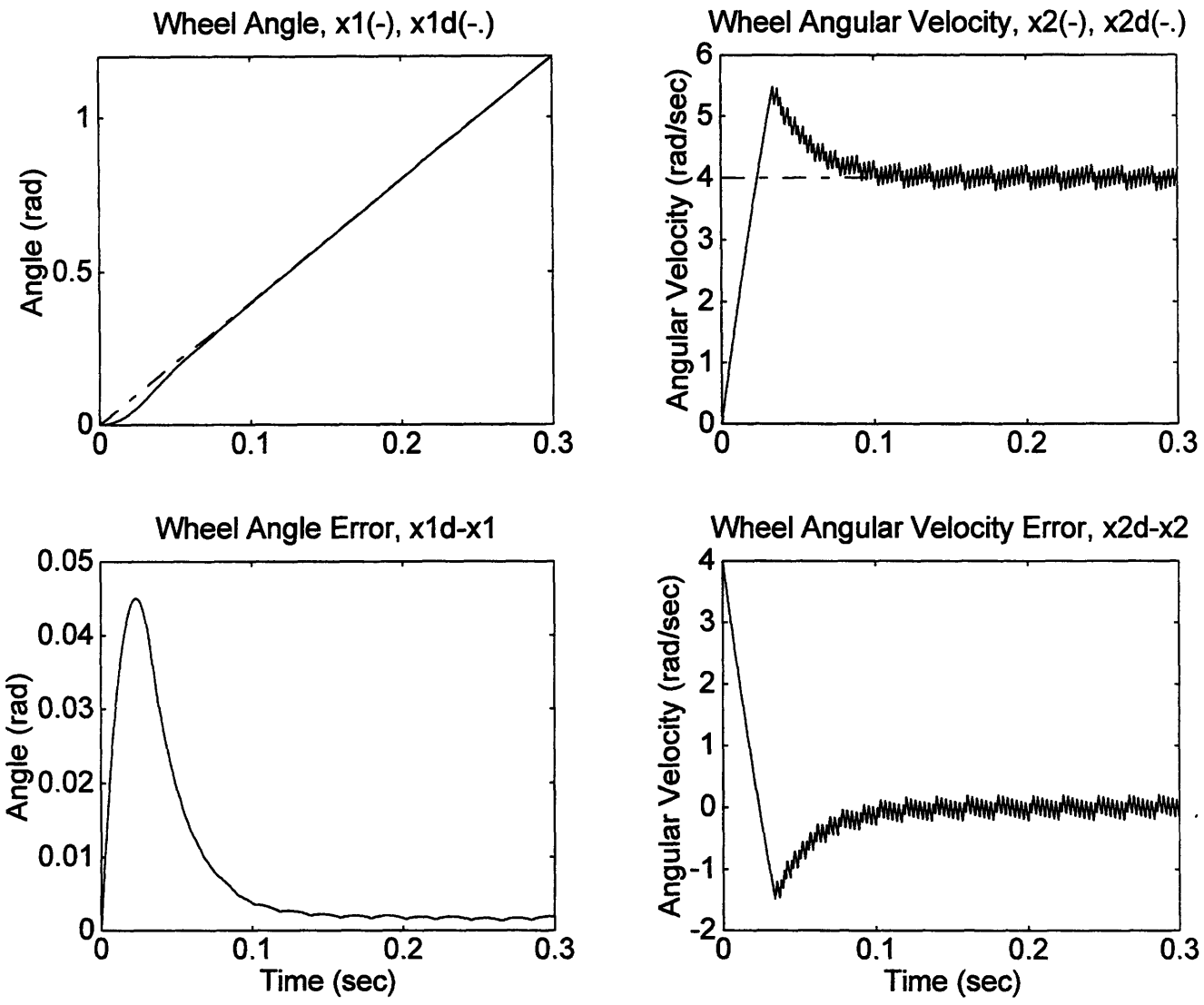

Figure 5.7.1. Simulation of sliding mode control in Chapter 5.2. with ± 24 V switching and no environmental disturbances: The reference position command is a ramp function and 1 KHz control switching frequency. Notice that the position and velocity of the EOD vehicle follows the desired command input well. Chattering exist in especially vehicle's velocity. However, for an operation on rough terrain, this speed chattering is not a significant problem.

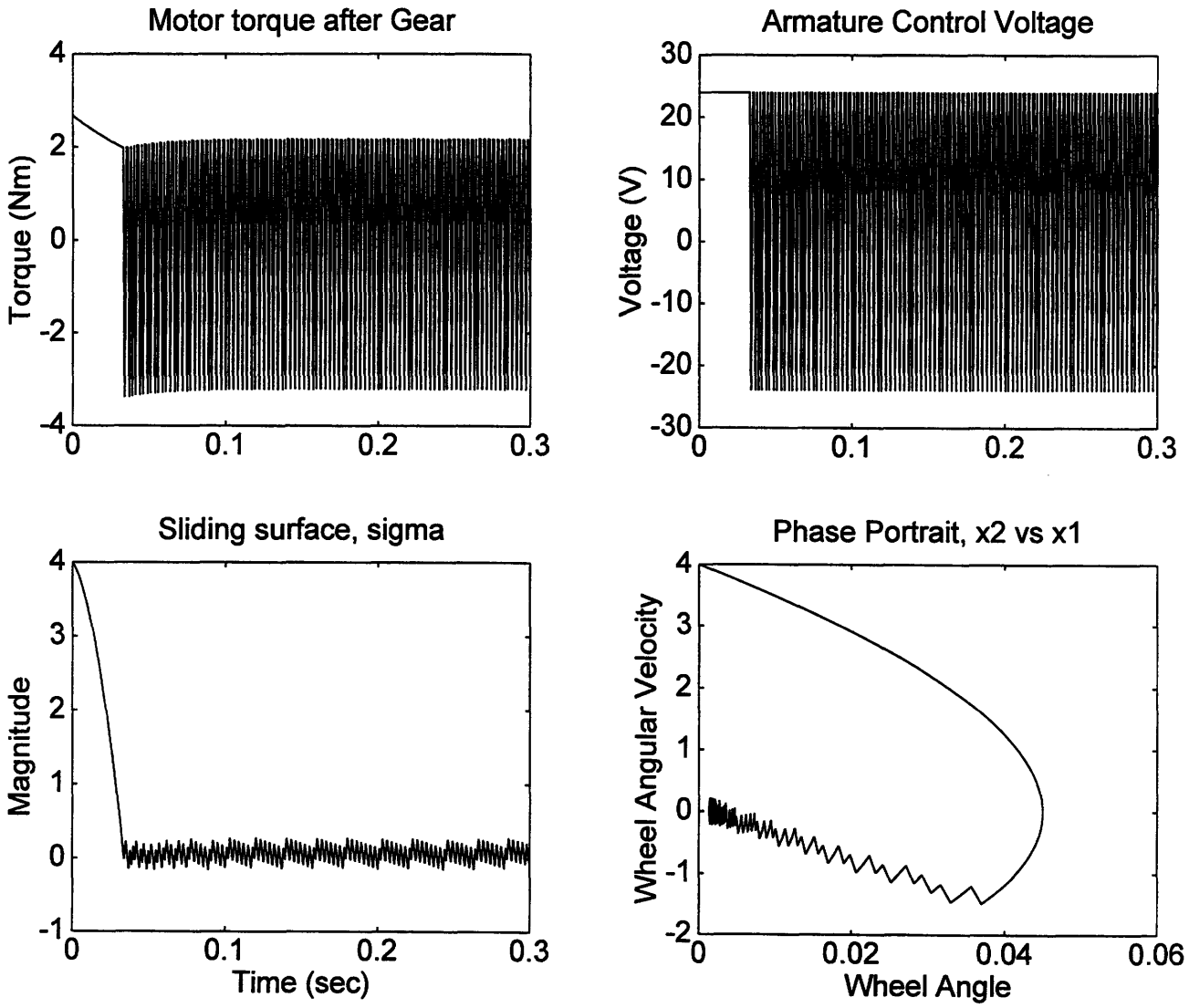

Figure 5.7.2. Continued from previous simulation results: The reference position command is a ramp function and 1 KHz control switching frequency. Sliding surface does exist with some chattering.

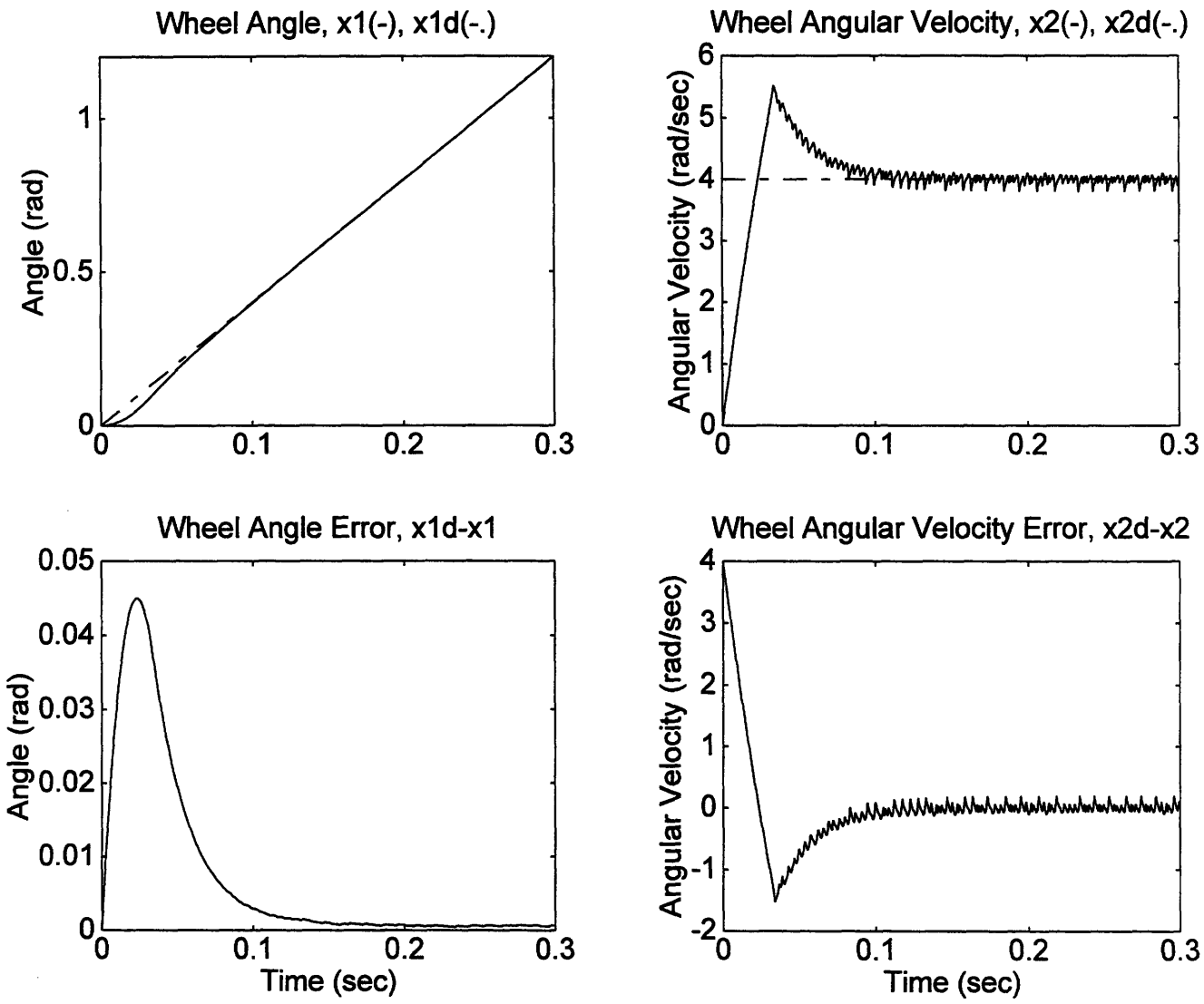

Figure 5.7.3. Same simulation of sliding mode control in same condition in Figure 5.7.1. and Figure 5.7.2. but with a difference of 24 V and 0 V switching. Performance of the controller is very similar to the previous controller. Ideally the output should be same if the switching frequency were infinite.

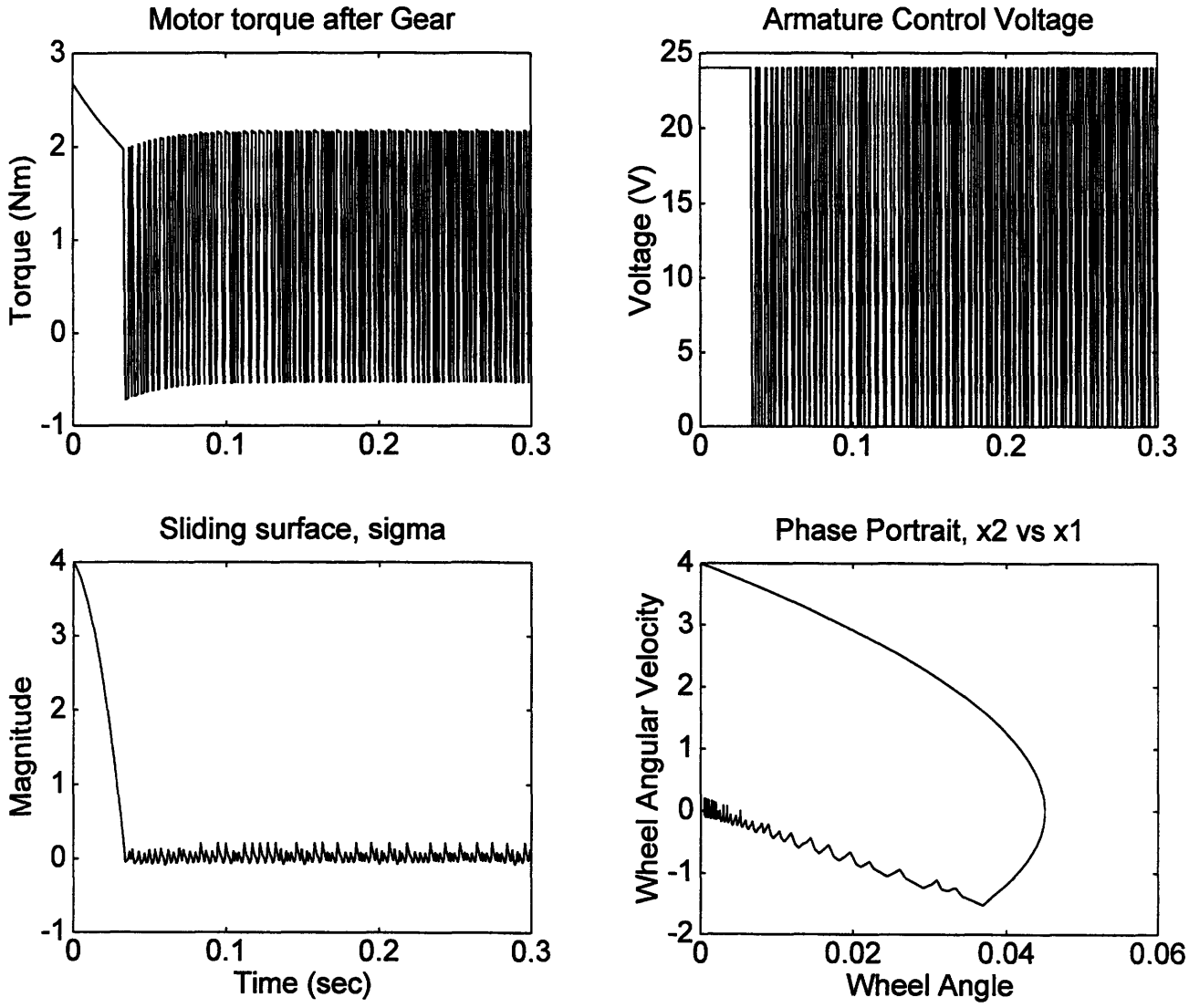

Figure 5.7.4. Continued from previous simulation results: Armature voltage is switching between 24 V and 0 V. This way power loss by charging MOSFETs and motor inductor is minimized.

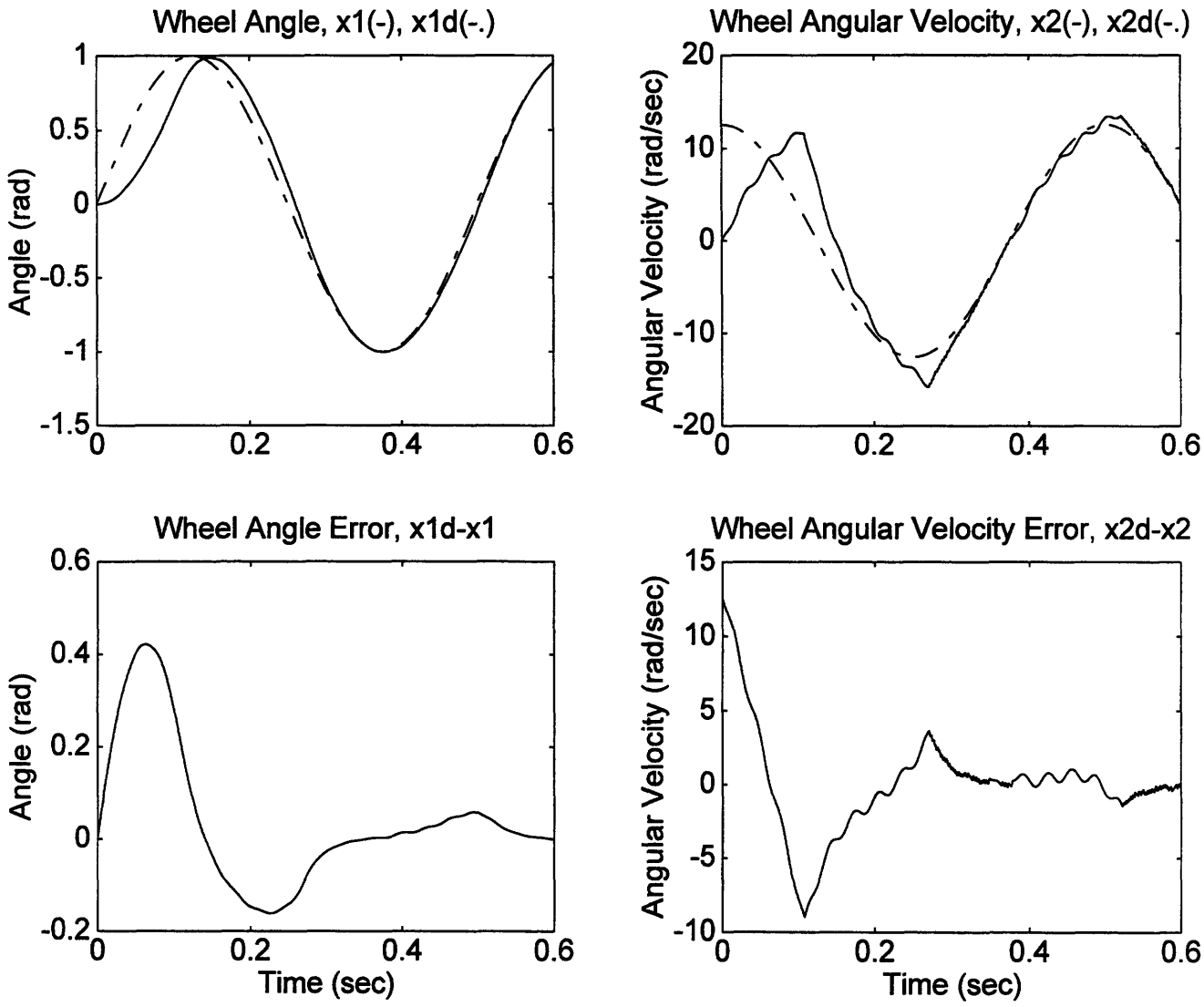

Figure 5.7.5. Simulation of sliding mode control with ± 24 V switching and significant environmental disturbances: The reference position command is a sine function and 1 KHz control switching frequency. Notice that the position and velocity of the EOD vehicle follows the desired command input well despite fast command position input and large disturbance in Figure 5.7.6.

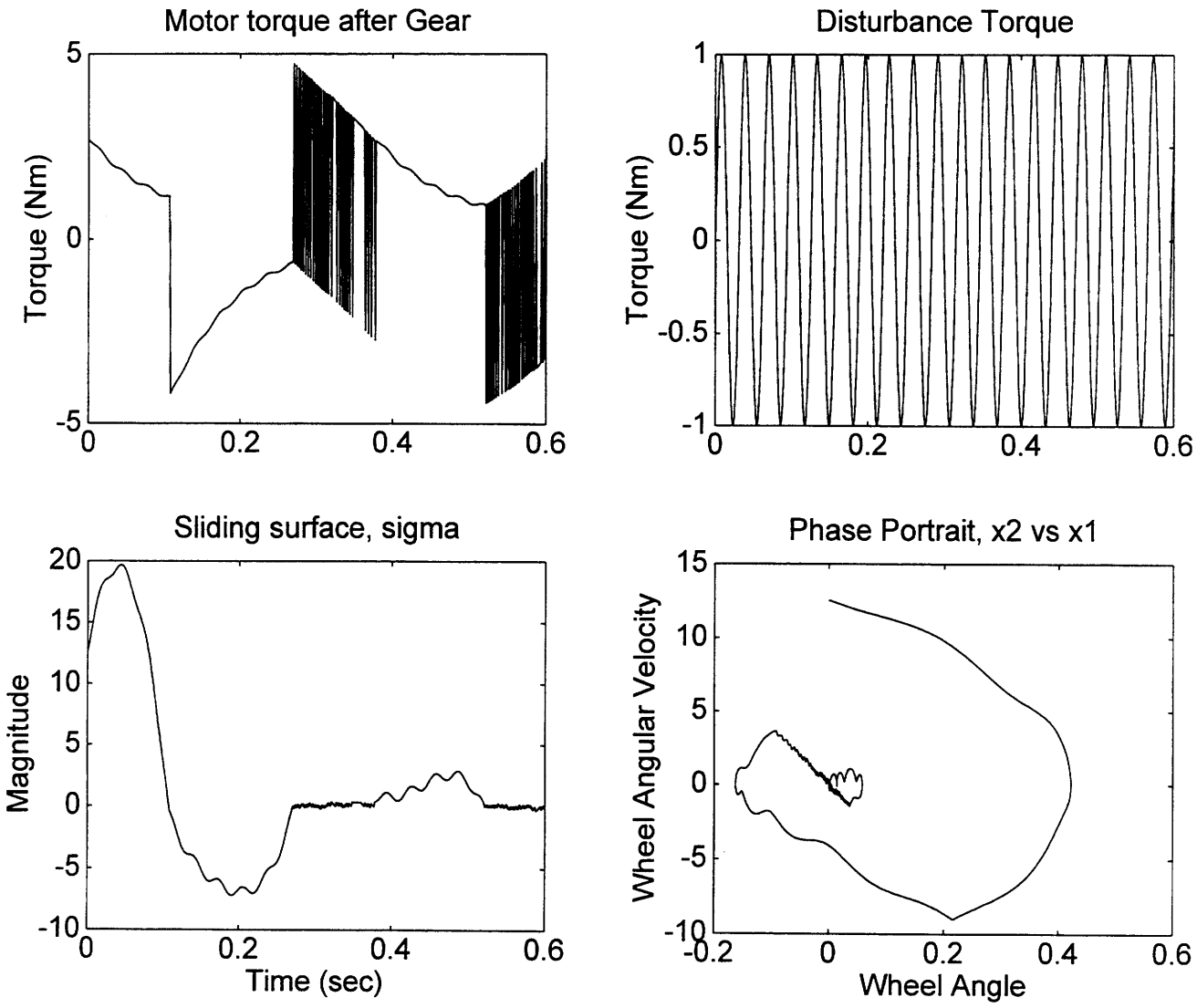

Figure 5.7.6. Continued from previous simulation results: Disturbance torque is sinusoid with 200 Hz frequency. Also magnitude of disturbance is 20 % of motor's stall torque. Despite these condition sliding surface still stays around zero for most of time.

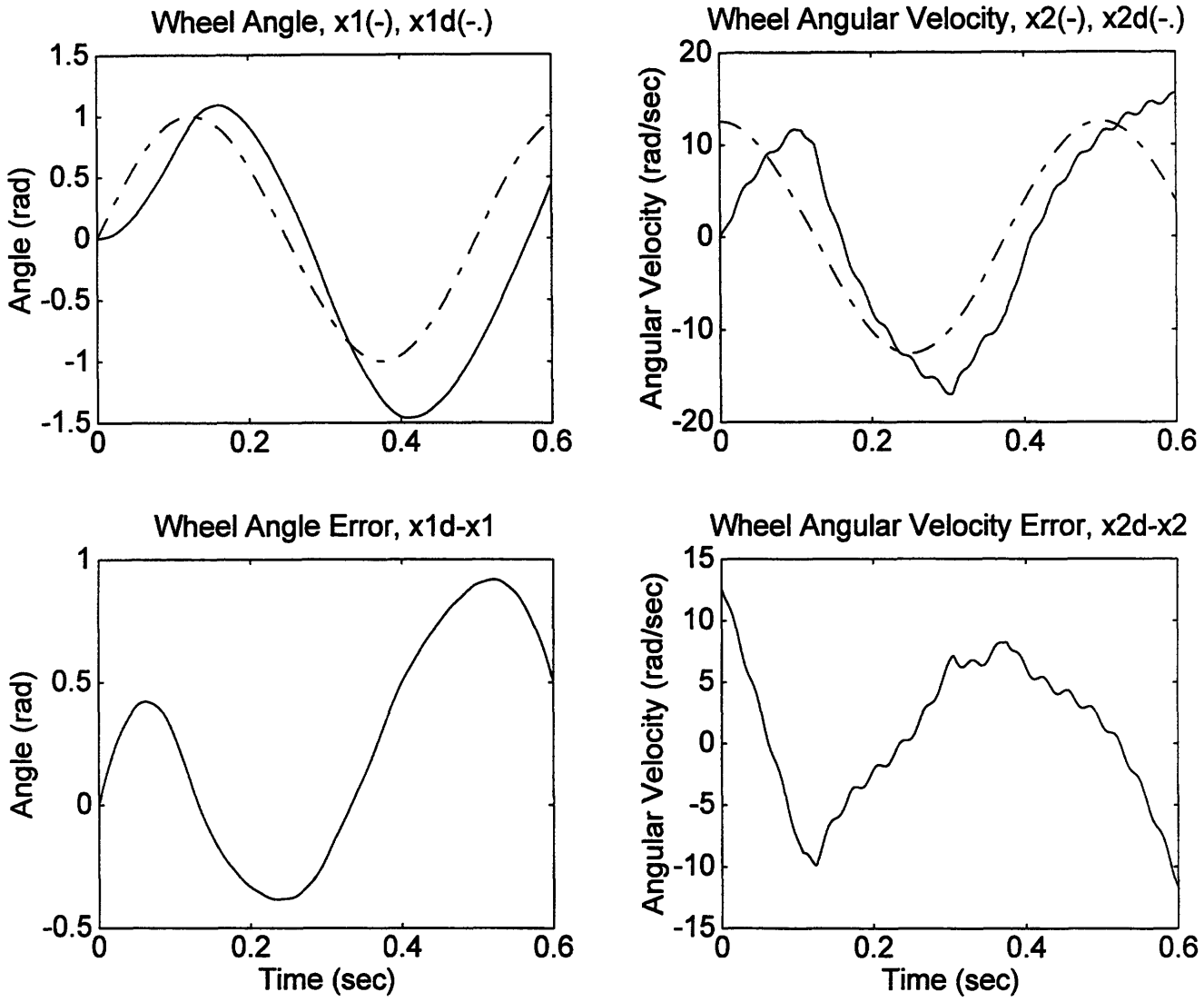

Figure 5.7.7. Simulation of sliding mode control with 24 V and 0 V switching and significant environmental disturbances: The reference position command is a sine function and 1 KHz control switching frequency. Notice that the position and velocity of the EOD vehicle follows the desired command input in some degree with steady state error despite fast command position input and large disturbance in Figure 5.7.8.

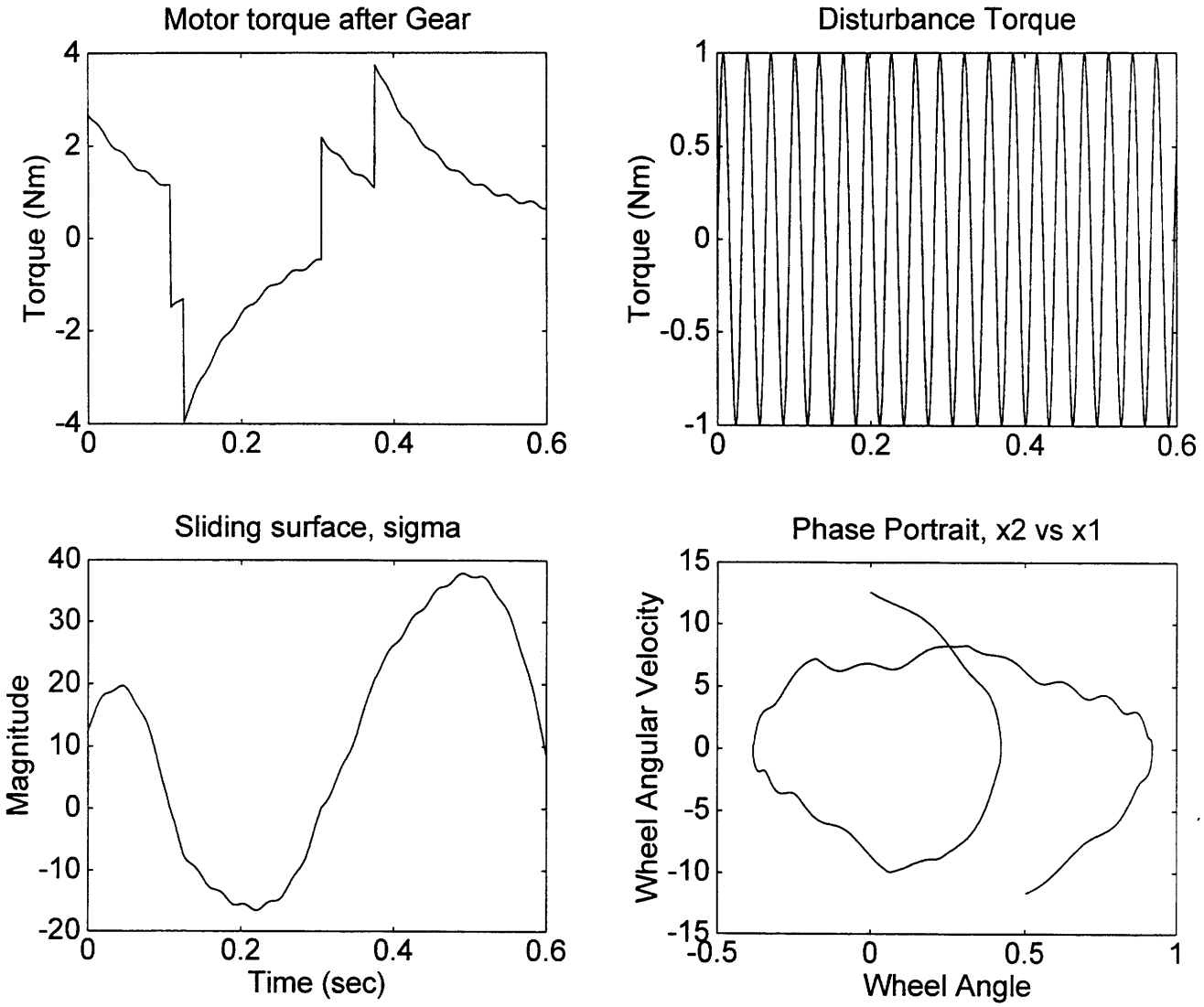

Figure 5.7.8. Continued from previous simulation results: Disturbance torque is sinusoid with 200 Hz frequency. Also magnitude of disturbance is 20 % of motor's stall torque. Notice that sliding surface does not exists since switching to 0 V does not have enough power to compensate sinusoidal disturbances. But remember that this disturbance is very unlikely for the EOD vehicle operation.

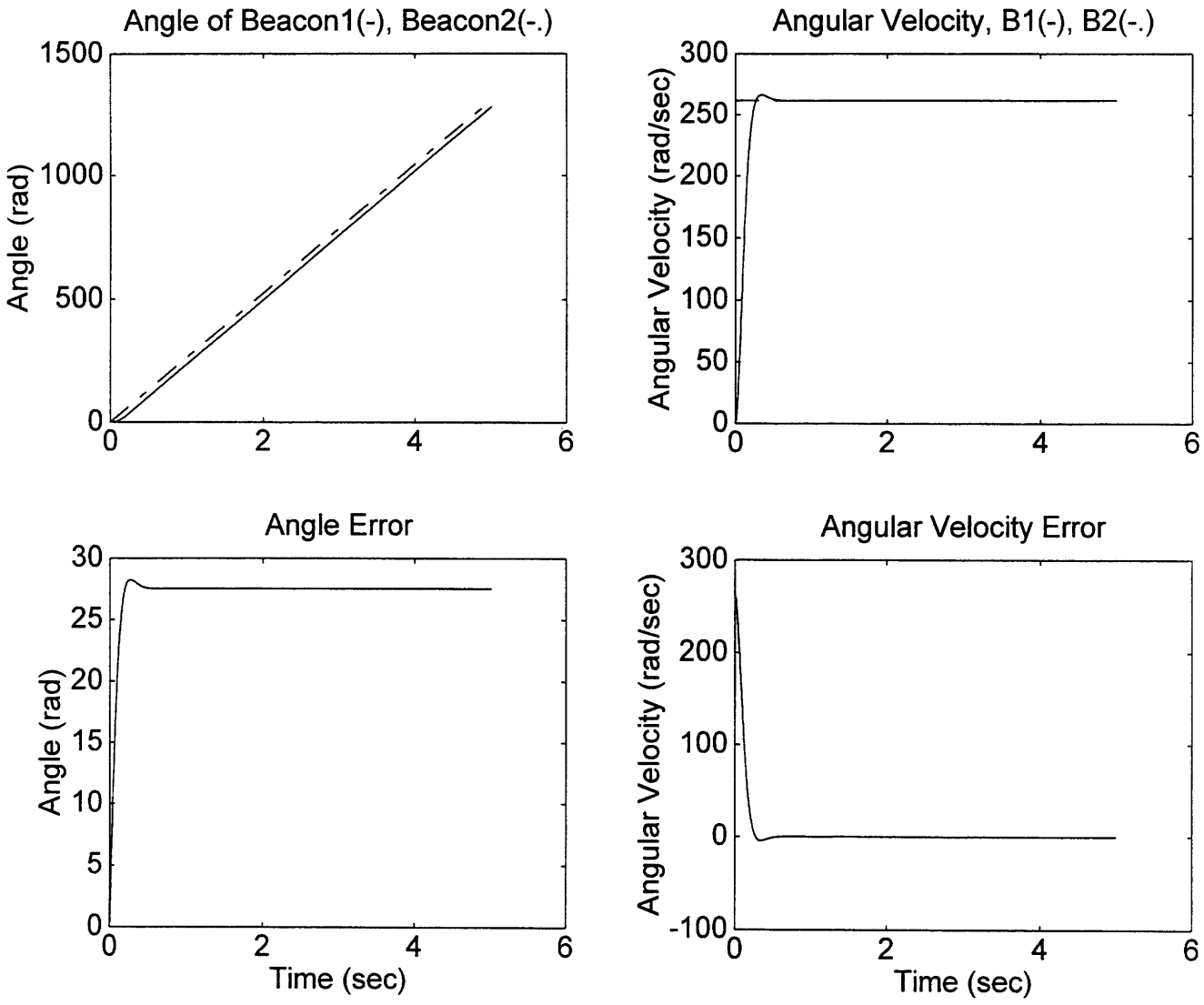

Figure 5.7.9. Beacon2 angular velocity is synchronized to beacon1's without steady state error with LQR control. Angle of beacon2 has a steady state error but this is acceptable since beacon2 only has to be locked on a certain phase angle.

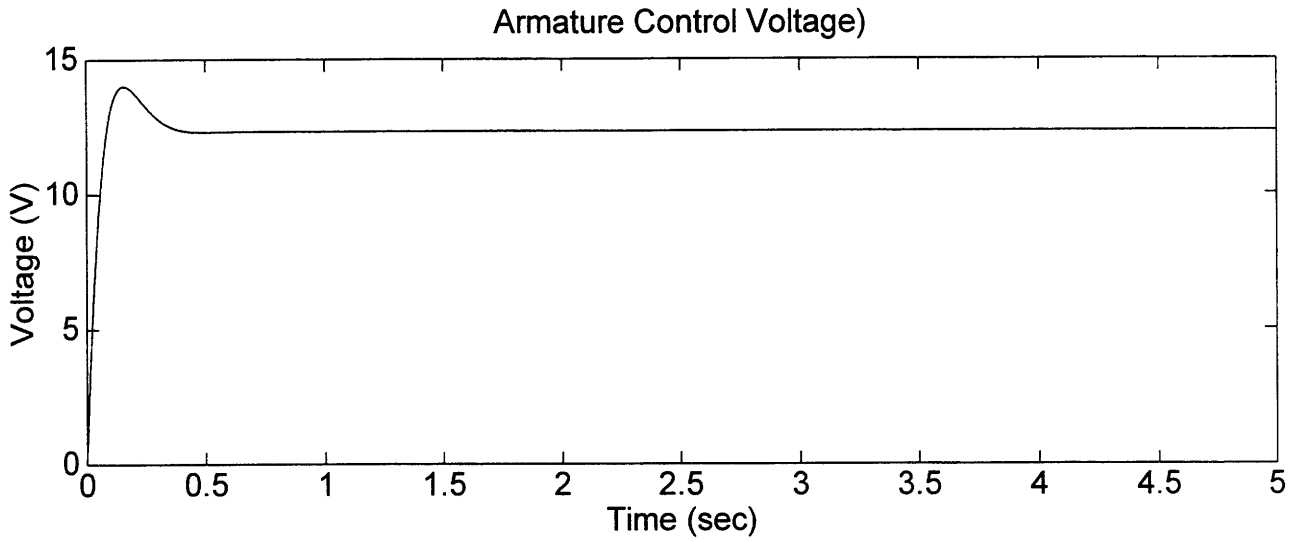

Figure 5.7.10. Control voltage is within battery maximum battery voltage or power supply. Thus this LQR controller will not be saturated.

CHAPTER 6

Summary and Conclusions

6.1. Summary

This paper treated general problems in design and integration of electrical and control part of a small autonomous vehicle. Due to size of the vehicle, many design and implementation factors are discussed. Mainly power efficiency, compactness and robustness are considered in electrical design. Even the choice of motor control algorithm was chosen based on hardware compactness and power transfer efficiency.

Electrical sensors and actuators must be compact and consume low power. Determining which electronics impact on power consumption most is very important, and driver motors are main power hungry electronics for the EOD vehicles. Design of proper and energy efficient motor driver circuit is more important than any other electronics without compromising its performance. The sliding mode control implemented in a 8 bit microprocessor and using H-bridge without DA converters nor PWM generator is a new concept and hasn't been well known in industries. Same time performance is not compromised like in National Semiconductor's LM18245. Design of motor electronics should consider vehicle's controllability for its performance, and this new motor circuit is designed specifically for compactness and good control performance. Selection of motor also be based on some anticipated mathematical model of vehicle and its functional specifications. Provided models in Chapter 4 should help better for future vehicle design. Also anti-aliasing filter for a gyro and its impact on heading angle estimation by bode plots of error dynamics are provided to help to choose a right anti-aliasing filter. LPS was made many changes and improvement to even to operate properly which originally designed last only few operations. A better choice of radio receiver solved many communication problems. For synchronization problem, continuous voltage regulators and beacon2 motor synchronization circuit are already implemented. Some calibrations are left to operate LPS properly.

Modeling and control of vehicles are very important issue since autonomy of vehicle needs a precise, reliable and predictable vehicle motion control. Complete vehicle dynamics are modeled in Chapter 4 in hoping for better vehicle design and component selections for future development not depending on previous version of vehicle model. Control issue must be addressed strongly in low level software not with benign assumptions of vehicle dynamic control. Chapter 5 introduces several good motion

control algorithms especially with sliding mode control. Also servo LQR and disturbance accommodating control were introduced in process of motor control. Two different sliding mode control are simulated and are proven to be robust and high performance in simulation.

6.2. Conclusions and Suggestions for Further Work

Autonomy of vehicles requires many sensors and good motion control actuators. Power management is very important to balance different parts of electronics. Sonar sensor, gyro and LPS were discussed as some of sensors in EOD vehicles. It is essential to plan ahead of actual design process and what is needed and what is not. Of course it may be changed later, but it is best to have an overall plant for electronics and power consumption calculations before all things are started. Getting a rough quantitative number for all these requirements will be very helpful for later development and revision stage. Be aware of small details, i.e. mounting space for electronics, connector types and sizes, EMI, proper coaxial cable use, proper understanding and usage of RF connectors like BNC, SMA, SMB, F-type, N-type and BNC to SMA adapters, wire harnessing with proper size gage based on voltage and current level, anticipated power consumption calculation for new electronics, expandability for future, and so on.

BIBLIOGRAPHY

1. _____, "Amplifier Reference Manual," Analog Devices, Inc., 1992
2. _____, "Amplifier Applications Guide," Analog Devices, Inc., 1992
3. Askeland, Donald R., "The Science and Engineering of Materials," PWS-KENT, Boston, Massachusetts, 1989
4. Beer, Ferdinand P. and Johnston, E. Russell, Jr., "Vector Mechanics for Engineers: Statics and Dynamics," McGraw-Hill Publishing Company, New York, 1988
5. Brogan, William L., "Modern Control Theory", Prentice Hall, Englewood, New Jersey, 1991
6. Chajes, Alexander, "Principles of Structural Stability Theory," Prentice Hall, Englewood Cliffs, New Jersey, 1974
7. DeCarlo, Raymond A., Zak, Stanislaw H. and Matthews, Gregory P., "Variable Structure Control of Nonlinear Multivariable Systems: A tutorial," IEEE Automatic Control, 1988
8. DeLaune, Jon, "MTTL and MECL Avionics Digital Frequency Synthesizer," Motorola Inc., AN-532
9. Dorf, Richard C., "Modern Control Systems," Addison-Wesley Publishing Company, Massachusetts, 1992
10. _____, "Electronics Now," September, 1993
11. Geiger, Dana F., "Phaselock Loops for DC Motor Speed Control," Wiley-Interscience Publication, 1981
12. _____, "GyroChip II: Solid-State Rate Sensor Operational Manual," Systron Donner Internal Division, A BEI Electronics Co., California
13. Johnson, C.D., "Theory of disturbance-accommodating controllers," Control and Dynamic Systems, vol. 12, p.387, 1976
14. Kalman, R.E., "On the general Theory of Control Systems,"
15. Leitmann, George, "The Calculus of Variations and Optimal Control," Plenum Press, New York, 1981
16. _____, "Linear and Interface Integrated Circuits," Motorola Inc., DL 128, REV 3, 1990
17. _____, "Linear Applications Handbook," National Semiconductor Corporation, 40041, California, 1991
18. _____, "LMD 18200 3A, 55V H-Bridge," National Semiconductor Corporation, California, 1996
19. _____, "LS/S/TTL Logic Databook," National Semiconductor Corporation, 40044, California, 1989
20. _____, "Miniature Drive Systems," Micro Mo Electronics Inc., Florida, 1992
21. Nash, Garth, "Phase-Locked Loop Design Fundamentals," Motorola Inc., AN-535, 1994
22. _____, "Power MOSFET Transistor Data," Motorola Inc., DL 135, REV 3, 1989
23. Sedra, Adel S. and Smith, Kenneth C., "Microelectronic Circuits," Saunders College Publishing, 1991

24. Sifer, J.F., Prouty, S.J. and Mak, P.H., "Advanced Concepts for Launch Vehicle Control," IEEE, 1991
25. _____, "Small-Signal Transistors, FETs and Diodes Device Data," Motorola Inc., DL 126, REV 3, 1991
26. _____, "Special Purpose Linear Devices Databook," National Semiconductor Corporation, 400104, California, 1989
27. Serway, Raymond A., "Physics: For Scientist & Engineers with Modern Physics," Saunders College Publishing, 1990
28. Slotine, Jean-Jacques E. and Li, Weiping, "Applied Nonlinear Control," Prentics Hall, Englewood Cliffs, New Jersey, 1991
29. Spong, Mark W. and Vidyasagar, M., "Robot Dynamics and Control,' John Wiley & Sons, Inc., 1989
30. Tedeschi, Frank P., "The Active Filter Handbook," TAB BOOKS, Pennsylvania, 1979